# EFFECTS OF GEOSYNTHETIC REINFORCEMENT ON THE SEISMIC PERFORMANCE OF BURIED PIPES

By

Büşra Nur Kılınç

B.S., Civil Engineering, Boğaziçi University, 2021

Submitted to Kandilli Observatory and Earthquake Research Institute

in partial fulfilment of requirements for the degree of

Master of Science

Graduate Program in Earthquake Engineering

Boğaziçi University

2024

# ACKNOWLEDGMENTS

I am profoundly appreciative of my supervisor, Prof. Dr. Ayşe Edincliler, for her priceless guidance throughout my studies. Her deep expertise and broad experience have been a great source of motivation in my academic life.

I would also like to thank my committee members, Doç. Dr. Gülüm Tanırcan and Prof. Dr. Selçuk Toprak for their contributions.

My sincere thanks go to the technicians who assisted me during my experiments in Prof. Dr. Mustafa Erdik Shake Table Laboratory at the Kandilli Observatory and Earthquake Research Institute of Boğaziçi University. I would also like to express my gratitude to Prof. Dr. Gökhan Baykal for his consistent encouragement and guidance throughout my academic research, which has significantly shaped my ideas and direction.

The experimental box used in this thesis is the product of the project supported by Boğaziçi University Research Fund Grant Number BAP14020. I would like to thank Boğaziçi University Scientific Research Projects for their support. I would also like to thank Superlit Company for providing the pipes used in the experiments.

Finally, I would like to express my deepest gratitude to my mother for her tremendous understanding and encouragement throughout my journey. Also, special thanks to V.Efe Kılınç who is a mechanical engineer candidate for his support during my experiments.

# ABSTRACT


## EFFECTS OF GEOSYNTHETIC REINFORCEMENT ON THE SEISMIC PERFORMANCE OF BURIED PIPES

Buried pipelines are critical for transporting water, sewage, gas, and other essential utilities, and their failure during seismic events can lead to significant disruptions and damages. This thesis examines the effect of different geogrid layer arrangements on the seismic behaviour of buried High-Density Polyethylene (HDPE) pipes through a series of shaking table experiments. The study evaluates the effectiveness of different geogrid reinforcement configurations on the seismic performance of the buried pipe. A comprehensive experimental program was conducted, involving 15 shaking table tests under 3 different earthquake motions. Geogrid layers were positioned, and five cases were examined: an unreinforced control case, pipe wrapping with geogrid, two layer of geogrid, three layer of geogrid and four layer of geogrid. The test results demonstrate that geosynthetic reinforcement might improves the seismic performance of buried pipes. In particular, the tests showed that the different geogrid arrangements resulted in varying improvement percentages in the seismic performance of buried pipes. These findings highlight the potential use of geogrids to enhance the seismic performance of buried pipe, offering valuable insights for designing more safe pipe systems in earthquake-prone regions.

# ÖZET

## GEOSENTETİK DONATININ GÖMÜLÜ BORULARIN SİSMİK PERFORMANSI ÜZERİNDEKİ ETKİLERİ

Gömülü boru hatları, su, atık su, gaz ve diğer temel hizmetlerin taşınmasında kritik öneme sahiptir. Bu boruların sismik olaylar sırasında başarısız olması, önemli kesintilere ve hasarlara yol açabilir. Bu tez, gömülü Yüksek Yoğunluklu Polietilen (HDPE) boruların sismik davranışı üzerinde farklı geogrid tabaka düzenlemelerinin etkisini bir dizi sarsma masası deneyleri aracılığıyla incelemektedir. Çalışma, gömülü borunun sismik performansı üzerindeki farklı geogrid takviye konfigürasyonlarının etkinliğini değerlendirmektedir. Üç farklı deprem hareketi altında 15 sarsma masası testi içeren kapsamlı bir deney programı gerçekleştirilmiştir. Geogrid tabakaları stratejik olarak konumlandırılmış ve beş farklı senaryo incelenmiştir: takviye edilmemiş kontrol durumu, geogrid ile boru sarmalama, iki tabaka geogrid, üç tabaka geogrid ve dört tabaka geogrid. Test sonuçları geogrid takviyenin gömülü boruların sismik performansını iyileştirebileceğini göstermektedir. Özellikle, testler farklı geogrid düzenlemelerinin, gömülü boruların sismik performansında farklı iyileşme yüzdeleriyle sonuçlandığını ortaya koymuştur. Bu bulgular, gömülü altyapının yapısal bütünlüğünü artırmak için geosentetiklerin potansiyel kullanımını vurgulamakta ve deprem riski yüksek bölgelerde daha güvenli boru sistemleri tasarlamak için önemli bilgiler sunmaktadır.

# TABLE OF CONTENTS

ACKNOWLEDGMENTS ..... iii

ABSTRACT ..... iv

ÖZET ..... v

TABLE OF CONTENTS ..... vi

LIST OF FIGURES ..... ix

LIST OF TABLES ..... xviii

LIST OF SYMBOLS AND LIST OF ACRONYMS/ABBREVIATIONS ..... xix

1. INTRODUCTION ..... 1

1.1. General ..... 1

1.2. Scope of Investigation ..... 2

1.3. Objectives of the Thesis ..... 3

1.4. Problem Statement ..... 4

1.5. Organization of the Thesis ..... 5

2. LITERATURE REVIEW ..... 6

2.1. Introduction ..... 6

2.2. Geosynthetics ..... 14

2.2.1. Geosynthetics Studies ..... 17

2.3. Studies with Geogrid ..... 27

2.4. Experimental Analyses - Full-Scale Laboratory Testing ..... 28

2.5. Soil-Pipe Interaction ..... 33

2.6. Numerical Studies ..... 40

2.7. Mathematical Modelling ..... 45

3. EXPERIMENTAL PROGRAM ..... 49

3.1. Introduction ..... 49

3.2. Experimental Facility ..... 49
3.2.1. Test equipment ..... 50
3.3. Physical Modelling - Shaking Table Test Program ..... 59
3.3.1. Experimental setup and Sample Preparation ..... 59
3.3.2. Earthquake Motions ..... 64
4. EXPERIMENT RESULTS ..... 66
4.1. Case 1 ..... 67
4.1.1. Acceleration Response ..... 67
4.1.2. Displacement Response ..... 70
4.1.3. Settlement ..... 72
4.2. Case 2 ..... 72
4.2.1. Acceleration Response ..... 72
4.2.2. Displacement Response ..... 75
4.2.3. Settlement ..... 76
4.3. Case 3 ..... 77
4.3.1. Acceleration Response ..... 77
4.3.2. Displacement Response ..... 80
4.3.3. Settlement ..... 81
4.4. Case 4 ..... 82
4.4.1. Acceleration Response ..... 82
4.4.2. Displacement Response ..... 85
4.4.3. Settlement ..... 86
4.5. Case 5 ..... 87
4.5.1. Acceleration Response ..... 87
4.5.2. Displacement Response ..... 90
4.5.3. Settlement ..... 91
5. DISCUSSION AND CONCLUSION ..... 93
5.1. Effect Of Geogrid Arrangement Type ..... 94
5.1.1. Acceleration Response ..... 94
5.1.2. Displacement Response ..... 98

5.1.3. Spectral Acceleration ..... 100
5.1.4. Effect of Geogrid Configuration with Depth ..... 103
5.2. Effect Of Geogrid Layer Number ..... 104
5.2.1. Acceleration Response ..... 105
5.2.2. Displacement Response ..... 108
5.2.3. Spectral Acceleration ..... 111
5.2.4. Effect of Number of Geogrid Layer with Depth ..... 114
5.3. Effects of Earthquake Motions ..... 116
6. CONCLUSIONS ..... 118
REFERENCES ..... 121

# LIST OF FIGURES

Figure 2-1. Full bore rupture due to lateral ground movement, 2017 [4]. ..... 7

Figure 2-2. A rupture in oil pipeline (Garvebhavipalya and Bandepalya off National highway) [4]. ..... 8

Figure 2-3. Wrinkled pipe in Kullar, Izmit during the 1999 Kocaeli Earthquake [7]. ..... 9

Figure 2-4. Pipeline damages in Gurlevik Transmission Line, Adiyaman [10]. ..... 10

Figure 2-5. Buried gas pipeline crimped at the fault [9]. ..... 10

Figure 2-6. Water distribution network and pipeline damage in the Kahramanmaraş earthquake on February 6, 2023 [10]. ..... 11

Figure 2-7. Cross sectional distortion and ovalization and wrinkling of the water transmission pipe in the February 6, 2023, Kahramanmaraş earthquake [11]. ..... 12

Figure 2-8. Cross-sectional details of the full-scale test [18]. ..... 18

Figure 2-9. Protective sand layer with geofoam [20]. ..... 19

Figure 2-10. Test modelling [21]. ..... 20

Figure 2-11. Cross-sectional view illustrating numerical modelling of the EPS cover system [24]..……21

Figure 2-12. Schematic view of test set up [25]. ..... 22

Figure 2-13. Test results for effect of geofoam location on pipe vertical deformation [26]……..... 23

Figure 2-14. Test results for effect of geofoam density on pipe vertical deformation [26]……..... 24

Figure 2-15. Different combinations of pipe and EPC [27]. ..... 24

Figure 2-16. Reinforced arrangements a) horizontal arrangement; b) inverted U arrangement; c) envelope arrangement [28]. ..... 25

Figure 2-17. Different reinforcement arrangements [29]. ..... 27

Figure 2-18. Cross Section of Experiment [44]. ..... 30

Figure 2-19. Reinforcement arrangements: horizontal ground surface [45]. ..... 30

Figure 2-20. Reinforcement arrangements: pipe buried in an embankment [45]. ..... 31

Figure 2-21. Arrangement of geosynthetics [47]. ..... 32

Figure 2-22. Experimental Setup [48]. ..... 33

Figure 2-23. Test configuration [50]. ..... 34

Figure 2-24. Pullout test model [59]. ..... 36

Figure 2-25. Test Setup [64]. ..... 38

Figure 2-26. Experimental Setup [59]. ..... 39

Figure 2-27. Model container and shaking table [65]. ..... 39

Figure 2-28. 3D plot of peak response acceleration ratios with height and input peak acceleration [65]. ..... 40

Figure 2-29. Buried pipeline system in liquefaction zone [68]. ..... 41

Figure 2-30. Soil/structure interaction mechanisms due to waves passage [69] ..... 42

Figure 2-31. Variation of burial depth and spacing of pipes [72]. ..... 43

Figure 2-32. Displacement vs length [72]. ..... 44

Figure 2-33. FEM model [67]. ..... 45

Figure 2-34. Mathematical theory of loads on Pipe [57]. ..... 47

Figure 3-1. Shaking Table at KOERI. ..... 50

Figure 3-2. The Test Box Used in Pullout and Shaking Table Performance Tests ..... 51

Figure 3-3. Soil box front view and side view with dimensions (mm). ..... 51

Figure 3-4. Compaction of sand. ..... 52

Figure 3-5. The grain size distribution of Silivri Sand. ..... 53

Figure 3-6. Pipe Dimensions. ..... 54

Figure 3-7. Geogrid used in the experiments. ..... 55

Figure 3-8. Accelerometers and LVDT arrangement front view of box. ..... 57

Figure 3-9. Side View of Box with Accelerometer Arrangement. ..... 57

Figure 3-10. Top View of Box with Accelerometer Arrangement. ..... 58

Figure 3-11. Accelerometers, A12, A13, A14, A15 and A16 on the sand. ..... 58

Figure 3-12. Experimental model for Case 1. ..... 60

Figure 3-13. Geogrid arrangement for Case 2. ..... 61

Figure 3-14. Experimental model for Case 2. ..... 61

Figure 3-15. Experimental model for Case 3. ..... 62

Figure 3-16. Geogrid layers placement for Case 3. ..... 62

Figure 3-17. Experimental model for Case 4. ..... 63

Figure 3-18. Geogrid layers placement for CASE 4. ..... 63

Figure 3-19. Experimental model for Case 5. ..... 64

Figure 3-20. Kocaeli Earthquake input motion acceleration-time history [77]. ..... 65

Figure 3-21. El-Centro Earthquake input motion acceleration-time history [77]. ..... 65

Figure 3-22. Kobe Earthquake input motion acceleration-time history [77]. ..... 65

Figure 4-1. CASE 1: Time-history, Fourier amplitude spectrum, response spectrum graphs for A14 under all Earthquake motions. ..... 68

Figure 4-2. CASE 1: Time-history, Fourier amplitude spectrum, response spectrum graphs for A7 under all Earthquake motions. ..... 69

Figure 4-3. CASE 1: Time-history, Fourier amplitude spectrum, response spectrum graphs for A1 under all Earthquake motions. ..... 70

Figure 4-4. CASE 1: The displacement measurements of D20 under all Earthquake motions……..... 71

Figure 4-5. CASE 1: The displacement measurements of D17 under all Earthquake motions……71

Figure 4-6. CASE 1: The displacement measurements of D19 under all Earthquake motions……72

Figure 4-7. CASE 2: Time-history, Fourier amplitude spectrum, response spectrum graphs for A14 under all Earthquake motions. ..... 73

Figure 4-8. CASE 2: Time-history, Fourier amplitude spectrum, response spectrum graphs for A7 under all Earthquake motions. ..... 74

Figure 4-9. CASE 2: Time-history, Fourier amplitude spectrum, response spectrum graphs (A1) for all Earthquake motions. ..... 75

Figure 4-10. CASE 2: The displacement measurements of D17 under all Earthquake Motions……76

Figure 4-11. CASE 2: The displacement measurements of D20 under all Earthquake Motions……76

Figure 4-12. CASE 2: The displacement measurements of D19 under all Earthquake Motions……77

Figure 4-13. CASE 3: Time-history, Fourier amplitude spectrum, response spectrum graphs for A14 under all Earthquake motions. ..... 78

Figure 4-14. CASE 3: Time-history, Fourier amplitude spectrum, response spectrum graphs for A7 under all Earthquake motions. ..... 79

Figure 4-15. CASE 3: Time-history, Fourier amplitude spectrum, response spectrum graphs (A1) for all Earthquake motions. ..... 80

Figure 4-16. CASE 3: The displacement measurements of D17 under all earthquake motions……80

Figure 4-17. CASE 3: The displacement measurements of D20 under all earthquake motions……81

Figure 4-18. CASE 3: The displacement measurements of D19 under all earthquake motions……81

Figure 4-19. CASE 4: Time-history, Fourier amplitude spectrum, response spectrum graphs for A14 under all earthquake motions. ..... 83

Figure 4-20. CASE 4: Time-history, Fourier amplitude spectrum, response spectrum graphs for A7 under all earthquake motions. ..... 84

Figure 4-21. CASE 4: Time-history, Fourier amplitude spectrum, response spectrum graphs (A1) for all earthquake motions. ..... 85

Figure 4-22. CASE 4: The displacement measurements of D17 under all Earthquake Motions……86

Figure 4-23. CASE 4: The displacement measurements of D20 under all Earthquake Motions……86

Figure 4-24. CASE 4: The displacement measurements of D19 under all Earthquake Motions……87

Figure 4-25. CASE 5: Time-history, Fourier amplitude spectrum, response spectrum graphs for A14 under all Earthquake motions. ..... 88

Figure 4-26. CASE 5: Time-history, Fourier amplitude spectrum, response spectrum graphs for A7 under all Earthquake motions. ..... 89

Figure 4-27. CASE 5: Time-history, Fourier amplitude spectrum, response spectrum graphs for A1 under all Earthquake motions. ..... 90

Figure 4-28. CASE 5: The displacement measurements of D17 under all Earthquake Motions……91

Figure 4-29. CASE 5: The displacement measurements of D20 under all Earthquake Motions……91

Figure 4-30. CASE 5: The vertical displacement measurements of D19 under all Earthquake Motions. ..... 92

Figure 5-1. Time history for Case 2 (on pipe) under Kocaeli Earthquake (Iznik station)……95

Figure 5-2. Time history for Case 3 (on pipe) under Kocaeli Earthquake motion (Iznik station)……95

Figure 5-3. Time history for Case 2 (on pipe) under El-Centro Earthquake motion (Imperial Valley station). ..... 95

Figure 5-4. Time history for Case 3 (on pipe) under El-Centro Earthquake motion (Imperial Valley station). ..... 96

Figure 5-5. Time history for Case 2 (close to surface) under Kocaeli Earthquake motion (Iznik station). ..... 96

Figure 5-6. Time history for Case 3 (close to surface) under Kocaeli Earthquake motion (Iznik station). ..... 97

Figure 5-7. Time history for Case 2 (close to surface) under El-Centro Earthquake motion (Imperial Valley station)..... 97

Figure 5-8. Time history for Case 3 (close to surface) under El-Centro Earthquake motion (Imperial Valley station)..... 98

Figure 5-9. Maximum horizontal pipe displacements for Case 1, Case 2, and Case 3 under El-Centro Earthquake motion. ..... 99

Figure 5-10. Maximum horizontal pipe displacement for Case 1, Case 2, and Case 3 under Kobe Earthquake motion. ..... 100

Figure 5-11. Response spectrum for A14 (close to surface), Case 1 under Kocaeli Earthquake motion. ..... 101

Figure 5-12. Response spectrum for A14 (close to surface), Case 2 under Kocaeli Earthquake motion. ..... 101

Figure 5-13. Response spectrum for A14 (close to surface), Case 3 under Kocaeli Earthquake motion. ..... 101

Figure 5-14. Response spectrum for A7 (on pipe), Case 1 under Kobe Earthquake motion……102

Figure 5-15. Response spectrum for A7 (on pipe), Case 2 under Kobe Earthquake.... 102

Figure 5-16. Response spectrum for A7 (on pipe), Case 3 under Kobe Earthquake.... 103

Figure 5-17. Variation of acceleration with depth under El-Centro Earthquake motion for Case 1, Case 2 and Case 3..... 104

Figure 5-18. Case 3 - Time history for A14 (close to surface) under Kocaeli Earthquake motion (Iznik station)..... 105

Figure 5-19. Case 4 - Time history for A14 (close to surface) under Kocaeli Earthquake motion (Iznik station)..... 105

Figure 5-20 .Case 5 - Time history for A14 (close to surface) under Kocaeli Earthquake motion (Iznik station)..... 106

Figure 5-21. Time history for A14 (close to surface) under El-Centro Earthquake motion (Imperial Valley station) for Case 3. ..... 106

Figure 5-22. Time history for A14 (close to surface) under El-Centro Earthquake motion (Imperial Valley station) for Case 4. ..... 107

Figure 5-23. Time history for A14 (close to surface) under El-Centro Earthquake motion (Imperial Valley station) for Case 5. ..... 107

Figure 5-24. Time history for A14 (close to surface) under Kobe Earthquake motion (KJMA station) for Case 3. ..... 108

Figure 5-25 Time history for A14 (close to surface) under Kobe Earthquake motion (KJMA station) for Case 4. ..... 108

Figure 5-26. Time history for A14 (close to surface) under Kobe Earthquake motion (KJMA station) for Case 5. ..... 108

Figure 5-27. Maximum horizontal pipe displacement at D20 for Case 1, Case 3, Case 4, and Case 5 under Kobe Earthquake motion. ..... 109

Figure 5-28. Comparison of maximum horizontal pipe displacement at D20 for Case 1, Case 3, Case 4, and Case 5 under El-Centro Earthquake motion. ..... 110

Figure 5-29. Response spectrum for A7 (on pipe), Case 3 under Kocaeli Earthquake motion……112

Figure 5-30. Response spectrum for A7 (on pipe), Case 4 under Kocaeli Earthquake motion……112

Figure 5-31. Response spectrum for A7 (on pipe), Case 5 under Kocaeli Earthquake motion……112

Figure 5-32. Response spectrum for A7 (on pipe), Case 3 under Kobe Earthquake motion……113

Figure 5-33. Response spectrum for A7 (on pipe), Case 4 under Kobe Earthquake motion……114

Figure 5-34. Response spectrum for A7 (on pipe), Case 5 under Kobe Earthquake motion……114

Figure 5-35. Variation of maximum acceleration with depth under El-Centro Earthquake motion for Case 1, Case 3, Case 4, and Case 5. ..... 115

Figure 5-36 Acceleration improvement percentage for all cases under all earthquake motions (A14). ..... 117

# LIST OF TABLES

Table 2-1. Literature Review Main Topics. ..... 13

Table 3-1. Soil properties ..... 53

Table 3-2. Pipe properties. ..... 55

Table 3-3. Details of accelerometer locations. ..... 56

Table 3-4. Details of LVDTs and potentiometer locations. ..... 59

Table 3-5 Summary of Cases ..... 60

Table 3-6. Earthquake motions selected for this study. ..... 64

# LIST OF SYMBOLS AND LIST OF ACRONYMS/ABBREVIATIONS

| | |
|---|---|
| a | Acceleration |
| A | Accelerometer |
| f | Frequency |
| E | Young's modulus |
| Sa | Spectral acceleration |
| t | Thickness |
| Cc | The Coefficient of Uniformity |
| Cu | The Coefficient of Curvature |
| SP | Poorly Graded Sand |
| Hz | Hertz |
| ρ | Density of the backfill soil |
| ν | Poisson's ratio |
| PGA | Peak ground acceleration |

| | |
|---|---|
| FEM | Finite element model |
| EPS | Expanded Polystyrene |
| FLAC | Fast Lagrangian Analysis of Continua |
| USCS | United Soil Classification System |
| 2D | Two dimensional |

# 1. INTRODUCTION

## 1.1. General

Pipes have an important role in the transportation of liquid or gaseous materials. Energy resources like oil and natural gas, drinking water, wastewater, and sewage are examples of transported substances. It is also defined as a lifeline due to the importance of the material it carries. Pipeline transportation is the most preferred transportation method because it is a more economical, energy-efficient, environmentally friendly, reliable, and convenient method than the other modes of transportation like intermodal transportation and package carriers. The pipes are buried considering some aesthetic concerns, economic situation, and environmental effects. However, buried pipes are significantly affected by ground motion and seismic waves caused by earthquakes. Therefore, seismic design is extremely important as buried pipes extend for kilometres underground, because these carry dangerous liquids with explosive properties such as oil and natural gas [1].

Pipes are exposed to dynamic loads like earthquakes and static loads like traffic loads. In this thesis, seismic motions are considered. Fault movement, seismic waves formed by energy discharge under the ground, and liquefaction cause rupture and cracking in pipes. These effects differ according to length, diameter, pipe material properties, and soil properties. Considering all these effects, it is important to offer a solution after examining the behaviour of pipes under dynamic loads.

Buried pipelines can be divided into two main categories by considering the connection type; these are the continuous and segmented pipes. Depending on the material they carry, pipes can be placed under the ground. Connection type is one of the most important parameters of seismic design. Segmented type of pipe means welded pipes. According to past earthquakes, segmented pipes are more vulnerable to seismic waves than continuous pipes because welding reduces the strength of the pipe.

Pipes can be categorized as rigid or flexible based on the material from which they are produced. Steel, iron, and concrete pipes are defined as rigid, while polyethylene pipes are defined as flexible. Pipes which play an important role in the transport of liquid and gaseous materials used to be made of cast iron, both for the dangerous materials they carry and for various economic reasons. Nowadays, rigid pipes have been replaced by more flexible HDPE pipes. Recently, the use of flexible pipes has become more popular than the use of rigid pipes. The biggest reasons for the widespread use of flexible pipe are that they have more advantageous characteristics and material properties such as corrosion resistance, chemical resistance, light weight, flexibility, long-term tensile strength, watertight joints, abrasion–wear resistance, impact strength, hydraulic efficiency, longer lengths, water quality, thermal insulation, flame resistance, cost efficiency, environmental benefit [2].

The expectations from geogrid reinforcement focus on enhancing soil stability and minimizing seismic risks. Geogrids are expected to improve soil-structure interaction, reduce horizontal deformations, and increase the soil's load-bearing capacity. Additionally, they help distribute seismic forces more evenly, reducing stress on structures like pipelines, especially at critical points such as the pipe crown. Geogrids also mitigate the risk of liquefaction, stabilize soil layers during seismic events, and ultimately lower the seismic vulnerability of infrastructure [3].

## 1.2. Scope of Investigation

This thesis examines the effect of different geogrid layer arrangements on the seismic behaviour of buried pipes through a series of shaking table experiments. To achieve the objectives of the thesis, five cases were analysed with varying configurations of geogrid placement. The control case, referred to as Case 1, was conducted without the use of geosynthetics, while the other cases involved geogrid applications. Case 2 involved wrapping the pipe with geogrid, and Cases 3, 4, and 5 involved placing different numbers of geogrid layers as follows:

- CASE 1: Without any geogrid (Control Case).
- CASE 2: Wrapping the pipe with geogrid.
- CASE 3: Placing one layer of geogrid under the pipe and one layer above the pipe.
- CASE 4: Placing one layer of geogrid under the pipe and two layers above the pipe.
- CASE 5: Placing one layer of geogrid under the pipe and three layers above the pipe.

By comparing the results of these experiments, the effectiveness of using geosynthetics in improving the seismic performance of buried pipes was evaluated.

The experimental design involved creating controlled seismic loading conditions to simulate real earthquake scenarios. Various seismic motions were applied to assess their impact on the buried pipes. The materials used, including the specific types of geosynthetics and the properties of the pipe and surrounding soil, were carefully selected to ensure reliable results.

## 1.3. Objectives of the Thesis

This thesis focuses on the seismic performance of buried pipes and examines the effect of geogrid reinforcement arrangement types. The impact of different geogrid layer arrangements on the pipes' behaviour during earthquake motions was determined through a series of shaking table tests. The effectiveness of each geogrid configuration was assessed by comparing the test results, and the best configuration was identified from the cases analysed in this thesis. Full-scale physical experiments were conducted to identify the performance of the buried pipe under earthquake motions.

## 1.4. Problem Statement

Buried pipelines are critical components of urban infrastructure, responsible for transporting water, sewage, gas, and other essential utilities. Despite their importance, these pipelines are vulnerable to seismic events, which can lead to significant damage and disruptions in service. Earthquakes impose complex dynamic loads on buried pipes, causing stress and strain that can result in deformation, cracking, or even complete failure of the pipeline system.

One of the primary challenges in ensuring the resilience of buried pipelines is understanding their behaviour under seismic loading conditions. Traditional methods of pipeline construction may not adequately address the demands imposed by such events. Therefore, there is a need for solutions that can enhance the seismic performance of these systems.

Geosynthetics, such as geotextiles and geogrids, have emerged as potential materials for improving the seismic performance of buried pipes. These materials can reinforce the soil surrounding the pipeline, providing additional support and stability. However, the effectiveness of geosynthetics in mitigating seismic damage to buried pipes remains an area of research.

This thesis addresses the effectiveness of geogrid reinforcement by investigating the geogrid arrangement and the number of geogrid layers on the seismic performance of buried pipes. By conducting the full-scale physical experiments, the study aims to provide a comprehensive understanding of how geosynthetics can enhance the behaviour of buried pipelines during seismic events. The findings are expected to advance the design of safer and more reliable infrastructure systems, thereby enhancing resilience in communities that depend on these essential services.

## 1.5. Organization of the Thesis

This thesis is organized into six chapters. Chapter 1 provides an introduction and overview of the study. Chapter 2 presents a comprehensive literature review. Chapter 3 represents the experimental. Chapter 4 focuses on results of shaking table experiments. Finally, Chapter 5 presents the discussion and conclusion of the test results.

# 2. LITERATURE REVIEW

## 2.1. Introduction

This chapter includes the previous studies of geotechnical improvement of buried pipes with and without using geosynthetics. This chapter aims to review past studies for further research on the seismic performance of buried pipes.

With increasing urbanization, the importance of infrastructure facilities has also increased. The population density caused by urbanization leads to increase pipe capacity. Therefore, the effects of the earthquake motion should be taken into consideration while the pipes are being designed and placed. Also, it is necessary to pay attention to the improvement of the underground structures so that the ground movements do not affect daily life negatively. Recent theoretical and physical studies have also enabled us to observe the behaviour of buried pipes under earthquakes.

There are many studies about pipes in literature. This study focuses on buried pipes. Buried pipes are also divided into two main categories, that is, segmented and continuous pipes. Within the scope of this study, literature was reviewed considering the continuous buried pipes.

Examination of the infrastructure facilities falls within the field of geotechnical earthquake engineering and there are few studies on the research topic. When an earthquake disaster is considered, the first thing that comes to mind is superstructures. For this reason, the behaviour of the superstructures under earthquakes has been investigated by many scientists. However, when the past earthquakes are examined, it is seen that the earthquake also caused serious damage to the infrastructure. With the increasing population and urbanization, the economic and sociological damages caused by the earthquake have increased because the use of buried pipes carrying explosive or flammable fluids has also increased to meet the population's energy needs [5]. Figure 2-1 and Figure 2-2 show the bore rupture of oil pipes. There are numerous reports of these pipeline case studies



Figure 2-1. Full bore rupture due to lateral ground movement, 2017 [4].

Buried pipes are greatly affected by earthquakes and events caused by earthquake like fault movement, landslide, ground squeeze, and liquefaction. Earthquakes pave the way for expansion, and toxic and hazardous materials are released. Seismic hazards effects on the buried structures are permanent ground deformations, liquefactions, and fault rupture [1]. On the other hand, joint failure, cracking, and buckling are the common failure types of pipeline systems. There have been many earthquakes throughout history that have caused damage to buried pipes (Figure 2-2).

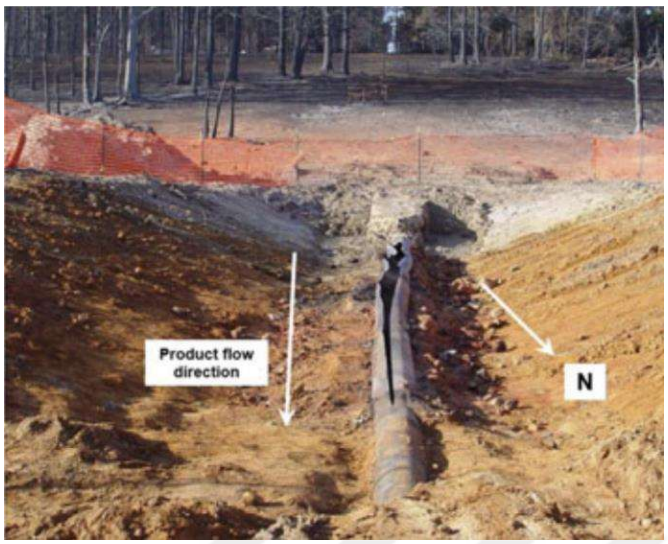



Figure 2-2. A rupture in oil pipeline (Garvebhavipalya and Bandepalya off National highway) [4].

The 1989 Loma Prieta earthquake in California, which caused widespread damage to roads, bridges, and pipelines in the San Francisco Bay Area. The 2011 Tohoku earthquake and tsunami in Japan caused extensive damage to the country's infrastructure, including pipelines and nuclear power plants. The 2010 Haiti earthquake, which devastated the country's infrastructure, including roads, bridges, and pipelines. The 1994 Northridge earthquake in California, which caused significant damage to roads, bridges, and pipelines in the Los Angeles area. The 2003 Bam earthquake in Iran, which caused widespread damage to the city's infrastructure, including pipelines and water systems. Tennant Creek (1999), Kocaeli (1999) and Chi-Chi earthquakes seem to have serious effects on buried pipes. The Tennant earthquake with a magnitude of 6.3 caused warping on buried pipes. The Kocaeli earthquake, with a magnitude of 6.6 Mw, caused the pipe to wrinkle, as shown in Figure 2-3 [6].



Figure 2-3. Wrinkled pipe in Kullar, Izmit during the 1999 Kocaeli Earthquake [7].

The 1964 Alaska earthquake caused more than 200 breaks on the gas pipe due to the landslides and ground cracking. The 1971 Fernando earthquake provoked the loss of water and pipe transportation services because of the pipe breaking due to liquefaction. The 1987 Ecuador earthquake caused the largest economic loss on pipes in history [6].

Hyoken -Nanbu earthquake poses considerable damage to the underground tunnels at Kobe in Japan. Many infrastructures were damaged in the Tohoku-Japan earthquake on March 11, 2011. The main reason for this is liquefaction as a result of the seismic motions. The water and sewer systems were severely damaged [8].



Figure 2-4. Pipeline damages in Gurlevik Transmission Line, Adiyaman [10].



Figure 2-5. Buried gas pipeline crimped at the fault [9].

The February 6, 2023, Kahramanmaraş earthquakes, with magnitudes of Mw 7.7 and Mw 7.6, caused significant damage to infrastructure across 13 provinces in Turkey, affecting over 14 million people. Buried utilities, including water, wastewater, and oil-gas pipelines, were extensively damaged. This led to disruptions in oil & gas and water supply by impacting over 14 million residents. In Gaziantep, critical damage to the Kartalkaya Water Transmission Line and the Düzbağ transmission line caused significant disruptions in water supply. Kahramanmaraş encountered severe damage in its water distribution system. In Adıyaman Province's Gurlevik transmission line, older steel pipes suffered tensile fractures, while newer ductile iron pipes remained intact. Following the earthquakes, Hatay Province undertook extensive reconstruction efforts, installing over 126 kilometers of new drinking water networks and 50 kilometers of wastewater lines. Gas pipelines, especially those supplying Kahramanmaraş, Gaziantep, and Hatay Provinces, sustained significant damage, resulting in temporary gas supply interruptions. Addressing and mitigating pipeline vulnerabilities is essential to enhancing the resilience of lifeline systems in the future [10].



Figure 2-6. Water distribution network and pipeline damage in the Kahramanmaraş earthquake on February 6, 2023 [10].



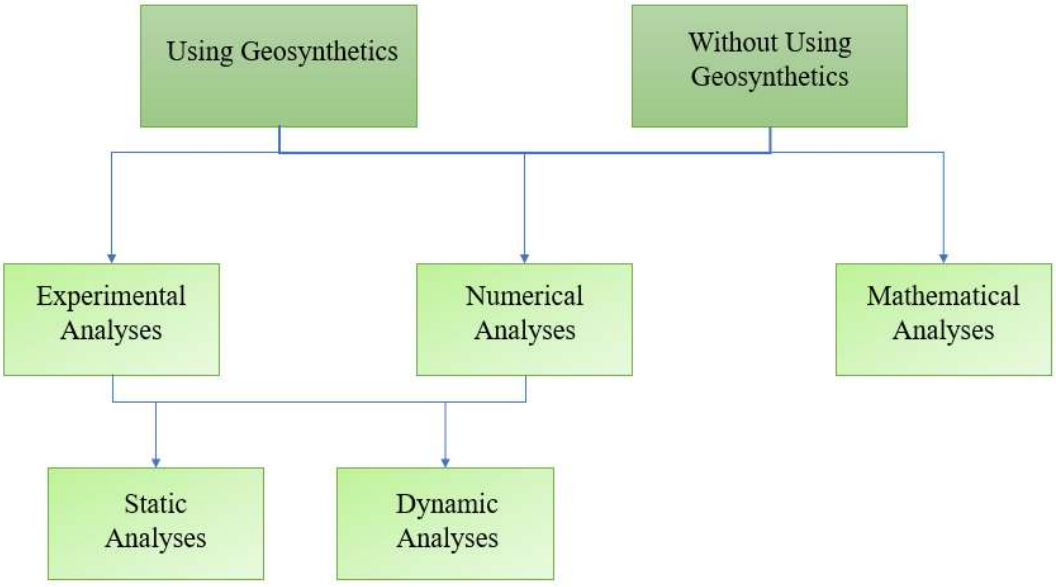
Figure 2-7. Cross sectional distortion and ovalization and wrinkling of the water transmission pipe in the February 6, 2023, Kahramanmaraş earthquake [11].

Due to the importance of the materials carried by the pipe, pipes designed to be buried underground for protection must be able to withstand both static and dynamic loads. So, geotechnical design is essential to define the soil and pipe interaction. While traffic loads, the weight of the buildings and similar structures on the pipeline system act as static loads, ground movements, swelling, and shrinkage act as dynamic loads. So, it is important to make improvements to buried pipes.

To protect the pipe trench against external static-dynamic loads, and soil pressure ground improvement methods have been applied. Some of the improvement methods of the buried pipe are the use of geosynthetics and a mixture of waste tire – sand and, sand granulated rubber mixture. Mitigation methods for buried pipes against failure can be examined in 5 categories. These are seismic design, reducing pipeline loading, changing pipeline configuration, and ground improvement. It is also important to perform kinematic interaction analysis to investigate the interaction between the soil and pipe and, to apply the mentioned methods.

In this thesis, the improvements of the buried pipes using geosynthetics by conducting series of shaking table tests. In this regard, the literature review is addressed in many ways. The main topic is the selection of improvement techniques. So, the literature review was done according to the studies using geosynthetics and without using it. Static analyses, dynamic analyses, mathematical and numeric modelling and experimental modelling techniques has also been included in the literature review. These are summarized as Table 2-1 that includes the titles of the studies in the literature and their relations with each other.

Table 2-1. Literature Review Main Topics.




Buried pipes have been addressed in many ways:

- Soil-pipe interaction
- Static analyses of buried pipelines
- Dynamic analyses of buried pipelines.
- Geotechnical improvement of the pipe trench
- Full-scale laboratory testing
- Mathematical modelling

Soil pipe interaction includes the soil-pipe interface research topics like soil pipe interface shear strength. Dynamic analyses include the stress analyses of pipe which exposed to geohazards. Geohazards includes to soil heave, lateral spreading, slope failure, liquefaction, and fault movement. Also, different studies have been carried out to improve the seismic performance of pipes. Geosynthetic as well as waste tire chips and fibre materials can be given as examples, but this thesis focuses on studies with geosynthetics.

## 2.2. Geosynthetics

Geosynthetics are engineered materials made from polymeric substances (such as polyethylene, polypropylene, or polyvinyl chloride) used in geotechnical and construction engineering. Geosynthetics can be used many different areas in geotechnical applications. It can be classified as mechanical, and hydraulic in terms of their functions. Filtration, drainage, barrier, erosion control and containment can be given as example of hydraulic functions. Separation, soil reinforcement, stabilization, containment, protection, and stress relief can be also as an example of the mechanical functions. In addition, geosynthetics have been used by many researchers to prevent the failure of buried structures against dynamic or static forces. Examples of geosynthetics include geotextiles, geogrids, geonets, geomembranes, geosynthetic clay liners, and geo-composites.

Types of Geosynthetics [12]:

- Geotextiles: These are permeable fabrics that, when used in association with soil, can separate, filter, reinforce, protect, or drain. They are typically made from polypropylene or polyester and come in two forms: Woven Geotextiles: Made by weaving fibers together, these are strong and durable, often used for reinforcement purposes. Non-Woven Geotextiles: Made by bonding fibers together (mechanically, chemically, or thermally), these are used for separation, filtration, and drainage. Overall, the choice between woven and non-woven geosynthetics depends on the specific application and the desired properties, such as tensile strength, permeability, filtration, and more.

- Geomembranes: These are impermeable membranes used for containment and environmental protection applications, such as liners for landfills, ponds, and canals.

- Geonets: These are net-like structures used for drainage purposes, providing a path for fluids to flow through.

- Geocomposites: These are hybrid materials combining the functions of geotextiles, geogrids, geonets, and/or geomembranes to perform multiple functions, such as drainage and reinforcement.

- Geocells: These are three-dimensional, honeycomb-like structures used for soil stabilization and erosion control.

- Geogrids: These are grid-like structures used primarily for reinforcement. They improve the structural integrity of soils and are commonly used in road construction and embankments.

Applications in Civil and Geotechnical Engineering [13]:

- Reinforcement: Geosynthetics are used to reinforce soils in applications such as retaining walls, steep slopes, and embankments. Woven geotextiles and geogrids are particularly useful for this purpose.

- Separation: Geotextiles are placed between different soil layers to prevent mixing and to maintain the integrity of each layer. This is crucial in road construction, where a layer of geotextile can prevent the mixing of subgrade and aggregate layers.

- Filtration: Non-woven geotextiles are often used to filter soil particles while allowing water to pass through. This application is common in drainage systems, where geotextiles prevent soil from clogging drainage pipes or channels.

- Drainage: Geonets and geocomposites are used to provide efficient drainage systems in landfills, roadways, and retaining walls, ensuring that water is effectively managed and does not cause structural problems.

- Containment: Geomembranes are used to line landfills, ponds, and canals, preventing the leakage of hazardous materials into the environment.

- Erosion Control: Geocells and geotextiles are used to prevent soil erosion on slopes, riverbanks, and coastal areas by providing a stable surface that resists the forces of wind and water.

Geogrids have been used in this thesis due to their significant benefits in soil reinforcement and stabilization. In geotechnical engineering, geogrids play a crucial role in enhancing the structural integrity of various constructions. Their open grid structure allows for effective interaction with the surrounding soil, creating a composite material with superior load-bearing capacity.

In road construction, geogrids reinforce the base and subbase layers, distributing loads more evenly and preventing rutting, which results in longer-lasting and more durable roadways, thus reducing maintenance costs over time. For retaining walls, geogrids reinforce the soil behind the walls, allowing for higher and steeper constructions by reducing lateral pressure and preventing wall failure. In projects involving embankments on weak or soft soils, geogrids provide a stable foundation by spreading the load over a larger area, reducing differential settlement, which is essential for the stability and safety of the structure.

Geogrids are also critical in stabilizing slopes, preventing landslides and erosion by reinforcing the soil and allowing for steeper slopes without extensive earthworks. This is particularly important in mountainous or hilly terrain. In railway construction, geogrids reinforce the ballast and sub-ballast layers, improving load distribution and reducing deformation, leading to more stable tracks and reduced maintenance costs.

The importance of geogrids in geotechnical engineering cannot be overstated. They significantly enhance the load-bearing capacity of soils, making them indispensable for projects requiring robust soil reinforcement. Geogrids also offer cost efficiency by reducing the need for additional fill materials and extensive earthworks, leading to overall savings in construction projects. Their environmental benefits include minimizing the need for excavation and the use of natural resources, contributing to more sustainable construction practices. Geotechnical structures reinforced with geogrids exhibit improved performance and durability, leading to longer service life and reduced maintenance requirements. Overall, geogrids are a vital component in modern geotechnical engineering, providing effective solutions for soil stabilization and reinforcement across a wide range of applications [13].

### 2.2.1. Geosynthetics Studies

James Mitchell's "Kettleman Hills waste landfill slope failure" is among the earliest projects on this topic. They looked on the low friction interface between geosynthetics and clays for stability studies. The development of geosynthetic research benefited greatly from the study by Mitchell et al. (1990). The most crucial contact between high density geomembrane and soil is identified utilizing a pull-out and direct shear test [14].

In 1996, Koerner was one of the first to investigate the usage of geosynthetics in pipes and tunnels. It has been demonstrated that geosynthetics are crucial to pipeline improvement, and remediation, covering pipes greater than 100 mm (4 in) in diameter into shipping tunnel [15]. Then, many researchers have conducted experimental studies on buried pipes. As a result of the studies, it has been realized that buried pipes are also vulnerable to both static and dynamic forces, which are suitable for displacement at least as much as the ground.

Some methods have been developed to reduce soil pressure on pipes and to protect them against dynamic loads. The most widely used examples of these are the improvement methods made with geosynthetics such as geofoam and geocell. Apart from these, the

mixture of waste rubber sand also increases the shear strength of the soil and makes a significant contribution to the pipe-soil interaction.

Geofoam, which is a geosynthetic improvement method, has been used in many studies in the literature. Geofoam, which is widely used in buried structures such as pipes and retaining walls, has generally been studied in the literature under static loading. It can be used to minimize the effect of static loads such as traffic loads on buried pipes by examining the effect of these loads on the pipe. Selvadurai (1989) pioneered the improvement of pipes with geosynthetics through his work. Geogrid was used on the concrete pipe to improve the uplift capacity in the pipes [16]. In later studies, the use of geocell and geofoam in addition to geogrid has become widespread. Khalaj et al (2017) investigated the behaviour of polyethylene pipe under static load using a non-woven geosynthetic - geocell. [17]

Kim (2010) investigated horizontal and vertical earth pressure by placing EPC protection just above the pipe and 1 m above the pipe as Figure 2-8 [18].

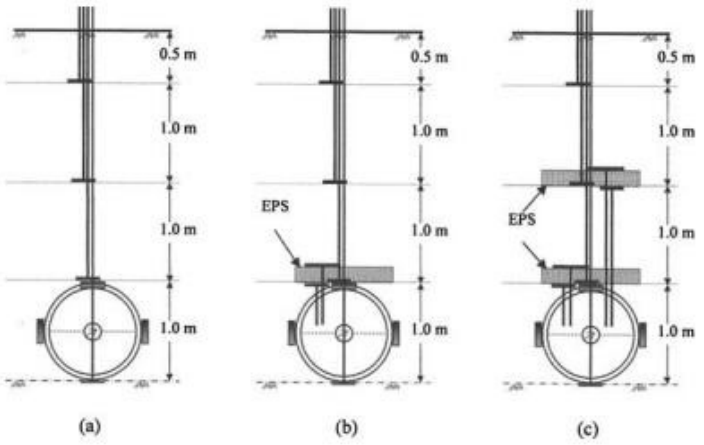



Figure 2-8. Cross-sectional details of the full-scale test [18].

The following study by Corey (2014), includes four large-scale static plate loading tests performed in a laboratory environment. The focus of the study was to investigate the effects of loads placed on 0.61 m diameter steel reinforced HDPE pipes, including pipe

deflection, soil pressure, pipe stress, and surface collapse. The study also investigated the effect of the presence or absence of geogrid reinforcement on sand in the tests. An important finding is that geogrid reinforcement reduces the longitudinal tensile stresses in the plastic shell of the pipe. Also, it enables to reduce lateral and shear stresses induced by the surface loads at the interface between the soil and pipe [19].

Anıl et al. (2012) placed 50 mm and 30mm thick geofoam on steel composite pipe and performed a drop test with impact force as shown in the Figure 2-9 [20].



Figure 2-9. Protective sand layer with geofoam [20].

Witthoef et al. (2008) examined geofoam improvements numerically by placing EPS of different lengths and thicknesses in a system as follows. The studies were done in the finite element programs, FLAC as seen in Figure 2-10 [21].

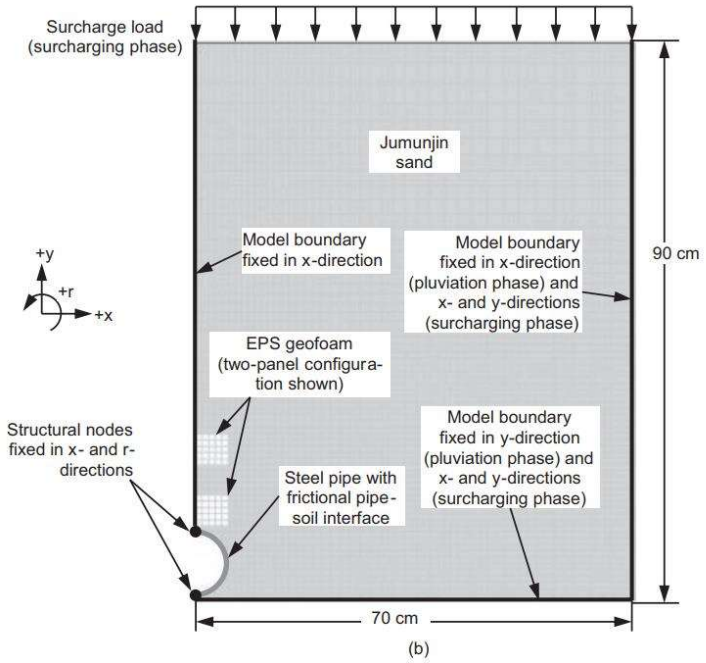



Figure 2-10. Test modelling [21].

Although there are few studies using geofoam in dynamic studies, there are no shaking table tests on pipes. Bathurst et al. (2007) used geofoam in the construction of rigid retaining walls to reduce the effect of dynamic loads. Laboratory tests were carried out by constructing a 1 m retaining wall on the shaking table. The dynamic forces were compared with the improved and unimproved test results, and a maximum reduction of 31% was observed at an acceleration of 0.7g [22].

An example of the use of geofoam in culverts, which is another underground structure, was given by Wang et al. (2021). According to the results obtained in field tests with 2 different thicknesses of geofoam and different types of sand, it was seen that geofoam helped to reduce the stress on the embedded concrete culvert. However, since the geofoam with higher density can be compressed less than the one with lower density, it has been concluded that it creates a second arc on the culvert by transferring stress [23].

Bartlett and Lingwall (2015), who conducted field tests and numerical studies to examine the effect of permanent displacements on the buried pipe and to prevent

deformations, used geofoam to create seismic resistance. In this study conducted at the University of Utah, the response of a buried steel pipe to permanent ground deformations such as faulting, liquefaction and settlement was investigated. The EPS was placed on the sliding part of the fault and the "peak uplift force" was examined according to the situation before it was placed as shown in Figure 2-11. As a result of the experiment, it was concluded that the test using geofoam required more displacement to reach the same peak uplift force and showed 10 times less rigidity than the vertical spring constant. The experiment was conducted using ductile steel pipeline. It was observed that EPS reduces bending and shear stress. EPS reduced the uplift force by 4 times and the displacement due to uplift was reduced by 2.75 times [24]. Beju (2017) used EPS geofoam and fly ash together by establishing a setup as shown in Figure 2-12 [25].

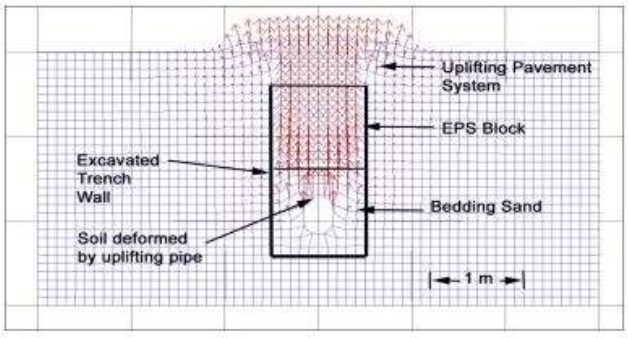



Figure 2-11. Cross-sectional view illustrating numerical modelling of the EPS cover system [24].

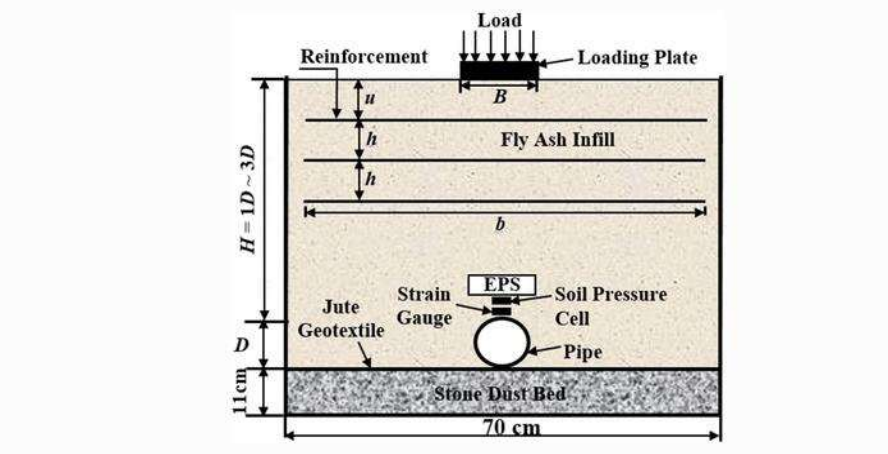



Figure 2-12. Schematic view of test set up [25].

The effect of geofoam location and density on the improvement of buried flexible pipes was investigated. Physical tests were conducted using a 1 m x 1 m x 0.6 m box, with a PVC pipe of 20 cm diameter used in the project. The pipe had an outer diameter of 200 mm, a wall thickness of 3.9 mm, and a length of 90 cm. The pipe stiffness was calculated as 1.68 MPa through a parallel plate load test conducted according to ASTM D-2412 [26].

Two different densities of geofoam were utilized, and the geofoams were placed at different depths above the pipe crown at 0 cm, 5 cm, and 10 cm for comparison. Geofoam creates a compressible zone over the pipe, which promotes soil arching and transfers the load above the pipe to the surrounding soil.

For the location effect, EPS geofoam plates with a density of 14.3 kg/m$^3$ and a thickness of 4cm were used. For the density effect, 2 cm-thick plates with densities of 16.3 kg/m$^3$ and 28 kg/m$^3$ were used in the experiments. The tests were conducted in a laminar box, with static loading applied on the sand using a 26 cm-diameter steel plate. Pneumatic load cells and two dial gauges were used for settlement measurements. A total of six experiments were performed.

The results showed that placing the geofoam 5 m above the pipe crown provided better improvement compared to placing it 10 m above. This suggests that having the geofoam closer to the pipe yields more effective results.

The vertical stress above the geofoam was calculated using the 2:1 method. It was observed that the geofoam with lower density, which is more compressible (14.3 kg/m$^3$), yielded more effective results, achieving improvements of approximately 300kPa. However, for higher load levels, the geofoam with a density of 28 kg/m$^3$ performed more effectively, providing improvement up to approximately 550kPa. Therefore, the effectiveness of the geofoam depends on the applied load level.

EPS (expanded polystyrene) foam becomes less significant after failure, rendering its location less important. When dealing with higher stress ranges, it is preferable to use a denser geofoam. Conversely, under lower stress levels, a lighter geofoam performs better as shown in Figure 2-13 and Figure 2-14 [26].

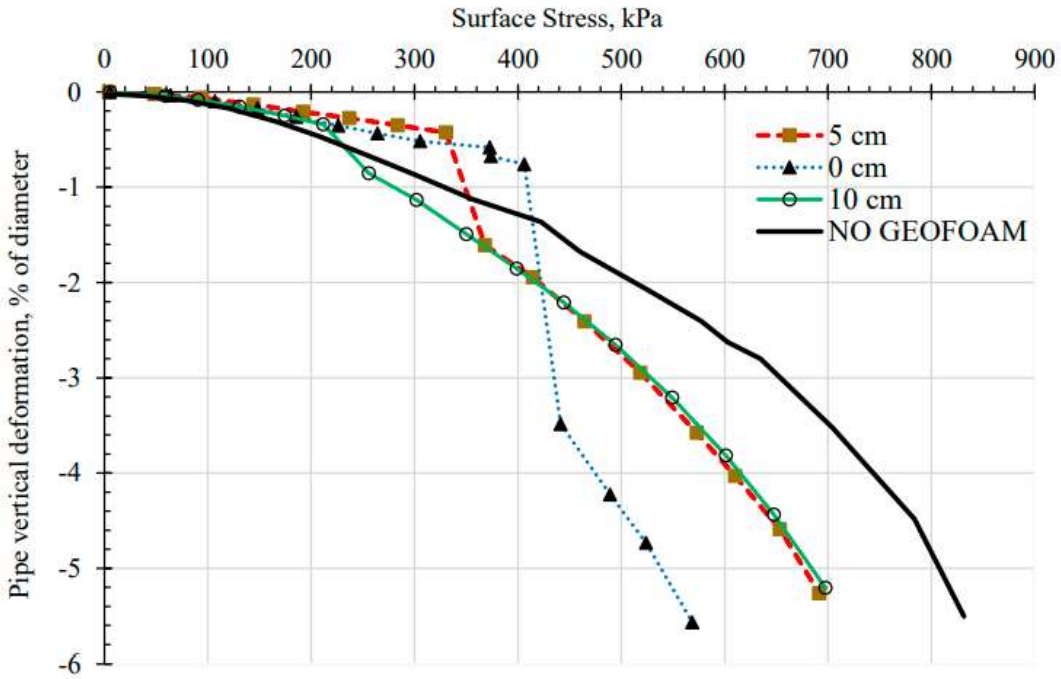



Figure 2-13. Test results for effect of geofoam location on pipe vertical deformation [26].

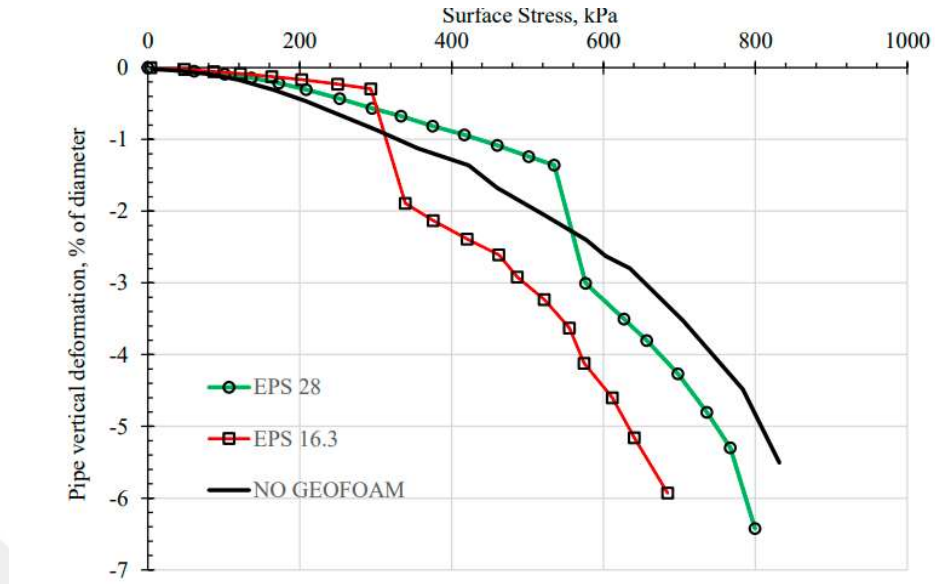



Figure 2-14. Test results for effect of geofoam density on pipe vertical deformation [26].

Another study on geofoams placed EPS geofoams with five different configurations, as shown in the figure, and subjected them to full-scale tests. The goal was to determine the most suitable EPS placement. They conducted study on HDPE pipes. Five different test setups were prepared, and pipe deformation was examined under vertical stress as indicated in Figure 2-15. It was observed that Test 1 provided better results in these tests. [27].

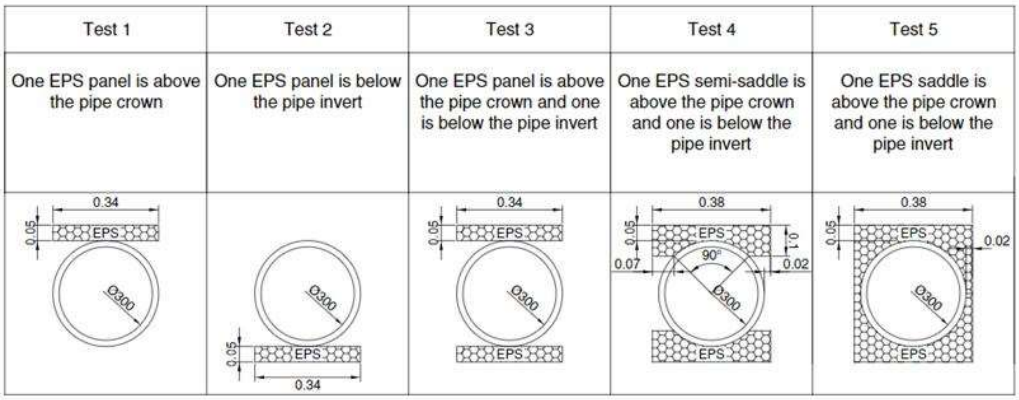



Figure 2-15. Different combinations of pipe and EPC [27].

Palmeira et al. (2010) conducted two different studies to improve the steel pipe (75mm diameter, 1.5mm thickness) using geogrids in various configurations as shown in the Figure 2-16. They compared two different types of geosynthetics placed in single horizontal layer, inverted U arrangement, and envelope arrangement. [28]

The findings revealed that in all geosynthetic arrangements, the horizontal stress on the pipe decreased. The envelope configuration proved to be more effective. The geosynthetics reduced both the strain and stress on the pipe's surface. These results indicate that the implementation of geogrids in different arrangements can significantly improve the performance and integrity of the steel pipe.

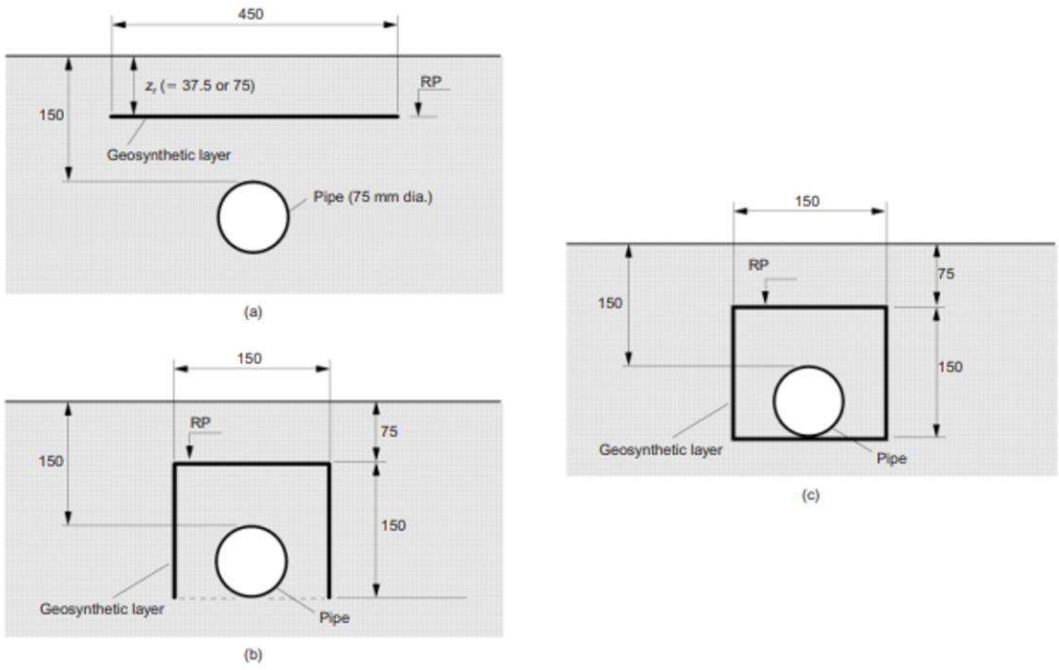



Figure 2-16. Reinforced arrangements a) horizontal arrangement; b) inverted U arrangement; c) envelope arrangement [28].

In another study, Palmeira et al. (2015) used a 75 mm, 1.4 mm thick, 16,000 mm long pipe that made use of geogrid in a laboratory experiment. The research explored the use of geosynthetics as anchorage for buried pipes in the oil industry. The study included model tests with various types of geogrids and anchorage arrangements to assess their

impact on the maximum pipe uplift forces. The results indicated that the presence of anchorage, particularly with geogrids, led to a significant increase in maximum pipe uplift forces compared to unanchored pipes, with an increase of up to 180%. Equations were developed to estimate the maximum uplift force for anchored pipes, and comparisons between predictions and measurements showed the potential for the use of geosynthetics for anchoring buried pipes. The paper highlighted the importance of preventing undesirable vertical or lateral displacements of buried pipes, which can result from the action of waves, buoyancy, and pipe buckling. Different construction techniques, including pipe burial and the use of rock or soil fill, were discussed as measures to protect and minimize damage to the pipes. The study emphasized the need for anchorage measures to avoid or reduce pipe buckling or lateral displacement, with a focus on the potential use of geosynthetics for anchoring buried pipes. The research conducted model tests with various types of geogrids and anchorage arrangements to evaluate their efficiency in increasing pipe uplift resistance as shown in Figure 2-17. The findings showed that the efficiency of geogrid anchorage was influenced by the type of geogrid and the arrangement utilized. The paper also discussed the influence of the deformations caused to the anchorage length and the passage of soil particles through the geogrid apertures on the performance of geogrid anchorage. The paper concluded that geosynthetics can be effectively used to anchor buried pipes, with beneficial effects in increasing pipe uplift resistance and reducing their displacements. The research also suggested the potential cost savings associated with using geosynthetics for anchoring pipes, especially in comparison with traditional solutions such as rock dump for offshore pipes [29].

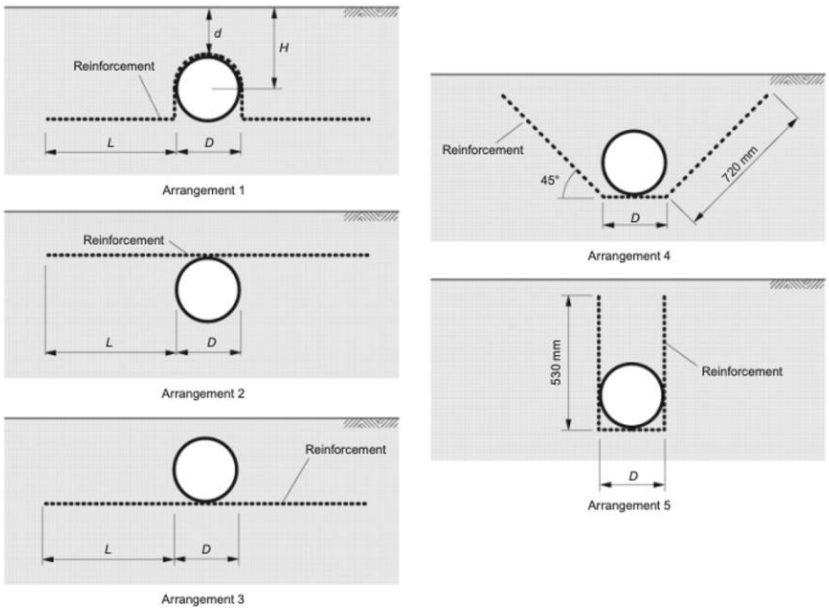



Figure 2-17. Different reinforcement arrangements [29].

## 2.3. Studies with Geogrid

Geogrids play a crucial role in enhancing soil performance under both static and dynamic loads. Advances in numerical modelling have improved the accuracy of geogrid design, enabling better prediction and mitigation of seismic effects on buried structures. Future research should continue to refine these models and explore new applications for geogrid reinforcement in earthquake-prone areas.

Geogrids, defined as geosynthetic materials, are polymeric reinforcements used primarily for soils, retaining walls, and highway applications, effectively reducing the need for pavement thickness [30]. These materials, produced in various grid forms including knitted, fabrics, are typically made from polyester and polyethylene [31]. The primary mechanism by which geogrids provide reinforcement is through tension that develops as the soil incorporating the geogrid is subjected to load, leading to bonding and interlock with soil aggregates [32]. The performance of geogrids depends on their material characteristics such as geometric configuration and physical properties. Key factors

influencing their mechanical behaviour include aperture size, open area percentage, and layer thickness.

Several studies have demonstrated the effectiveness of geogrids in soil reinforcement and load distribution. For instance, Ling et al. (2009) highlighted the ability of geogrids to improve the performance of retaining walls under seismic loading conditions [33]. Similarly, El-Sherbiny and Abdel-Rahman (2013) showed that geogrid reinforcement significantly enhances the stability of embankments subjected to seismic activity [34].

Numerous studies have investigated the relationship between geogrid layers and native soil under static loads, demonstrating significant improvements in load-bearing capacity due to geogrid reinforcement [35], [36]. Experimental research has shown that geogrid reinforcement of buried flexible pipes enhances performance under cyclic loads by distributing stresses and providing additional lateral support [37] [38] [39].

The role of geogrids in mitigating seismic effects, particularly those induced by faulting actions, has been explored through physical model tests and conceptual elasto-plastic model [40] [41] [42]. They indicate that geogrid-reinforced soils effectively disperse fault displacements, creating a wider shear zone and reducing horizontal strains. This action mechanism forms the basis for utilizing geogrid layers to mitigate seismic demands on buried pipes subjected to strike-slip actions.

## 2.4. Experimental Analyses - Full-Scale Laboratory Testing

Experimental studies in the literature have been conducted using many different small and large-diameter pipe types and soil types. Pipes with a diameter of less than 300 mm are considered small-diameter pipes, while the others are large-diameter pipes [43]. In addition to these, the effect of static and dynamic loads on buried pipes has been investigated by many researchers and experiments have been carried out using various improvement methods. Key studies prepared by Brachman et al. (2001), Kawabata et al. (2003), Tupa et al. (2007), Tafreshi et al. (2008), Pires et al. (2021), and Palmeira et al.

(2015) examine the effects of static loads on buried pipes. Additionally, Mir et al. (2002), Alzabeebee et al. (2019), and Wang et al. (2018) conducted studies investigating the behaviour of buried pipes under dynamic loads and fault movements.

Brachman et al (2001) designed the laboratory test to investigate the structural behaviour of a 220 mm diameter HDPE pipe embedded in a mixture of sand and coarse gravel with a density of 1760 kg/m³ in a 2.0 m wide, 2.0 m long and 1.6 m high box. This laboratory facility was specifically designed to test the performance for the evaluation of the structural response of small diameter buried pipes under vertical and horizontal stress. The test results can be used to identify factors that affect the durability and structural integrity of the pipe. These factors include the buried depth of the pipe, the characteristics of the ground in which it is placed, the diameter and material of the pipe. This analysis has demonstrated that the coarse gravel fill used in typical storage drainage levels has a substantial impact on the structural response of the pipe. When tested in coarse gravel as opposed to sand fill, the maximum pipe deflections and stresses were nearly twice as big. Due to the local bending effects brought on by the coarse gravel, significant changes in deflection and stress were also seen in coarse gravel when compared to sand fill [43].

Kawabata et al. (2003) investigated that the behaviour of a 150 mm diameter steel pipe buried in a reinforced embankment. The load was applied using 6 hydraulic jacks of 100 kN capacity as shown in the experimental diagram as shown in Figure 2-18. A biaxial load cell was used to accurately measure the load acting on the buried pipe. The settlement of the sand and the pipe deformations were investigated. Also, it was observed that as the pipe settled, the geogrid showed springing behaviour and the vertical load acting on the pipe decreased [44].

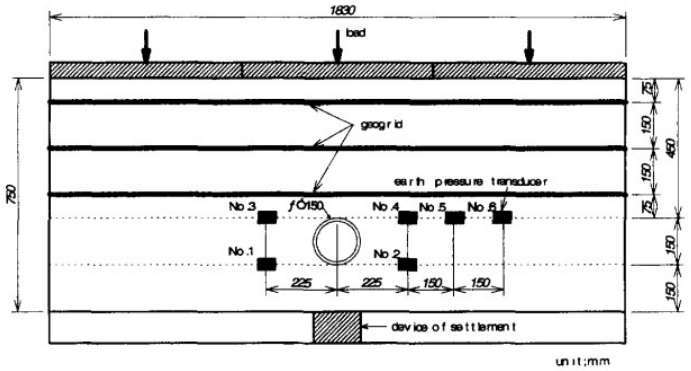



Figure 2-18. Cross Section of Experiment [44].

Tupa et al, (2007) described a lab experiment on the use of geosynthetic reinforcement to mitigate the effects of underground pressurized pipe collapse. Tests were done on various ground geometries, reinforcement kinds, and reinforcement configurations. The internal pressure of pipes has been considered, leading to the implementation of geosynthetic installations in various configurations as depicted in Figure 2-19 and Figure 2-20 [45].

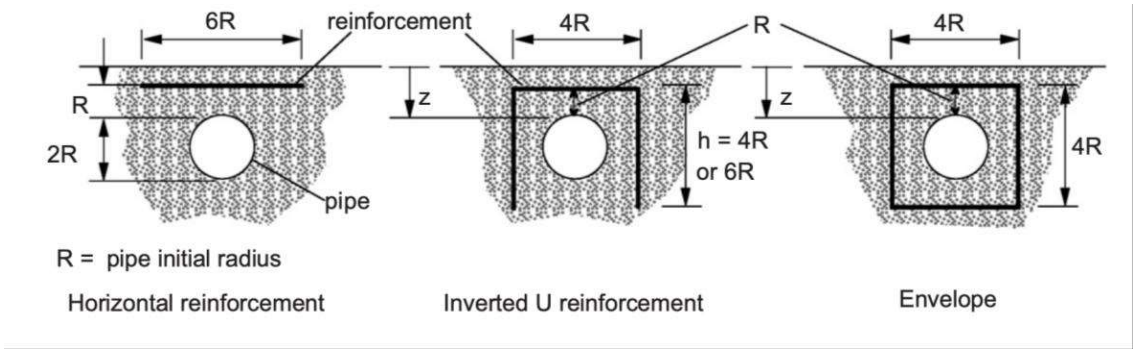



Figure 2-19. Reinforcement arrangements: horizontal ground surface [45].

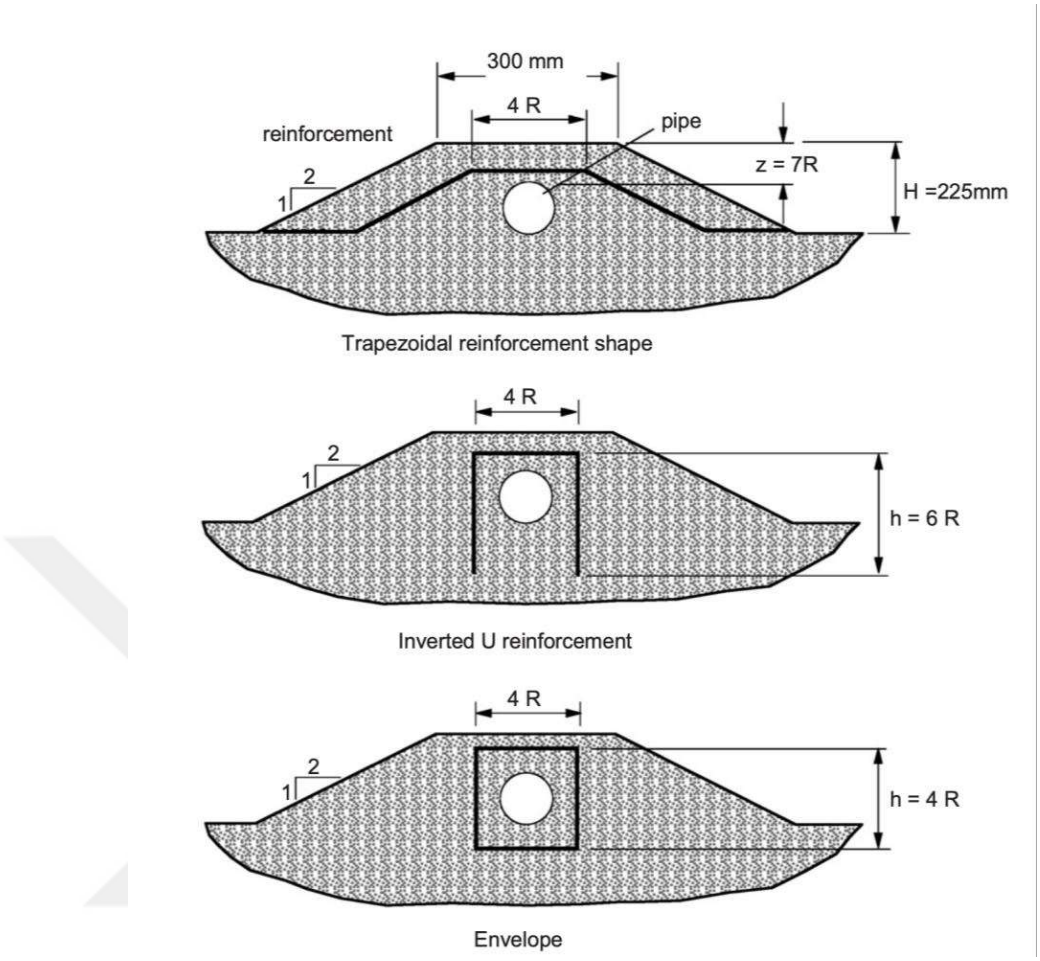



Figure 2-20. Reinforcement arrangements: pipe buried in an embankment [45].

The envelope configuration, in which the reinforcement covers the pipe and the soil, surpassed the other layouts in the study. The inverted U configuration comes next. When the same pressure level was transferred to the soil in the void expansion tests, the reinforced tests showed that the void shape stayed closer to the initial cylinder form than the unreinforced tests did. This shows that the reinforcement prevents the void from growing and keeps the soil more stable. One of the most important results of the study is that the reinforcing effect of geogrids is less than other geosynthetics because soil particles can pass through the grid openings.

In a laboratory test conducted by Tafreshi et al. (2008), static and repetitive loads were applied on a 110 mm diameter, 2.03 mm thick and 210 mm long pipe made of HDPE material. In this study, the research aimed to investigate how the pipe deforms with and

without reinforcement under vehicle loads. Due to the small diameter of the HDPE pipe, its effect on vehicle loads was particularly emphasised. The pipe strain reduction factor (PDRF) and settlement reduction factor (SRF) were investigated. The effect of geosynthetics placed in different locations at 1.5-3 times the pipe diameter. The geosynthetics were placed at various relative densities, namely 42%, 57%, and 72%. The results show that vertical diameter change (ΔD) and soil surface settlement (SSS) can be reduced to a certain extent. The reduction rates for ΔD and SSS were determined as 56% and 65%, respectively [46].

In a different study, measured vertical pipe strain under static stress in the laboratory using cohesionless soil-sand. Pires et al. (2017) looked at how geosynthetic reinforcement affected the mechanical behaviour of soil-pipe systems. Comparisons were made between the tests with and without geosynthetic treatment. There were 4 different geosynthetic arrangements. Pipes buried in reinforced soils would be less vulnerable to surface overstress-related damage. Furthermore, it was determined that enveloped shape (c) geosynthetic improvement is more effective (Figure 2- 21) [47].

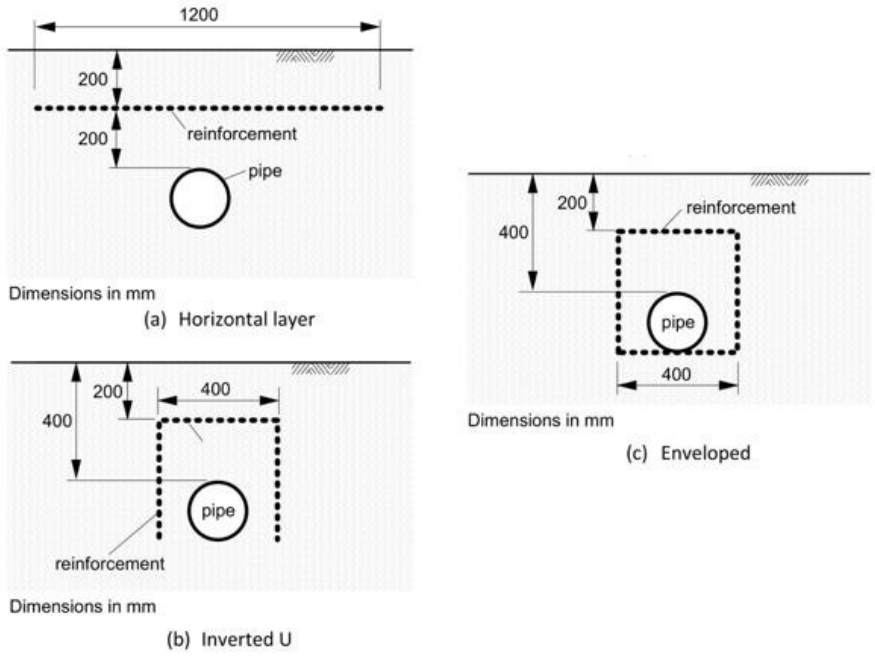



Figure 2-21. Arrangement of geosynthetics [47].

The study testing small diameter pipes was done by Wang et al. (2018). The 220 mm diameter HDPE pipe was investigated by setting up 2 different test setups. The soil box used in the experiment is 2.0 m wide × 2.0 m long and 1.6 m high. While it was sand tested in the first setup applying load and air bladders to ensure soil compaction, coarse gravel was tested in the second setup. When the tests made are compared, it is concluded that the deformations and strain in coarse gravel are more than the sand.

In a similar study in Figure 2-22, the internal pressure of the pipe was also considered. To restrain the movement of the pipe with 250 mm length and 90 mm diameter, geosynthetics were used as an improvement method. The model pipe was moved horizontally in the soil, and the resistance force acting on it as well as the soil pressure were both measured. To test the slip surface between the sand soil, lateral loading was used. The test results demonstrated that the suggested lightweight geosynthetics-based approach significantly increases thrust resistance [48].

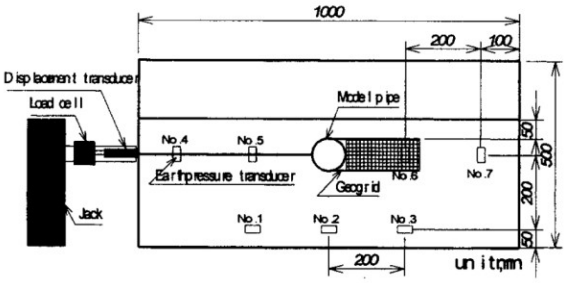



Figure 2-22. Experimental Setup [48].

## 2.5. Soil-Pipe Interaction

Soil resistance is a design parameter that is frequently used in geotechnical earthquake engineering such as foundation, pile systems, retaining walls. It is known that the interface force between the outer surface of the pile and the soil and the friction and shear forces formed at the interface play a major role in the strength of the pile. They encounter a similar situation with buried pipes. The forces occurring between the pipe wall and the soil play a major role in determining the behaviour of the pipe under static and

dynamic effects. Soil-pipe interface resisting capacity depends on the soil properties, fault type, slip length, pipe type and material.

O'Rourke et al. (1999) emphasized in his lecture at the Geotechnical & Structural Engineering Congress that the relationship between the Normal Soil Force on the Pipe Surface and the Normal Force on the Pipe Axis is key in the Soil-Pipe Modelling approach.

Soil resistance has been studied on different soil types and structures, the first known example of this in the literature the study of Potyondy (1961). Various tests and techniques can be performed to find the ground interface shear strength [49].

Dove et al. (1999) investigated the shear mechanism between the high-density geomembrane and Ottawa sand using the basic friction theory. They defined friction force as a component of two shear forces; “adhesion” and “plowing”. In addition, the peak interface strength and shear behaviour controlled by soil shape, type, hardness and applied stress were investigated [50].

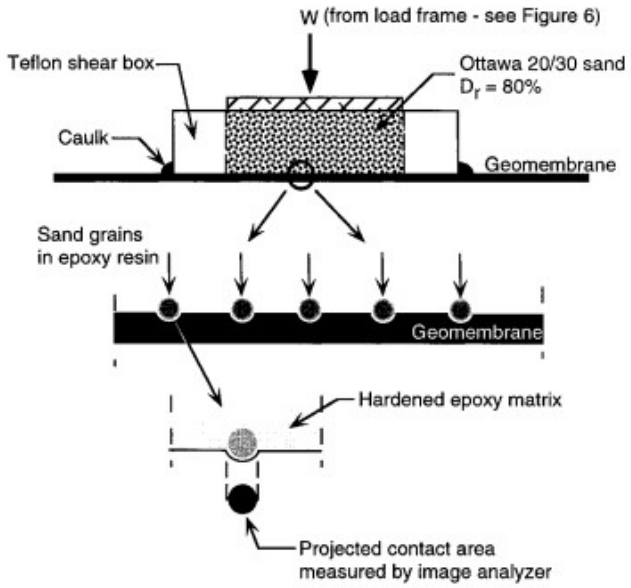



Figure 2-23. Test configuration [50].

Ring shear test [51] and direct shear test [52], and cylinder shear test [53] were used to determine the soil-ground interface shear strength properties. The peak friction coefficient was studied by DeJong et al. (2005). They concluded that the coefficient of friction depends on the particle surface, the excessive consolidation rate and compressive stress, the soil density, and the geomembrane surface properties [54].

On the other hand, Boukpeti et al. (2017) revealed that the interface shear strength varies depending on the soil type; clay, silt, or sand and investigated the sand-pipe interface resistance. They considered marine clays and measured the clay-pipe resistance by applying interface shear strength. In the study, unlike the others, the pipe is covered with 3 different layers. Then, these layers with different roughness values were compared with each other. Soil-interface slip resistance, excessive consolidation ratio and roughness were measured by applying ISM test to marine clays. The smaller interface roughness value (Ra= 2 μm) has a lower interface cutoff value than the larger interface roughness value (Ra= 8 μm). He concluded that lower interface shear resistance occurs at large displacements. In other words, displacement is considered as a measure of resistance. However, the displacement could not be measured precisely because the shear box used by Boukpeti et al in the project allows limited movement. This has been one of the disadvantages of the project [55].

The soil-pipe interface has been investigated by many different methods. An example of this is given by Quej et al. (2024). He analysed already damaged pipe to be used in his study, and the corrosion was investigated, and the earth-pipe interface characterization was made with electrochemical equipment [56].

Anderson et al. (2005) investigated the soil-pipe interaction with full-scale tests at the University of British Columbia. A pipe was placed in a 3 x 5 m earthen box and the axial tensile test was applied. This test shows deviations of up to 1m, which is a large value. Axial and transverse soil loadings were loaded on the pipe and the response of the soil and pipe was investigated. As a result of the experiments, it was observed that the pipe diameter decreased due to the tensile stress and the soil was curved in the shear zone. In addition, it was determined the interfacial friction angle decreased in the shear region [57].

Bilgin et al. (2006) proved that the interface shear friction behaviour is dependent on soil content, grain size, water content and material of the pipe [58]. Tensile test on cast iron pipe was performed by Stewart et al. (2009) and Bilgin et al. (2009) [59], [60]. The relationship between the peel resistance properties and displacement of different soil types was investigated. As a result of the experiment, it was seen that dense soil has 2 times more tensile capacity than loose soil. In addition, the relationship between shear resistance and tensile force has been examined and it has been determined that these two terms are very close to each other. In the tests performed with HDPE pipe in Figure 2-24, it was observed by pullout and cyclic shear tests that the decrease in the pipe radius caused a change in the interface friction force. Since the decrease in the radius of the tube also causes the stress on the normal contact surface to be reduced, the interface friction force is also reduced in the same proportion [59]. In addition, the pull-out resistance also depends on the density of the soil, the burial depth of the pipe, the interface friction angle, the pipe diameter, the length, and the lateral earth pressure. As it is known, cast iron shows less tolerance to temperature than PVC pipes. The junction points of cast iron can cause additional stresses due to temperature changes. In the laboratory environment, pullout tests were performed to determine the surface shear force between soil and pipe. They confirmed with the findings that the junction points are weaker regions [61].

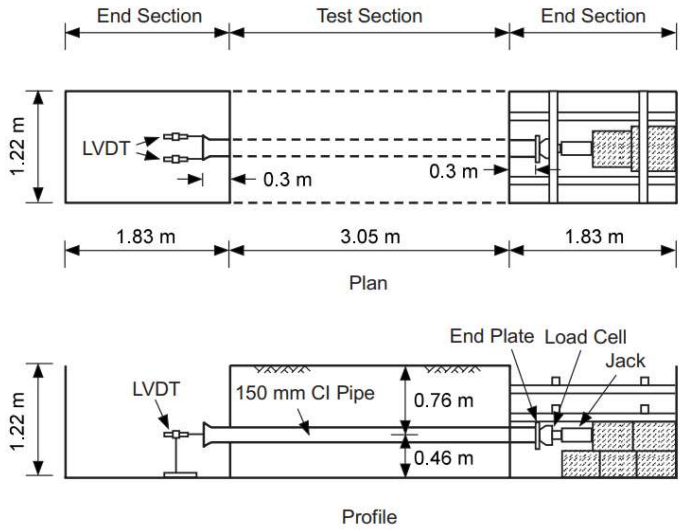



Figure 2-24. Pullout test model [59].

Eid et al. (2019) performed “torsional ring shear” and more than 450 “direct shear tests” using 4 different soils and 5 different solid surfaces with different plasticity values. The ratio of the interface friction angle with the soil and the relationship with the effective normal stress were investigated by experiments. As a result, it has been proven that as the plasticity of the soil increases, the peak and shear force decrease. [62]

Polypropylene is a thermoplastic polymer and is often used in pipe coatings. Lawrence et al. (2019) aims to determine interface shear strength of polypropylene pipeline coatings and granular materials at low stress level. In order to this, direct shear test and interface tests was done by using Winged Direct Shear Apparatus (WDSA) to observe different type of material behaviour. With the apparatus, instead of applying shear load to shear box directly, shear load is transferred by using ball seats and wings. Vertical and horizontal displacement was determined by using the Linear Variable Differential Transformers. Three sands and one coarser test sand were used in this project, and its peak-post peak, stress dilatancy behaviour, and direct shear results were compared. At the end, the researcher found that in addition to the hardness, interface friction depends on mostly grain size and soil type. Smaller grain size has a greater effect on interface strength [63].

Isaev et al. (2020) states that the soil-structure interface behaviour can be characterized by ultimate interface shear strength, residual interface shear strength and soil shear strength coefficient. In the Gersevanov Research Institute, consolidated drained (slow) and consolidated undrained (quick) test were conducted as direct shear tests by using polyethylene, hot-rolled steel, cold-rolled steel, and concrete as shown in figure. Selected soils were saturated gravelly sand, medium grained sand saturated, light loam and heavy loam with soft firm. At the end, they conclude that strength reduction factor $R_{int}$ depend on the surface roughness, type of the soil and interfacing soil condition. $R_{int}$ is also directly proportional to soil dispersion and liquidity index [64].

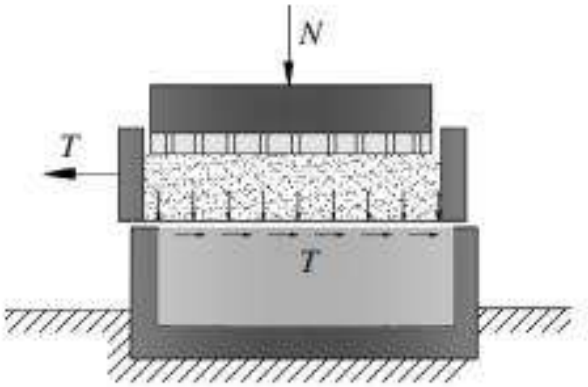



Figure 2-25. Test Setup [64].

Besides static and dynamic experimental test, researchers were investigating soil and pipe interface shear strength with different methodology. Bilgin (2009) used 2 types of tests to measure the interface shearing resistance between the pipe and the soil; pull/push tests and cyclic tests. Since the behaviour of polyethylene pipes is highly dependent on temperature, laboratory tests are performed at different temperatures. According to laboratory tests, it was observed that the pull-out resistance decreased directly proportional to the temperature. Also, shearing resistance decreased as the push-pull cycles test was applied. Pipes with small diameters have low contact stress, so shearing resistance is also low. Then, it was designed the experimental setup as follows. Before the pull- push tests, a certain amount of surcharge was applied as in the Figure 2-26 [59].

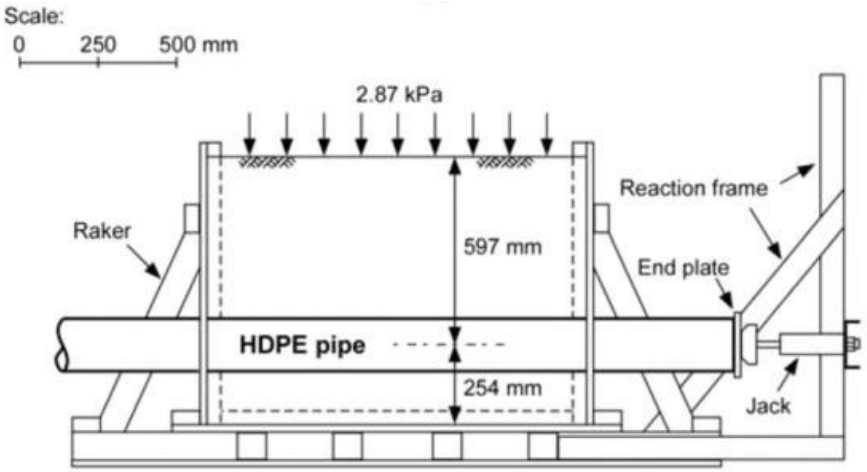



Figure 2-26. Experimental Setup [59].

Another study to investigate soil-pipe interaction was done by Yan et al. (2018). Large scale double shaking table test is applied with non-uniform and uniform excitations. When the uniform and non-uniform excitations are compared, it is seen that the non-uniform seismic excitations cause more catastrophic effect on pipe regarding displacement, amplitude of acceleration and strain. One of the reasons for this situation is that bending strain is neglected under uniform excitation, but for non-uniform excitation, it cannot be neglected. They also conducted large scale shaking table test program to determine pipe displacement under uniform and non-uniform excitations [65].




Figure 2-27. Model container and shaking table [65].

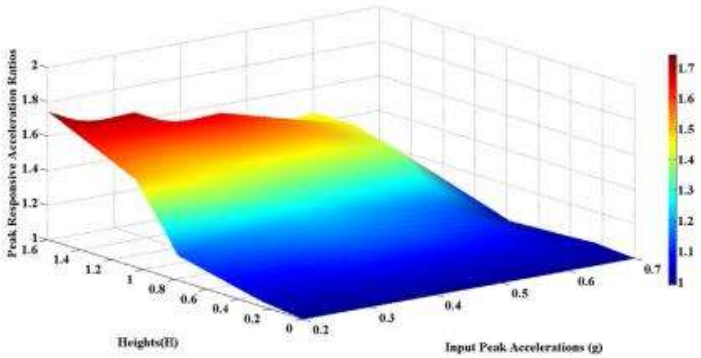



Figure 2-28. 3D plot of peak response acceleration ratios with height and input peak acceleration [65].

In addition to the HDPE pipe studies in literature, Feng (2022) and Alzabeebee (2019) used concrete pipes. Concrete pipes are generally modelled by considering piles with the same geometry as the pipe. Accordingly, to understand the interaction between concrete pipe and soil, Feng (2022) conducted the direct shear test with 5 different sand and 2 different clays with various water ratios. When comparing residual shear strength obtained from the test results, they reached that the concrete-saturated sand combination has lower residual shear stress than the concrete dry-sand interface [66], [67].

## 2.6. Numerical Studies

Numerical analyses are another way to analyse buried pipeline behaviour in addition to experimental, field, and mathematical analyses. Numerical analyses are essential to validate experimental analyses. In the literature, numerical analyses can be performed with many finite element programs. Some of the most popular programs in literature are PLAXIS, FLAC, ABAQUS, and ANSYS.

There are an increasing number of numerical analyses with simulation by using the finite element methods. These generally investigate the soil-pipe interaction.

One of the earliest numerical studies was done by Wang (1992). In the study, the seismic performance of buried water pipes has been examined. Also, cases with and without liquefaction analyses have been made. The pipe is modelled as follows and a finite element solution is developed using the energy method. The following figure shows the numeric modelling of the buried pipeline system with liquefaction zone done as indicated in Figure 2-29 [68].

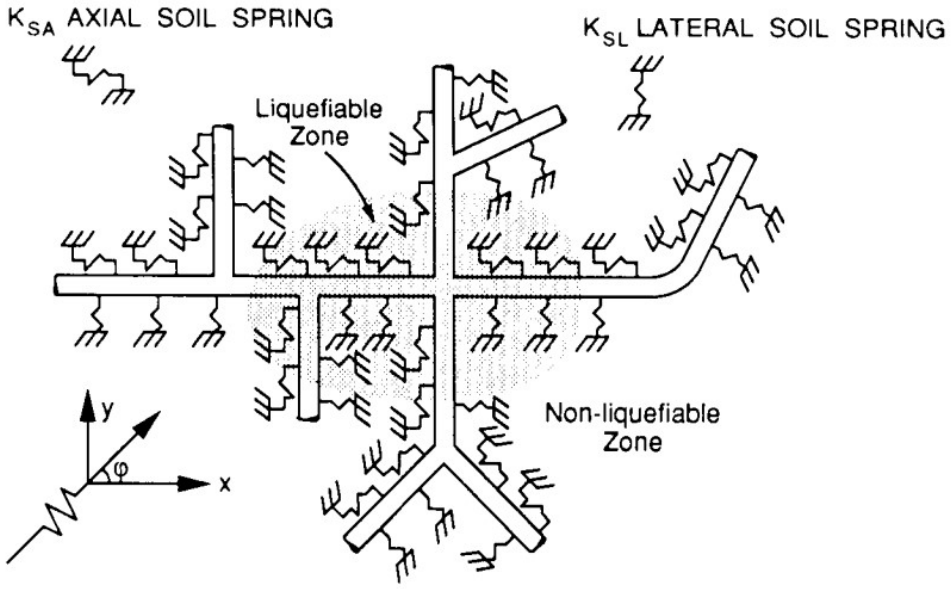



Figure 2-29. Buried pipeline system in liquefaction zone [68].

The deformations in the pipe during the earthquake were described by O'Rourke et al. (1999) with 2 geotechnical mechanisms [6].

1- Temporary deformations due to the passage of seismic waves

2- Permanent deformations caused by fault ruptures, landslides and liquefaction.

In linear pipes, deformations can be examined in two ways as transverse and longitudinal as shown in Figure 2-30. In longitudinal deformations, compression and tension are effective due to the propagation of the seismic wave [69].

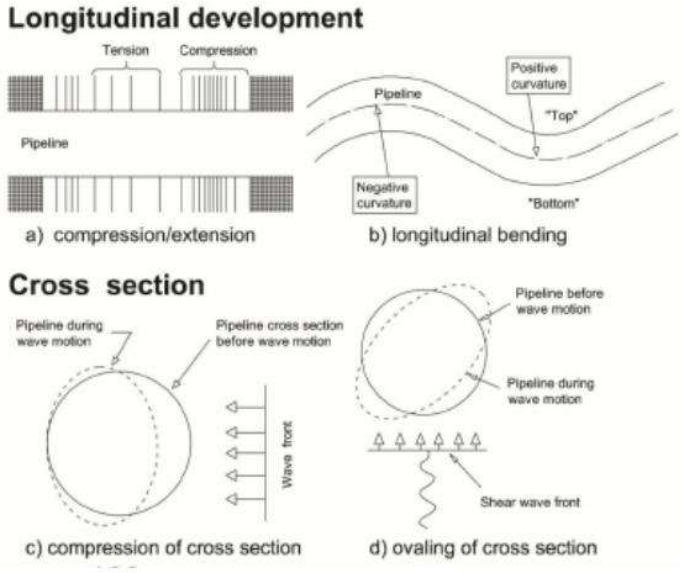



Figure 2-30. Soil/structure interaction mechanisms due to waves passage [69]

For the pipeline behaviour simulation, there are two different type of finite element analyses approach. The first one is beam-type elements for pipe and the other used for the soil modelling is nonlinear springs. Beam-type element models have been used for design pipelines by the American Society of Civil Engineers (ASCE) guidelines and the American Lifelines Alliance guidelines. Abaqus is one of the most preferred programs because it offers the user a master/slave relationship. Sarvanis (2018) modelled shell type elements for pipe and solid type element s for soil by using the ABAQUS in order to analyse soil-pipe interaction. Then strike slip fault crossing was investigated. Mohr-Columb model was used in the research. The model is divided into 1 m meshes and symmetry boundary condition is added. To get more realistic results, only the movement in the x direction is allowed and the vertical direction is restricted [70].

Sterling (1997) also made numerical modelling using the FLAC 3D program. The radial displacement is kept constant at the centre of the tube and the force towards the ground surface is neglected. Therefore, the results and observations did not match [71].

Sahoo et al. (2014) analysed single and double pipeline system with numerical investigation considering the effect of depth of single pipeline as shown in Figure 2-31, spacing between double pipeline, and the effect of PGD on buried pipe. The pipe is 2.1m length and 0.015m thickness. Also, water pressure was applied inside the pipe as 25kN/m$^2$. They reached final displacement is high at the middle of the pipe [72].

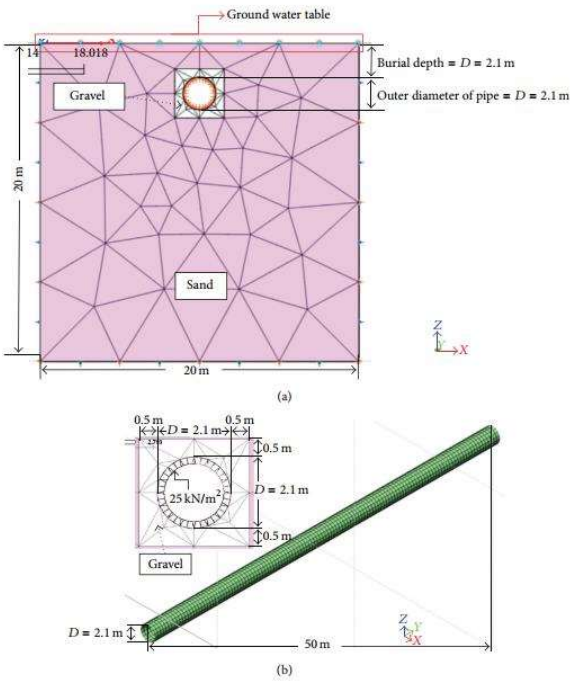



Figure 2-31. Variation of burial depth and spacing of pipes [72].

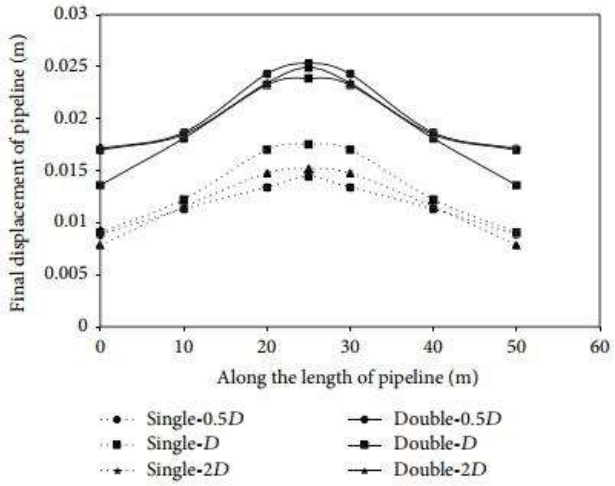



Figure 2-32. Displacement vs length [72].

Examination of buried pipes under static loads is quite a lot in the literature. However, its behaviour under dynamic-seismic loads has been studied in very few articles. Alzabeebee (2019) examines the seismic behaviour of buried pipes, and it is the first study to examine concrete pipes under shaking resistance. Before the shaking table test, displacement calculations were made using finite element programs – PLAXIS as shown in Figure 2-33. The aims of the study are seismic behaviour of buried concrete pipes with soil loads, to analyse bedding factors by using shaking table [67].

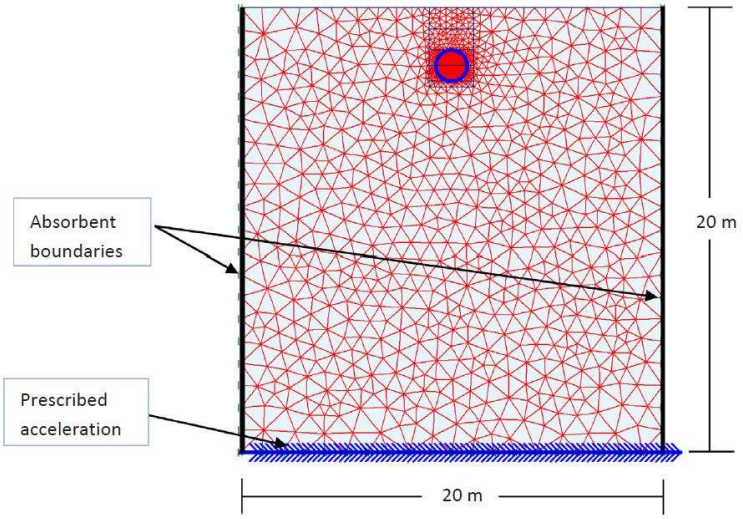



Figure 2-33. FEM model [67].

## 2.7. Mathematical Modelling

Buried pipes have been analysed in two different ways in the literature hydraulic and structural This study will focus on the structural analysis of buried pipes.

Static Design: Structures like parks, tunnels, highways, bridges, and other architectural buildings built on pipelines cause serious stress on pipelines. Therefore, besides the dynamic design of the pipes, the static design is also very important.

The static design of a buried pipe involves the analysis and calculation of the pipe's strength and stability under normal operating conditions and dead loads, such as the weight of the soil and water pressure. The following steps are typically involved in the static design of a buried pipe:

- Determination of the design loads
- Select the appropriate materials
- Calculation of the burial depth
- Perform structural analysis

- Evaluate the pipe's stability
- Design the pipe support system based on the results of the structural analysis and the stability evaluation.
- Installation and testing

Step 1 - Determination of the design loads: This involves identifying the types and magnitudes of loads that will act on the pipe, including soil weight, water pressure, live loads, and dead loads.

According to the “Guidelines for the design of buried steel pipe” from ASCE

Loads on buried pipes:

- Vertical earth loads like traffic load, embankment load,
- Internal pressure because of the hydrostatic force
- Seismic loads,
- Earthquake effects like liquefaction, uplift of the pipe, sliding, and fault movement.
- Temperature change and erosion.

Step 2 - Select the appropriate materials: The type of pipe material and its properties, such as its strength, ductility, and stiffness, should be selected based on the loading conditions and the specific requirements of the project.

Calculation of the burial depth: The burial depth should be determined based on the anticipated loads on the pipe and the strength of the soil. The depth should be sufficient to provide adequate support for the pipe and to prevent excessive deflection or deformation.

Perform structural analysis: This involves using mathematical models and computer simulations to determine the pipe's response to the loads and to calculate its deflection, stresses, and strains.

Evaluate the pipe's stability: The pipe's stability against buckling and lateral movement should be evaluated to ensure that it will remain in its intended position and will not collapse or move under normal operating conditions.

Design the pipe support system: A pipe support system may be required to maintain the pipe's stability and to distribute loads evenly along its length. The design of the support system should be based on the results of the structural analysis and the stability evaluation.

Installation and testing: The design should be checked against relevant codes and standards to ensure that it meets the minimum requirements for safety and performance.

The study of Anderson et al. (1913) is pioneer in their work on buried pipes. They have conducted ground-breaking research on sewage pipes, being among the first to define loads and develop mathematical models. As depicted in the adjacent figure, they have successfully employed mathematical modelling to define pipe loads as shown in Figure 2-34 [57].

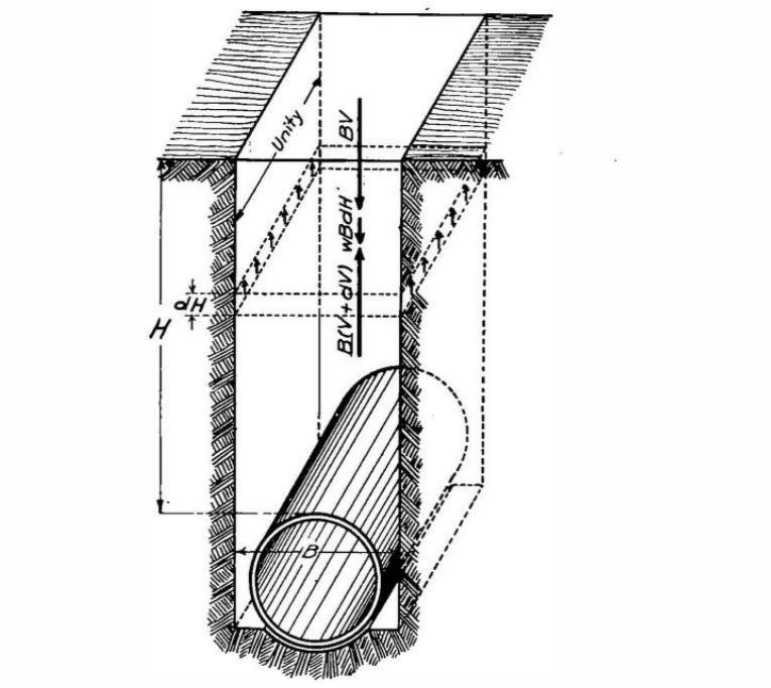



Figure 2-34. Mathematical theory of loads on Pipe [57].

Marston (1930) is one of the first theoretical study to emphasize soil loads on buried pipes. The study is for closed conduits [73]. Then, Spangler (1941) is the pioneer of the flexible buried pipe design. they developed “Iowa Deflection Formula” mathematical equations for the structural design of the buried pipes. They applied Marston’s theory for vertical loads with analytical and semi-empirical formulations. The calculations using the ring deflection theory was compared with the laboratory experiments. The results were found to be very close to each other [74].

Wang et al. (1985) investigate that buried pipe behaviour against fault movement by analysing mathematically. They found that in order to increase resisting capacity of the pipe considering fault movement depends on the following: [75]

(a) larger crossing angle
(b) smaller buried depth
(c) smaller pipe diameter
(d) smaller pipe frictional angle

The literature has studied seismic analyses of flexible buried pipes. Specifically, Moore (1989) researched buckling theories related to buried pipes. The magnitude of the hoop force experienced by the pipes is influenced by factors like trench geometry, compaction effects, and soil properties [43].

# 3. EXPERIMENTAL PROGRAM

## 3.1. Introduction

In this thesis, the seismic performance of buried pipes was investigated with and without the use of geogrids. Shaking table tests were conducted to assess the effect of different geogrid locations and arrangements on the seismic behaviour of the buried pipes. Additionally, the arrangement of the geogrids is studied by conducting experiments in the following 5 configurations. The seismic performance of each arrangement is then compared.

- CASE 1: Without using geogrid (Control Case).
- CASE 2: Wrapping the pipe with geogrid.
- CASE 3: Placing one layer of geogrid under the pipe and one layer above the pipe.
- CASE 4: Placing one layer of geogrid under the pipe and two layers above the pipe.
- CASE 5: Placing one layer of geogrid under the pipe and three layers above the pipe.

## 3.2. Experimental Facility

Experiments have been conducted at the Mustafa Erdik Shake Table Laboratory of Boğaziçi University Kandilli Observatory and Earthquake Research Institute (KOERI). In the experiments, a shaking table, soil box, sand, pipe, geogrids, and measuring devices were used. Details of the equipment are provided in the following sections. In the experiments 16 accelerometers, 5 laser displacement meters, and 1 data collection system were used.

### 3.2.1. Test equipment

3.2.1.1. Shaking table. The shaking table used in the experiments is a powerful tool for simulating seismic events. It can accommodate specimens up to 10 tons with its dimensions of 3 meters by 3 meters. The table generates horizontal vibrations using a servo-hydraulic actuator, mimicking real or synthetic motions with a force of up to 2g and a total lateral displacement of 24 cm (12 cm in each direction). Additionally, a modern digital control system and updated computer software ensure precise operation of the shaking table.



Figure 3-1. Shaking Table at KOERI.

3.2.1.2. Soil Box. The soil box used in this study was developed under the project BAP14020, titled "Effects of Seismic Loading on Soil-Pipe Interface Shear Resistance." Its purpose is to investigate and measure the impacts of earthquakes on the shear resistance of the soil-pipe interface. The box is made of steel material, chosen for its rigidity, and was specifically designed and manufactured for pullout and seismic performance tests as shown in Figure 3-2. The inner dimensions of the box are 90 cm in width, 120 cm in length, and 90 cm in height, while its overall dimensions, including the connection plate to the shaking table, are 129 cm in width, 221 cm in length, and 100 cm in height.

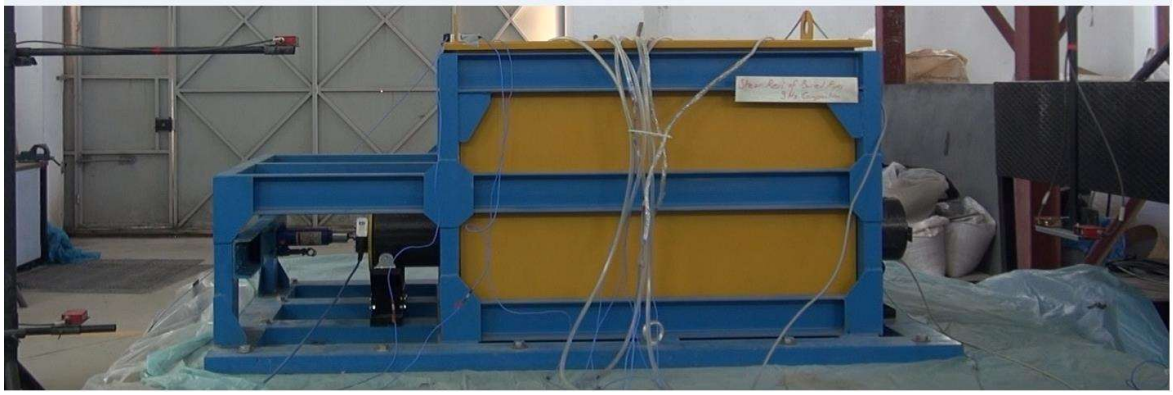


Figure 3-2. The Test Box Used in Pullout and Shaking Table Performance Tests

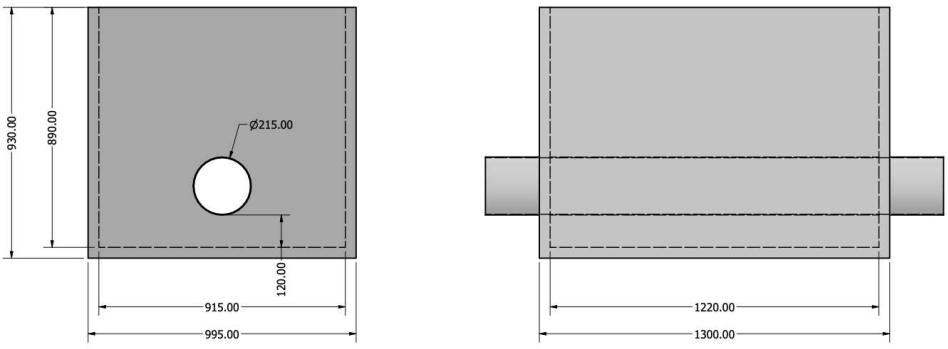



Figure 3-3. Soil box front view and side view with dimensions (mm).

3.2.1.3. Sand. The soil sample used in these experiments was Silivri Sand. The sand was carefully placed and compacted within the soil box to ensure uniform density and consistency throughout the experiment as seen in Figure 3-4. Additionally, before the experiments, a 9 Hz frequency wave was applied to further compact the sand and ensure uniformity as suggested by Bathurst et al. (2007). The careful preparation and compaction of the soil sample were critical to the success and accuracy of the experiments, as they directly influenced the interaction between the soil, pipe, and geosynthetics [22].



Figure 3-4. Compaction of sand.

To determine sand properties, a laboratory test was conducted. Soil properties are given in the Table 3-1 and grain size distribution of Silivri Sand is given in Figure 3-5.

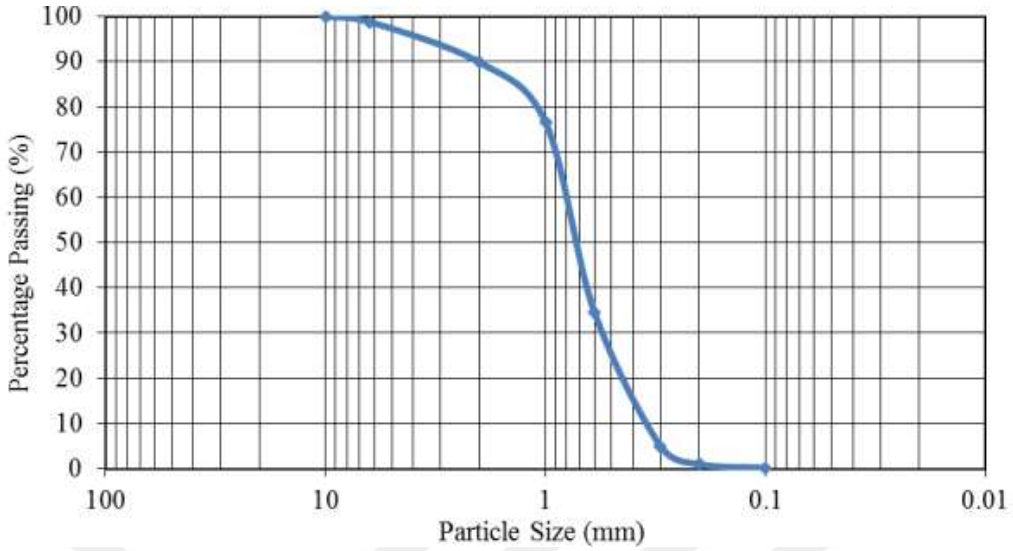



Figure 3-5. The grain size distribution of Silivri Sand.

From the direct shear test, the following properties were obtained.

Table 3-1. Soil properties

| **Property** | **Symbol** | **Value** | **Method** |
|---|---|---|---|
| **Soil Classification according to (USCS)** | SP | Poorly Graded Sand | ASTM D422-07 |
| **Unit weight** | $\gamma$ | 16.5k N/m$^3$ | ASTM D4253-00 |
| **Specific gravity** | $G_s$ | 2.7 | ASTM D854 |
| **Coefficient of uniformity** | $C_u$ | 2.5 | |
| **Coefficient of curvature** | $C_c$ | 1.1 | |
| **Internal friction angle** | $\varphi$ | 24 | ASTM D3080 |
| **Minimum void ratio** | $e_{min}$ | 0.37 | |
| **Maximum void ratio** | $e_{max}$ | 0.73 | |

3.2.1.4. Pipe. In the experimental studies conducted for the thesis, a High-Density Polyethylene (HDPE) pipe was used. Superlit Pipe Industries provided the HDPE pipe used in the experimental studies conducted for this thesis. The detailed properties of the pipe are outlined in Table 4.2. The pipe's wall thickness was 7.5 mm, with an internal diameter of 200 mm and an external diameter of 215 mm.




Figure 3-6. Pipe Dimensions.

Table 3-2. Pipe properties.

| **Property** | **Value** |
|---|---|
| **Material** | HDPE |
| **Elasticity Modulus, E (Mpa)** | 1000 |
| **Thickness (mm)** | 7.5 |
| **Pipe diameter- internal (mm)** | 200 |
| **Pipe diameter- external (mm)** | 215 |
| **Pipe length (mm)** | 1800 |
| **Cross-sectional area (A) ($m^2$)** | 0.004889 |
| **Moment of Inertia ($m^4$)** | $6.3476846\times10^{-6}$ |

3.2.1.5. Geogrid. Geogrids are employed to enhance the seismic performance of buried pipes. Geogrids are geosynthetic materials used to reinforce soils and similar materials. They are typically made from olymers such as polypropylene or polyester and are characterized by their open grid-like structure. The geogrid used in this study, as shown in the photograph below, has grid openings with a width of 3.5 cm.

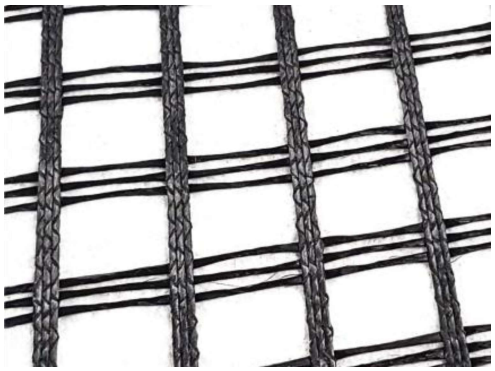


Figure 3-7. Geogrid used in the experiments.

In the experiments conducted for this thesis, geogrids are arranged in four different configurations to assess their effectiveness in improving the seismic performance of buried pipes. The configurations include wrapping the pipe with geogrid, placing geogrid layers under and above the pipe, and varying the number of layers above the pipe. These configurations aim to determine the optimal arrangement of geogrids for maximum seismic protection.

3.2.1.6. Instruments. Accelerometer: By mounting accelerometers on the shaking table, soil box, pipe and soil movement are measured. It is vital for ensuring that the shaking table replicating the desired earthquake motions. In the experiments, 16 accelerometers were used. It is defined as numbers A1, A2, A3, A4, A5, A6, A7, A8, A9, A10, A11, A12, A13, A14, A15, and A16. The locations were the same for all tests, given in the Table 3-3.

Table 3-3. Details of accelerometer locations.

| **Accelerometer** | **Location** |
|---|---|
| A1 | Shaking table |
| A2, A3, A4 | Soil box |
| A5, A7, A8, A9 | Pipe |
| A6, A10, A11, A12, A13, A14, A15, A16 | Soil |

Accelerometers A7, A8, and A9 are mounted on a pipe at distances of 22 cm, 66 cm, and 102 cm from the box, respectively as shown in Figure 3-8. Another set of accelerometers, A12, A13, and A14, are placed 20 cm above the first set at the same distances. A10 and A11 are placed at an equal distance to the right and left of A8, and A15

and A16 are placed 20 cm above them, respectively as Figure 3-8, Figure 3-9 and Figure 3-10. The arrangement of the accelerometers on the soil is shown in Figure 3-11.

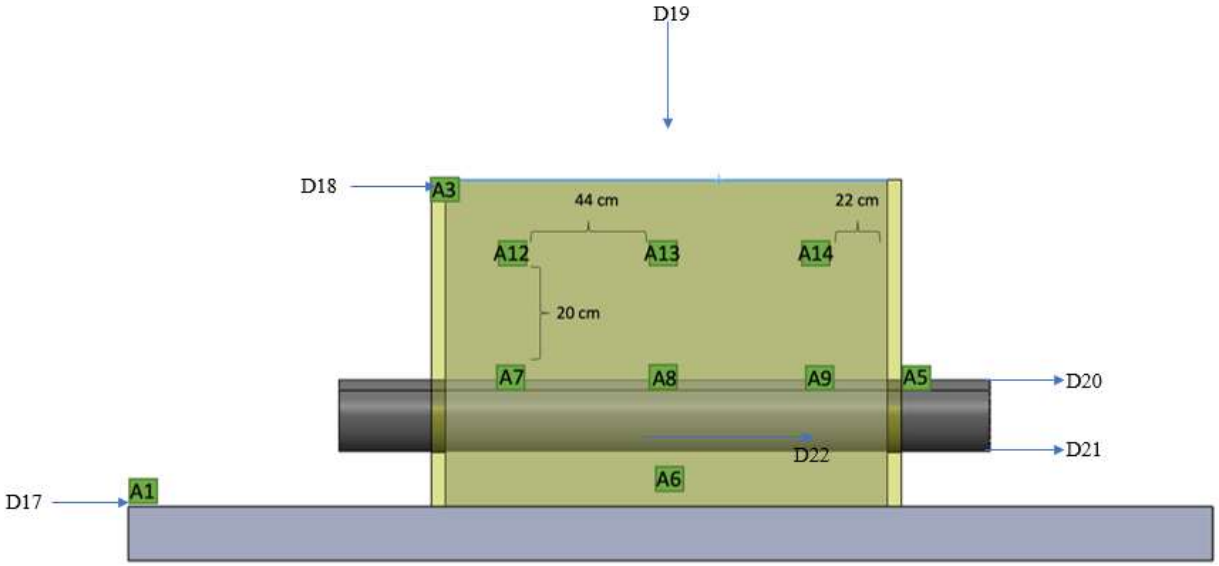



Figure 3-8. Accelerometers and LVDT arrangement front view of box.

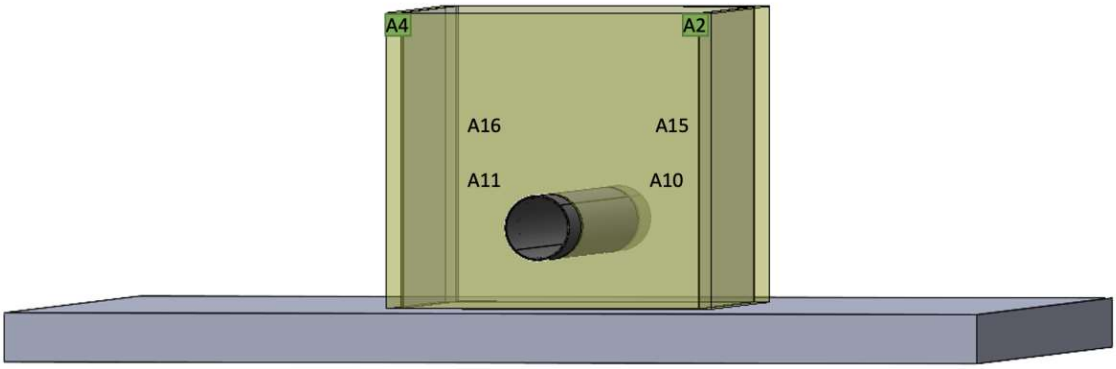



Figure 3-9. Side View of Box with Accelerometer Arrangement.

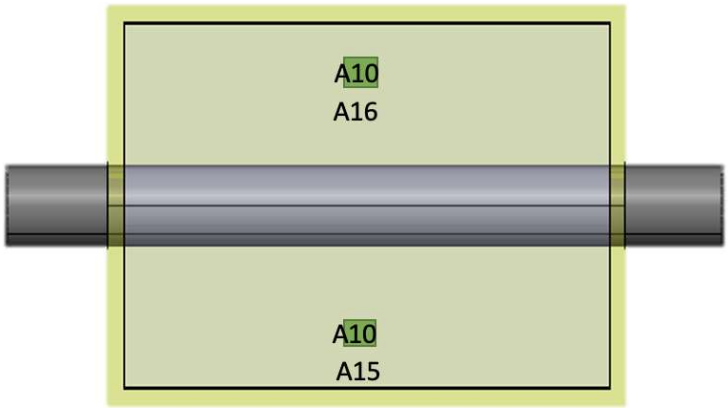



Figure 3-10. Top View of Box with Accelerometer Arrangement.



Figure 3-11. Accelerometers, A12, A13, A14, A15 and A16 on the sand.

Linear Variable Differential Transformers (LVDTs): Linear variable differential transducers (LVDTs) enable measuring displacement of the test model during shaking table experiments. In the experiments, 5 LVDTs and 1 potentiometer were used. It is defined as numbers D17, D18, D19, D20, D21, and D22. Their locations were the same for all tests, given in Table 3-4.

Table 3-4. Details of LVDTs and potentiometer locations.

| **Sensors** | **Location** |
|---|---|
| LVDT - D17 | Shaking table (x-direction) |
| LVDT - D18 | Soil box (y-direction) |
| LVDT - D19 | Vertical displacements on the surface (z-direction) |
| LVDT - D20, D21 | Outlet of pipe |
| Potentiometer - D22 | Inside the pipe |

## 3.3. Physical Modelling - Shaking Table Test Program

### 3.3.1. Experimental setup and Sample Preparation

In the experimental setup, the pipe was positioned inside a box, with 1200 mm of the pipe length contained within the box and 200 mm extending out from each side of the box. Additionally, the pipe was placed 120 mm above the bottom of the box.

A buried pipe and Silivri sand system was placed in an 89x92x122 cm box. Special care was taken to fill the sand used, especially to be dry and homogeneous at every point. Then, experiments were carried out by improving with geogrid in different geogrid arrangements under the same input motion. Table 3-5 shows the different arrangements made using geogrid. The obtained improved and unimproved test results are compared in the section 5. Before the tests, a 9 Hz signal was applied to the soil box to compact the sand and achieve a more uniform test sample. For all cases the relative density of the soil sample is 60%.

In the study, various configurations were tested to evaluate the seismic performance of the buried HDPE pipes as summarized in Table 3-5. The configurations are as follows:

Table 3-5 Summary of Cases

| | |
|---|---|
| CASE 1 | Unimproved |
| CASE 2 | Pipe wrapping |
| CASE 3 | 1 layer bottom of the pipe, 1 layer top of the pipe |
| CASE 4 | 1 layer bottom of the pipe, 2 layer top of the pipe |
| CASE 5 | 1 layer bottom of the pipe, 3 layer top of the pipe |

Case 1 - Unimproved: In this configuration, no geogrid was used. The pipe was buried without any additional reinforcement.

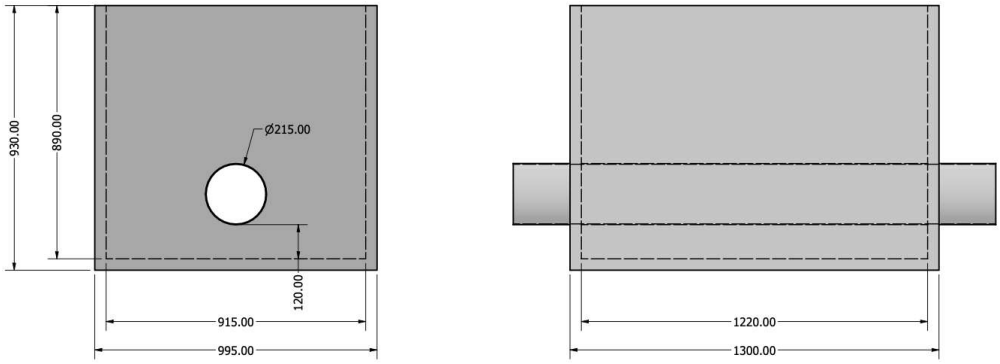



Figure 3-12. Experimental model for Case 1.

Case 2 – Wrapping the geogrid around the pipe: The 120 cm segment of the HDPE pipe, with an internal diameter of 20 cm, placed inside the box, was fully encased in geogrid. This configuration was designed to evaluate the impact of completely wrapping the pipe in geogrid on its seismic performance.

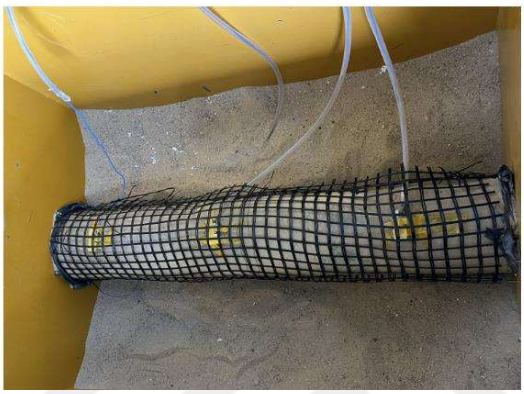


Figure 3-13. Geogrid arrangement for Case 2.

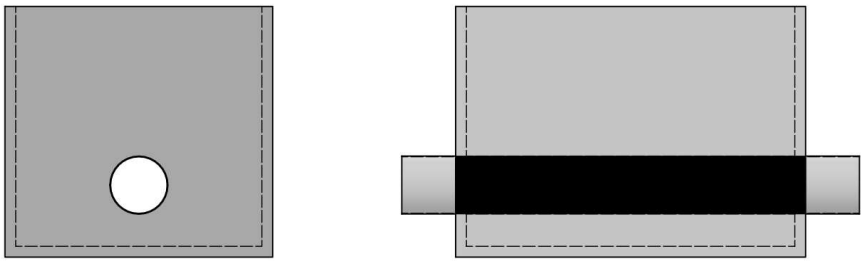


Figure 3-14. Experimental model for Case 2.

Case 3 - 2 layers of geogrid: There are 1 layer bottom of the pipe and 1 Layer top of the pipe in this case. As shown in the Figure 3-15 , the geogrid layer was placed 5 cm below the pipe (D/4) as suggested in the literature [45]. Another geogrid layer was positioned 5 cm above the pipe, shown in Figure 3-16. The geogrids were laid with a width equal to twice the pipe diameter. This arrangement was intended to provide reinforcement both above and below the pipe.

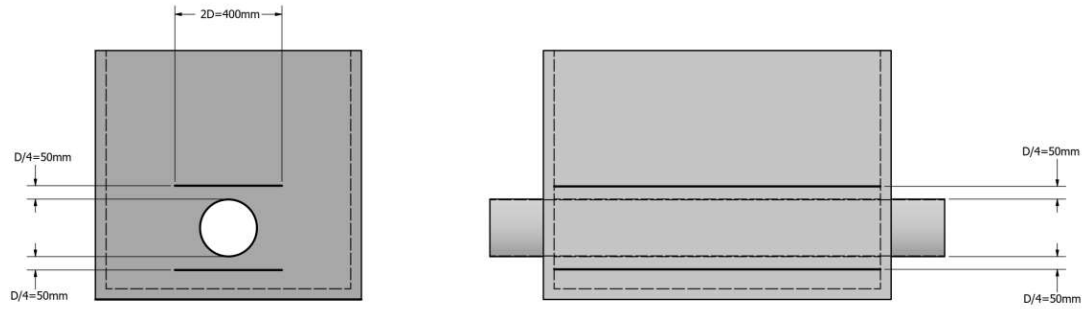



Figure 3-15. Experimental model for Case 3.



Figure 3-16. Geogrid layers placement for Case 3.

Case 4 - 3 layers of geogrid: There are 1 Layer Bottom of the Pipe and 2 Layer Top of the pipe in this case. Geogrids were placed 5 cm below the pipe, 5 cm above the pipe and another 10 cm above the pipe. An additional layer was then placed 5 cm below the pipe, with the same dimensions as in the previous cases. Similarly, the geogrid width is equal to twice the diameter of the pipe.

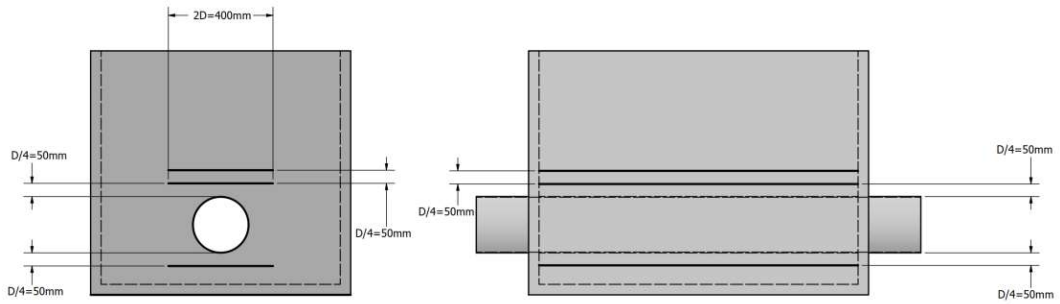



Figure 3-17. Experimental model for Case 4..



Figure 3-18. Geogrid layers placement for CASE 4.

Case 5 - 4 Layers of Geogrid: In this configuration, there is one layer of geogrid placed beneath the pipe and three layers positioned above it. As in the previous cases, the box was emptied, and a layer of geogrid was placed 5 cm below the pipe, followed by

layers placed 5 cm, 10 cm, and 15 cm above the pipe. The geogrid dimensions remained the same, with the width being twice the pipe's diameter.

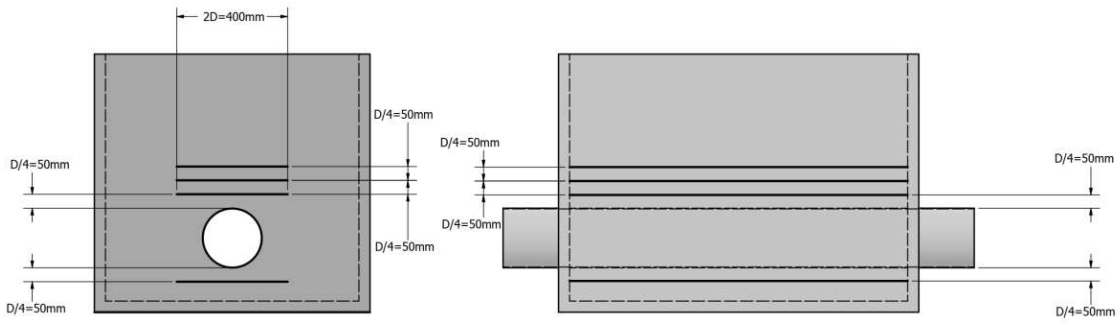



Figure 3-19. Experimental model for Case 5.

### 3.3.2. Earthquake Motions

In this study, 3 different earthquake motion were applied to examine the seismic performance of buried pipes under different configurations of geosynthetics. The following earthquake motions were selected for the study:

Table 3-6. Earthquake motions selected for this study.

| Earthquake name | Station | PGA (g) | Magnitude | DATE |
|---|---|---|---|---|
| **Kocaeli** | Iznik | 0.15 | 7.5 | 17.08.1999 |
| **El-centro** | Imperial Valley | 0.3 | 6.9 | 19.08.1940 |
| **Kobe** | KJMA | 0.82 | 6.9 | 16.01.1995 |

The acceleration time graphs of the applied earthquake motion are shown in Figure 3-20, Figure 3-21 and Figure 3-22:

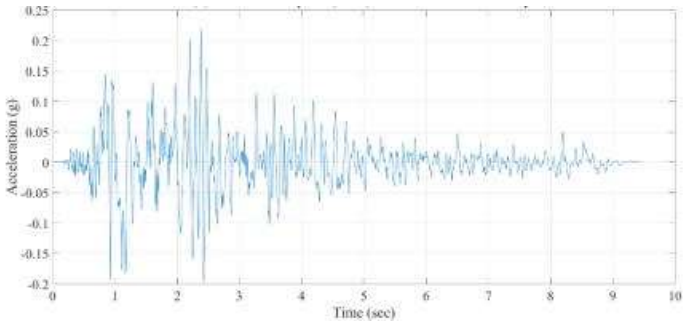



Figure 3-20. Kocaeli Earthquake input motion acceleration-time history [77].

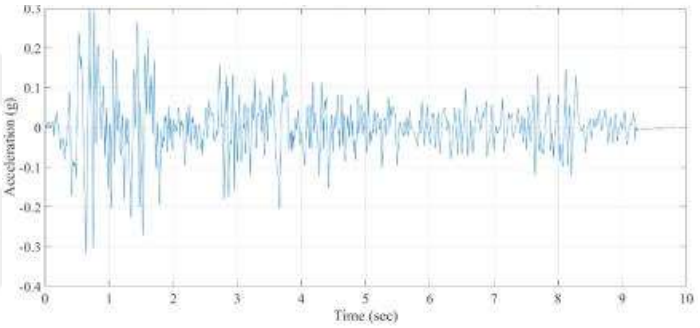



Figure 3-21. El-Centro Earthquake input motion acceleration-time history [77].

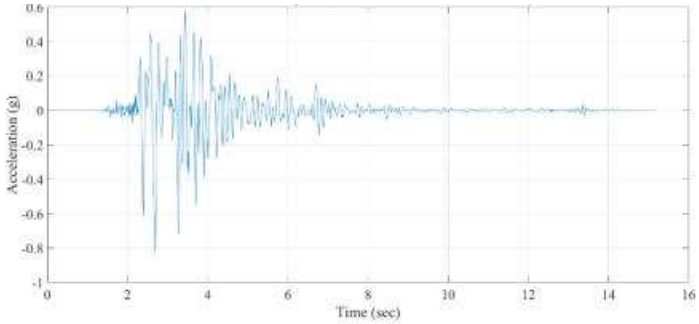



Figure 3-22. Kobe Earthquake input motion acceleration-time history [77].

# 4. EXPERIMENT RESULTS

In this section, the key findings from the experimental study are presented, focusing on the seismic responses of buried HDPE pipes under different cases. Many experiments were conducted to understand the effect of geogrids on the seismic performance of buried pipes. Five different cases under 3 different earthquakes were tested, resulting in a total of 15 experimental scenarios. Kocaeli Earthquake motion recorded at the Izmik Station, with a PGA of 0.22g El Centro earthquake motion recorded at the Imperial Valley Station with a PGA of 0.3 g and Kobe Earthquake with a PGA of 0.82 g were also used as input motions.

The thesis study consists of five different cases. Case 1 involves a scenario without geogrid, while Cases 2 to 5 include geogrid reinforcement. Detailed information about each case is provided in Chapter 3. Each case was tested under three different earthquake motions, and the shaking table tests were used to simulate the seismic events, with further details on the earthquakes given in Chapter 3.

The experimental results were obtained from measurements taken at different depths in the experimental setup. Specifically, data was collected from accelerometer A7, placed on the pipe, and from A14, located close to surface, 20 cm above the pipe. The earthquake input motions applied to the shaking table were measured by accelerometer A1. In each test, the horizontal displacement of the shaking table was measured with D20, representing the lateral displacement of the pipe. The lateral displacement of the shaking table was measure with D17 while vertical displacement of the test sample was recorded by D19.

For each case, the measured acceleration-time histories, horizontal displacement-time histories, vertical displacement-time histories, Fourier Amplitude Spectra, and Response Spectra were presented in the same graphs to allow for comprehensive comparison. Experimental results under all earthquake motions are presented in the Section 4-1 – Section 4-5.

## 4.1. Case 1

Case 1 was conducted without the use of geogrid and serves as the control case. Three earthquake motions were applied.

### 4.1.1. Acceleration Response

The results obtained from experiments conducted using the Iznik, El Centro, and Kobe earthquakes were obtained from the accelerometers placed on the pipe and close to surface. The corresponding time history, Fourier spectrum, and spectral acceleration graphs are presented in Figure 4-1, Figure 4-2, and Figure 4-3 respectively.

Under the Kocaeli earthquake motion, the initial maximum acceleration recorded at A1 was 0.149 g. The near-surface accelerometer at station A14 measured maximum acceleration of 0.169 g, indicating an amplification of approximately 14%. This shows that the surface layers significantly contributed to the increase in ground motion.

Similarly, under the El Centro earthquake motion, the maximum acceleration was measured at A1 as 0.291 g, which increased to 0.349 g at A14, resulting in a 20% amplification.

In the case of the Kobe earthquake motion, the maximum acceleration increased from 0.782 g at A1 to 0.912 g at A14, representing a 17% amplification. Although this amplification is less than that observed during the El Centro earthquake, it still indicates a notable increase in ground motion close to surface.

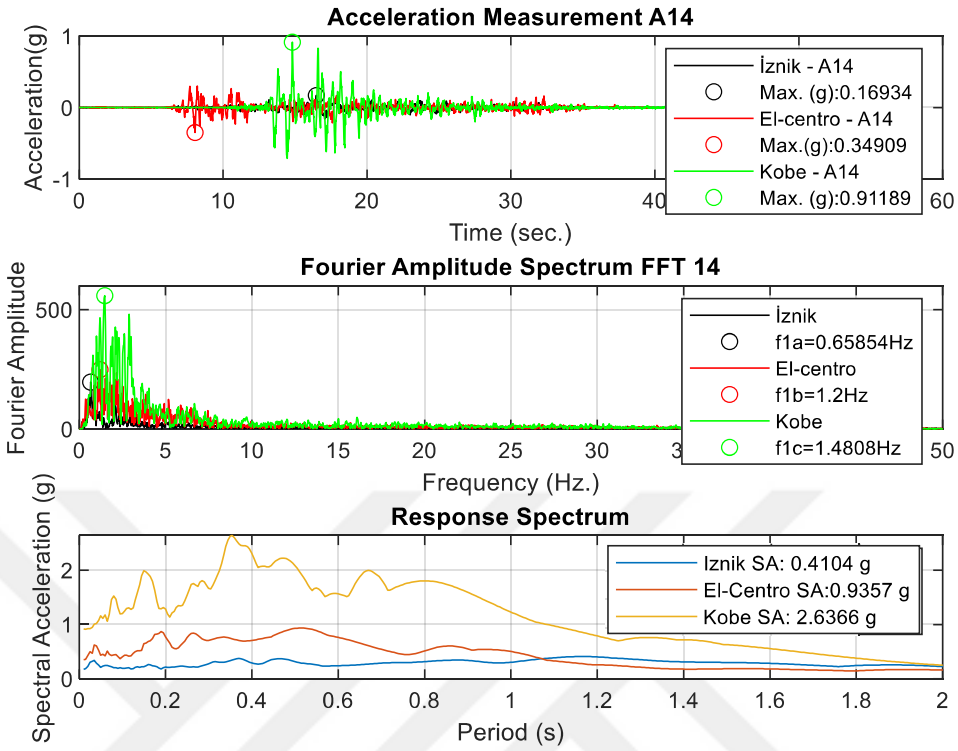



Figure 4-1. CASE 1: Time-history, Fourier amplitude spectrum, response spectrum graphs for A14 under all Earthquake motions.

The accelerometer on the pipe, A7, represented much more moderate amplification. In the Kocaeli earthquake, the value increased from 0.149 g at A1 to 0.156 g at A7 - only a 5% amplification. In the El Centro earthquake motion, the maximum acceleration increased from 0.291 g at A1 to 0.321 g at A7, showing a 10% amplification. While this increase is more remarkable compared to that of Kocaeli earthquake, it is still smaller than the surface amplification. For the Kobe earthquake, an increase similar to that of El Centro was observed: from 0.782 g at A1 to 0.882 g at A7, indicating a 13% amplification.

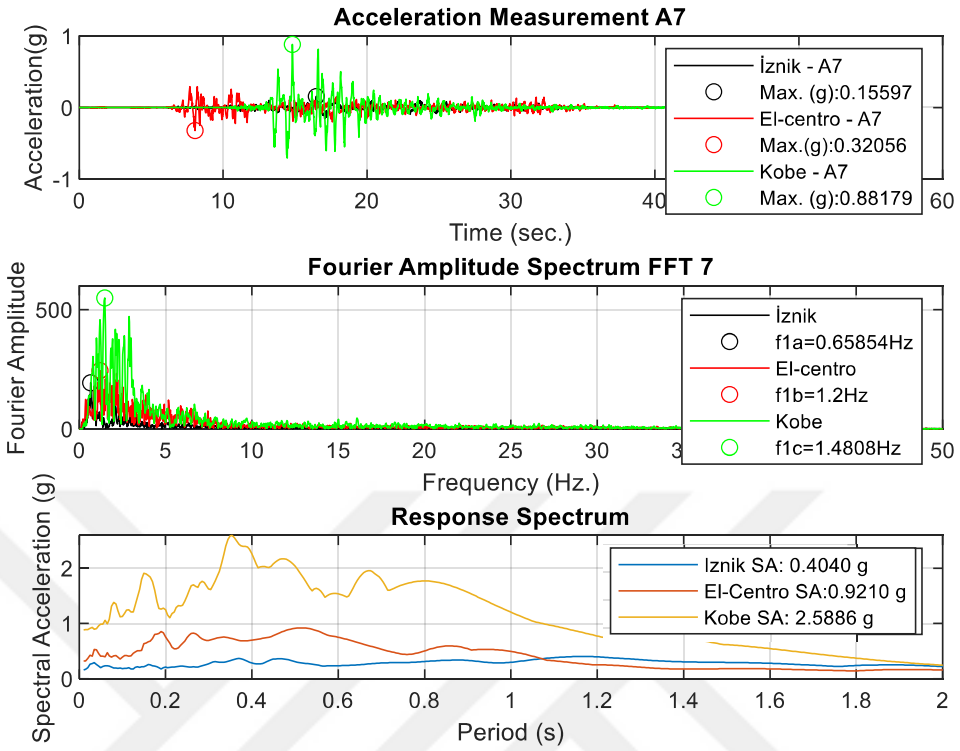



Figure 4-2. CASE 1: Time-history, Fourier amplitude spectrum, response spectrum graphs for A7 under all Earthquake motions.

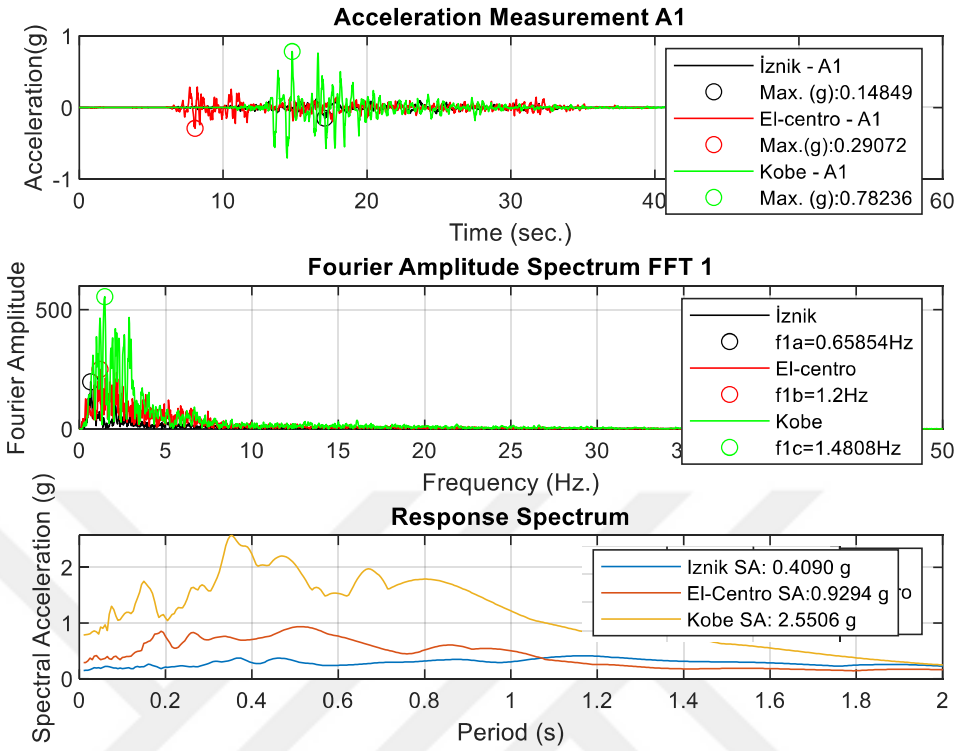



Figure 4-3. CASE 1: Time-history, Fourier amplitude spectrum, response spectrum graphs for A1 under all Earthquake motions.

### 4.1.2. Displacement Response

The lateral displacements measured by D20 can be seen in Figures 4-4 and 4-5. The El Centro earthquake motion resulted in the largest displacement value on the pipe, 9.83 cm was measured. The Kobe earthquake motion caused a displacement of 9.25 cm, while the Kocaeli earthquake (Iznik station) resulted in a pipe displacement of 7.66 cm.

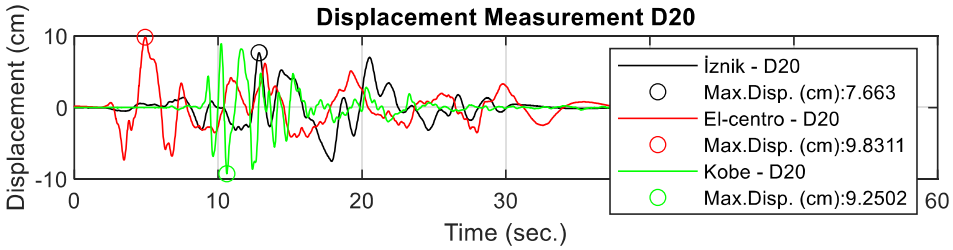



Figure 4-4. CASE 1: The displacement measurements of D20 under all Earthquake motions.

Figure 4-5 represents the lateral displacement of shaking table. The largest displacement measured under El-Centro earthquake motion with 9.52 cm.

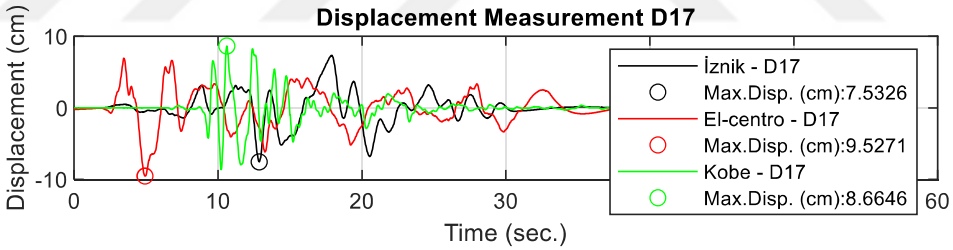



Figure 4-5. CASE 1: The displacement measurements of D17 under all Earthquake motions.

When the displacement of the shaking table under the El-Centro earthquake motion is 9.52 cm, as shown in Figure 4-4 and Figure 4-5, the displacement of the pipe is 9.83 cm. Accordingly, the displacement of the shaking table increased by 3% over that of the pipe. Similarly, under the Kobe earthquake motion, there was a 7% increase, and under the Kocaeli earthquake motion, a 2% increase in pipe displacement compared to the displacement of the shaking table.

### 4.1.3. Settlement

D19 shows the settlement of the surface of the test sample as the best scenerio. The largest settlement occurred under El-Centro earthquake with 0.42 cm.

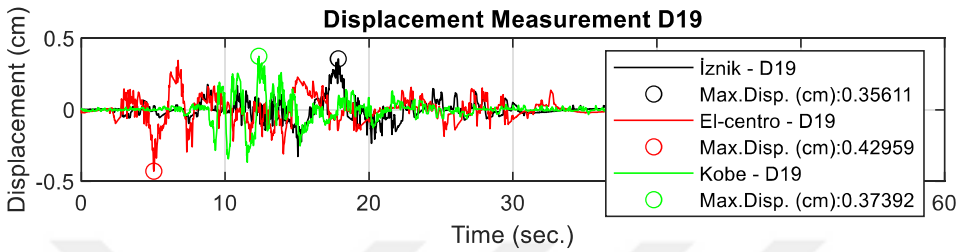



Figure 4-6. CASE 1: The displacement measurements of D19 under all Earthquake motions.

## 4.2. Case 2

The Kocaeli earthquake motion, El Centro earthquake motion, and Kobe earthquake motion were applied to the case of geogrid wrapping. The acceleration responses on pipe (A7) and close to surface (A14) compared with PGA of input motions (A1) and displacement responses are presented for the case of pipe wrapping with geogrid. The maximum acceleration and displacement responses are presented in this section.

### 4.2.1. Acceleration Response

Under the Kocaeli earthquake motion, the maximum acceleration measured close to surface (A14) was 0.158 g, showing an amplification of approximately 7% compared to the input motion. In the El Centro earthquake motion, the maximum acceleration close to surface was 0.304 g, indicating a minimal 2% amplification compared to the actual. For the Kobe earthquake motion, the PGA close to surface reached 0.881 g, reflecting a 13% amplification.

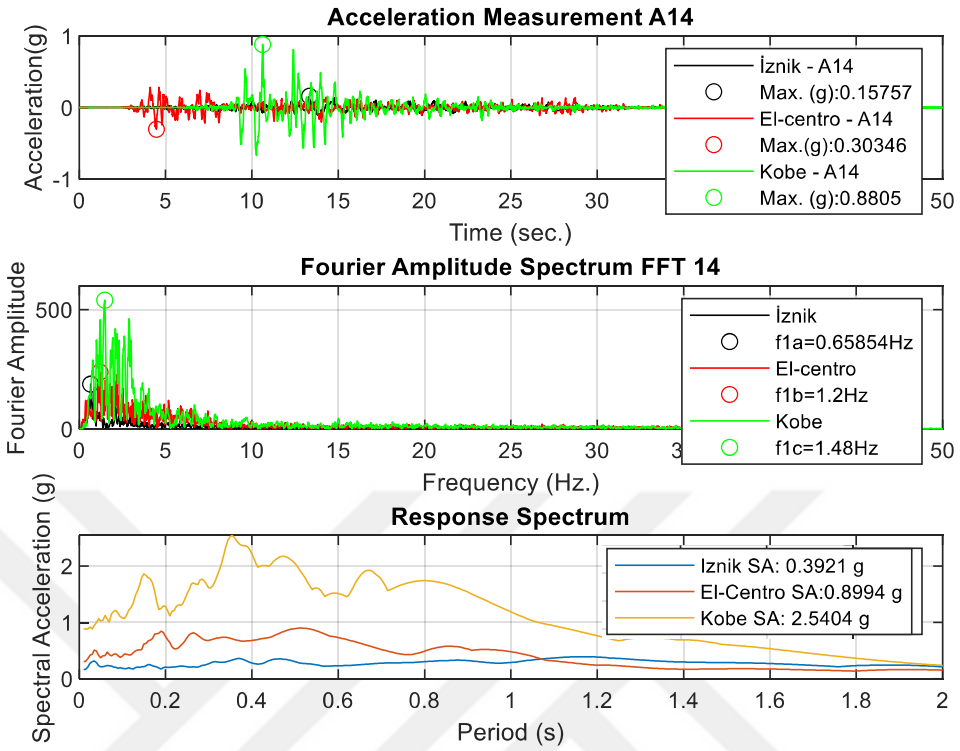



Figure 4-7. CASE 2: Time-history, Fourier amplitude spectrum, response spectrum graphs for A14 under all Earthquake motions.

The on-pipe measurements (A7) show different amplification patterns. In the Kocaeli earthquake, the PGA was 0.151g, with a slight 2% amplification. Under the El Centro earthquake motion, a recording of 0.3061g at A7 showed a 3% amplification. In contrast, under the Kobe earthquake has the highest amplification on the pipe, with the maximum acceleration increasing to 0.9350 g, marking a 20% amplification.

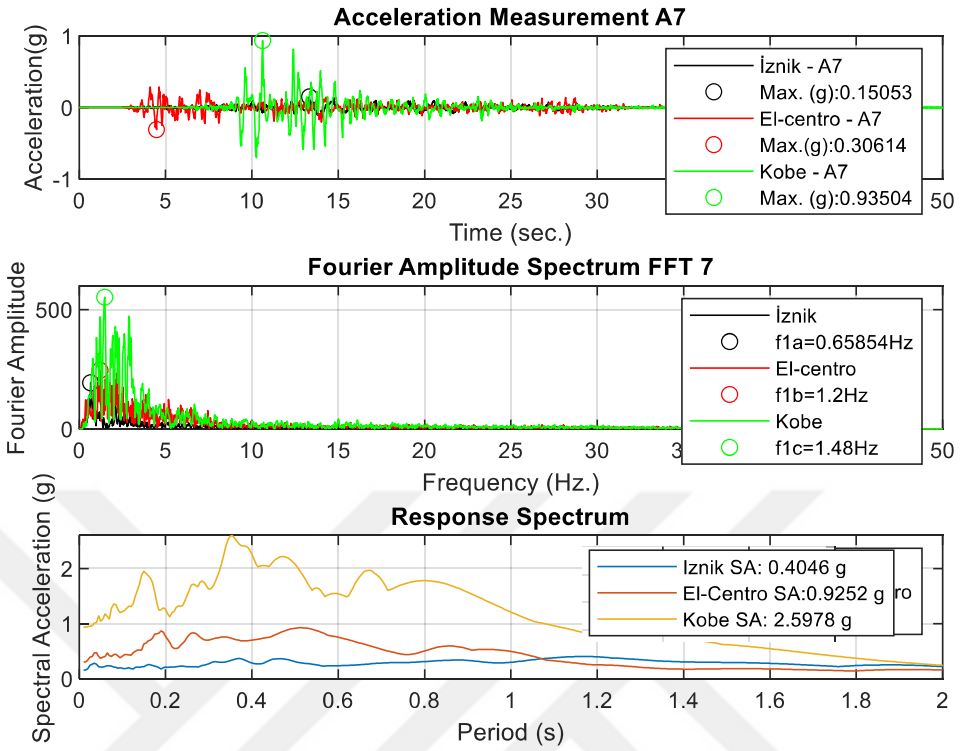



Figure 4-8. CASE 2: Time-history, Fourier amplitude spectrum, response spectrum graphs for A7 under all Earthquake motions.

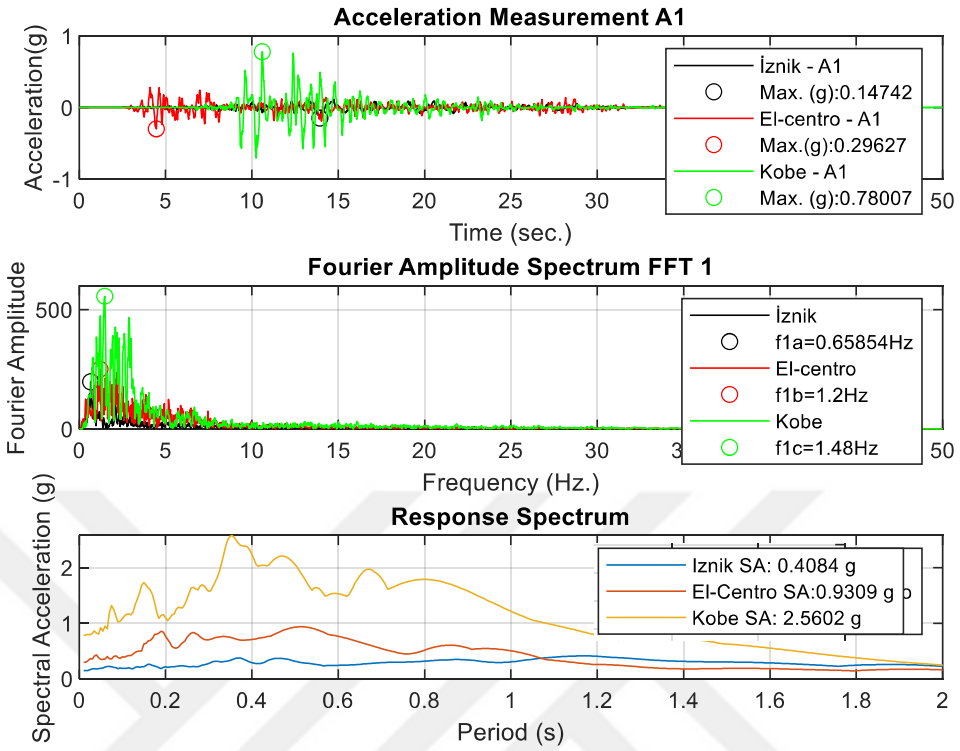



Figure 4-9. CASE 2: Time-history, Fourier amplitude spectrum, response spectrum graphs (A1) for all Earthquake motions.

### 4.2.2. Displacement Response

Figure 4-10 shows lateral displacement of the shaking table for all earthquake motions. The largest displacement was measured under the El-Centro earthquake motion, recorded as 9.61 cm.

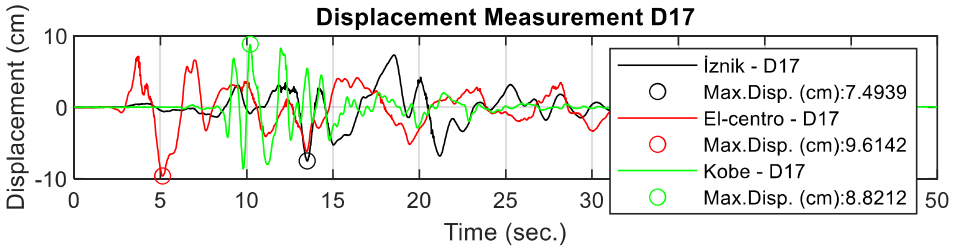



Figure 4-10. CASE 2: The displacement measurements of D17 under all Earthquake Motions.

The horizontal pipe displacement occurs in the case 2 shown in Figure 4-11.

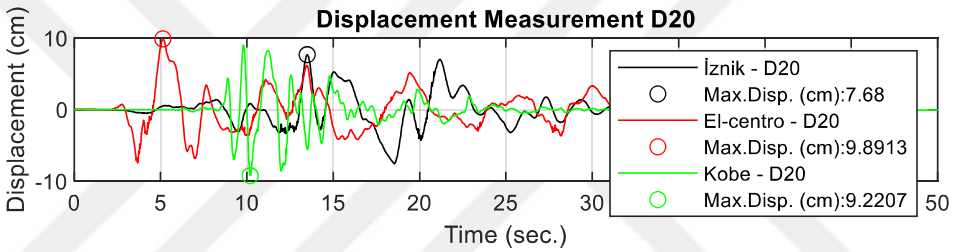



Figure 4-11. CASE 2: The displacement measurements of D20 under all Earthquake Motions.

When the displacement of the shaking table under the El-Centro earthquake motion is 9.61 cm, as shown in Figure 4-10 and Figure 4-11, the displacement of the pipe is 9.89cm. Accordingly, the displacement of the shaking table increased by 3% over that of the pipe. Similarly, under the Kobe earthquake, there was a 5% increase in displacement, and under the Kocaeli earthquake, a 2% increase in displacement from the shaking table to the pipe.

### 4.2.3. Settlement

In Figure 4-12, D19 shows the surface settlement of the Case 2. The largest settlement was observed under the El Centro earthquake motion, measured as 1.19 cm,

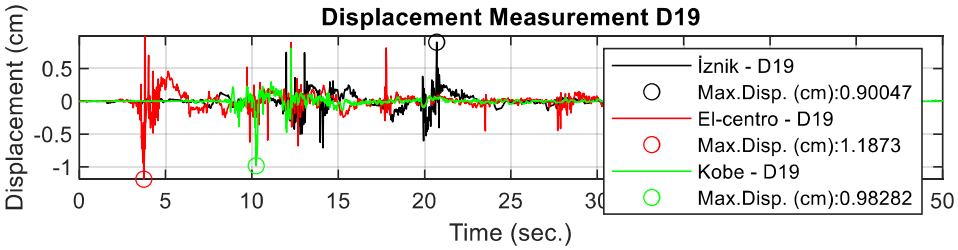



Figure 4-12. CASE 2: The displacement measurements of D19 under all Earthquake Motions.

## 4.3. Case 3

In this configuration, one layer of geogrid is placed beneath the pipe, while one layer is positioned above it. This section presents the resulting acceleration, displacement responses and settlement of the surface.

### 4.3.1. Acceleration Response

In the Figure 4-13, Figure 4-14 and Figure 4-15, maximum acceleration values values for the Kocaeli, El Centro, and Kobe earthquake motions are analysed based on their amplification close to surface (A14) compared to the earthquake's actual maximum acceleration values of input motions.

Under the Kocaeli earthquake motion, the surface maximum acceleration (A14) was 0.1464 g, almost identical to the earthquake's actual maximum acceleration of 0.146g, indicating no significant amplification at the surface. Under the El Centro earthquake motion, the PGA close to surface (A14) was 0.303g, reflecting 4% amplification compared to the actual earthquake maximum acceleration of 0.291g.

Under the Kobe earthquake motion, the surface maximum acceleration was 0.9248 g, showing a more considerable 21% amplification over the earthquake's actual maximum acceleration of 0.7655. The Kobe earthquake motion exhibited the largest amplification at close to the surface, particularly highlighting the significant increase in ground motion at A14 compared to the actual maximum acceleration of input motions.

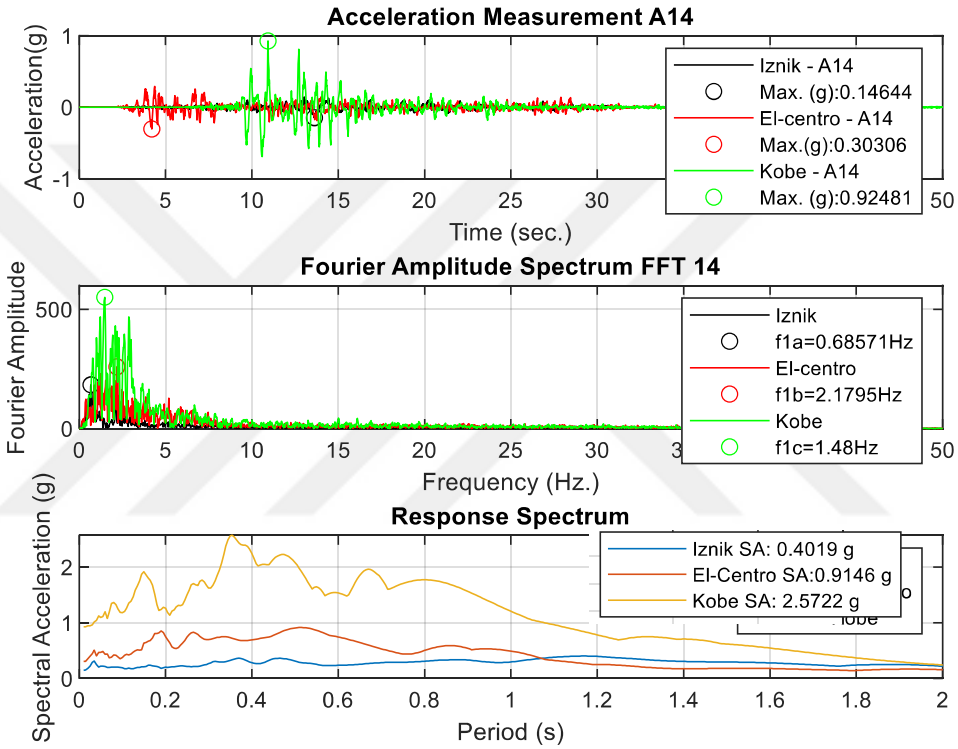



Figure 4-13. CASE 3: Time-history, Fourier amplitude spectrum, response spectrum graphs for A14 under all Earthquake motions.

In the case of the Kocaeli earthquake motion the maximum acceleration at A7 was 0.1460 g, similar to the actual maximum acceleration. Regarding El Centro earthquake motion, the pipe measurement at A7 was 0.3017 g, showing a small 4% amplification over the actual maximum acceleration. Under the Kobe earthquake motion, the maximum acceleration at A7 was 0.938 g, reflecting a significant 22% amplification compared to the earthquake's actual maximum acceleration.

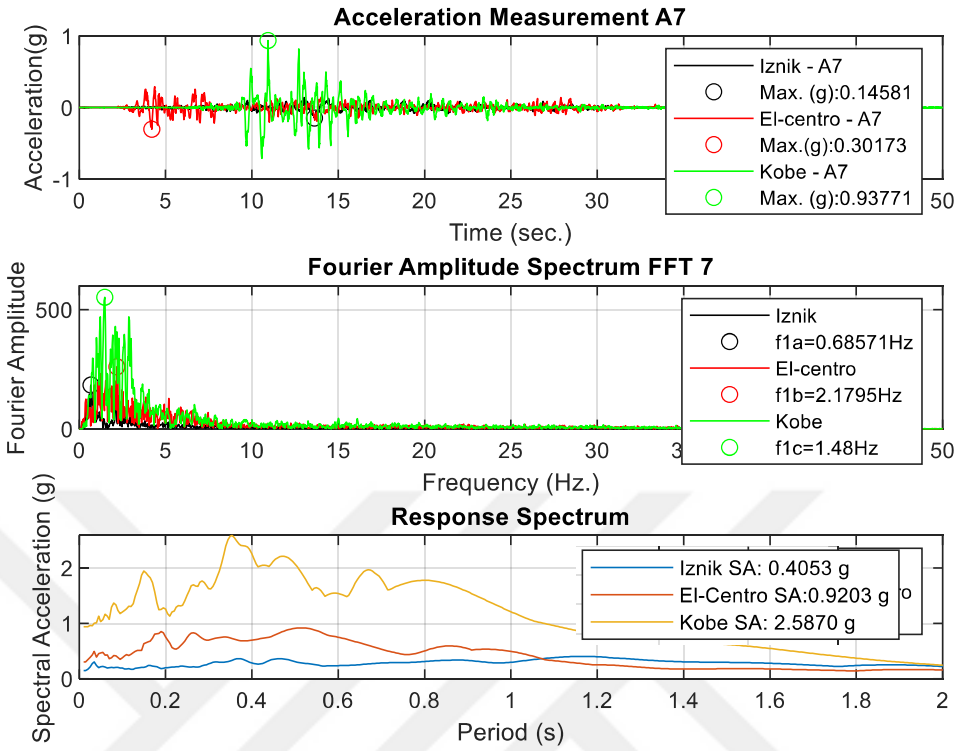



Figure 4-14. CASE 3: Time-history, Fourier amplitude spectrum, response spectrum graphs for A7 under all Earthquake motions.

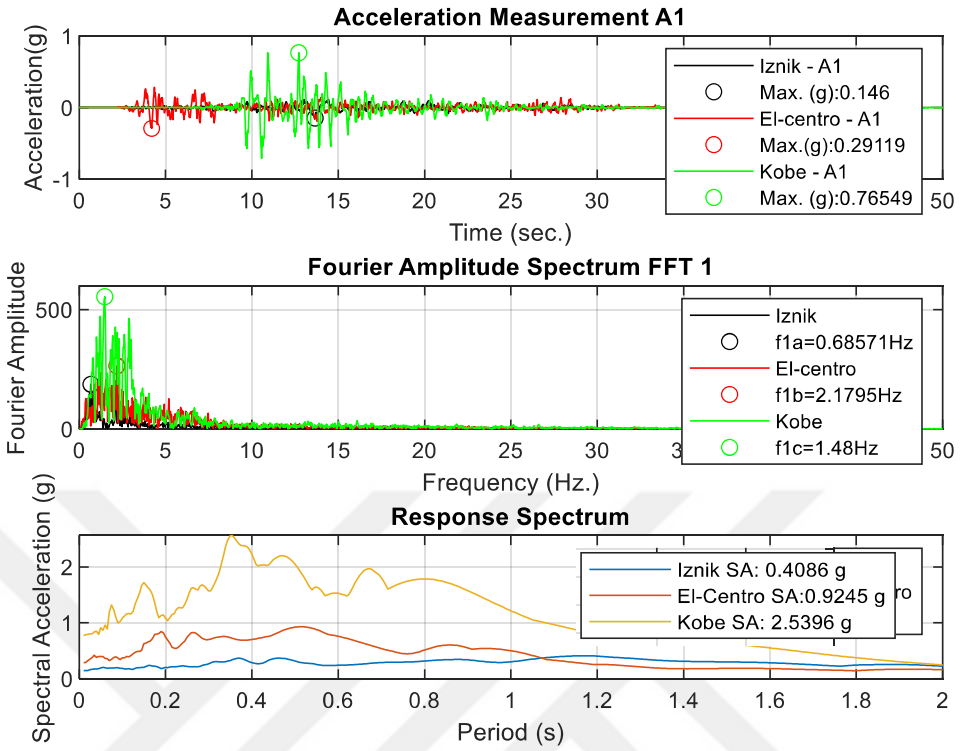



Figure 4-15. CASE 3: Time-history, Fourier amplitude spectrum, response spectrum graphs (A1) for all Earthquake motions.

### 4.3.2. Displacement Response

Figure 4-16 and Figure 4-17 represent lateral displacements of pipe and shaking table under all earthquake motions.

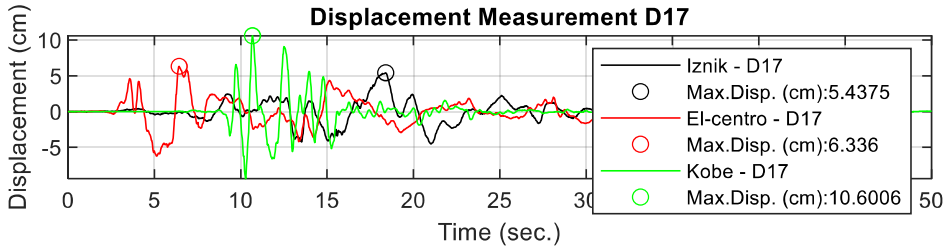



Figure 4-16. CASE 3: The displacement measurements of D17 under all earthquake motions.

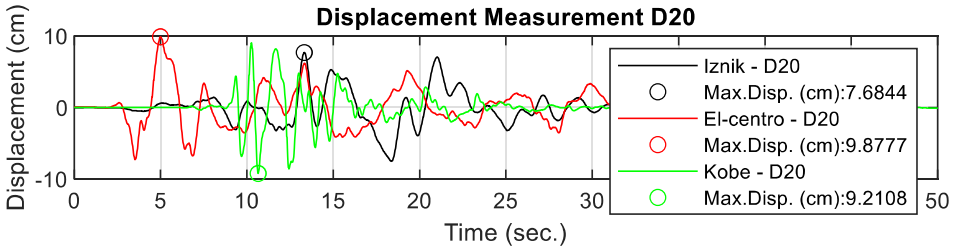



Figure 4-17. CASE 3: The displacement measurements of D20 under all earthquake motions.

As shown in Figures 4-16 and 4-17, the displacement of the shaking table increased by 41% compared to that of the pipe under the Kocaeli earthquake motion. Similarly, under the El-Centro earthquake, there was a 56% increase in displacement from the shaking table to the pipe. In contrast, under the Kobe earthquake, a 13% decrease in displacement was observed in the pipe compared to the displacement of the shaking table.

### 4.3.3. Settlement

D19 shows the surface settlement. The higher surface settlement was observed in Kobe earthquake motion in scenario of 2 layer of geogrid with 0.68 cm.

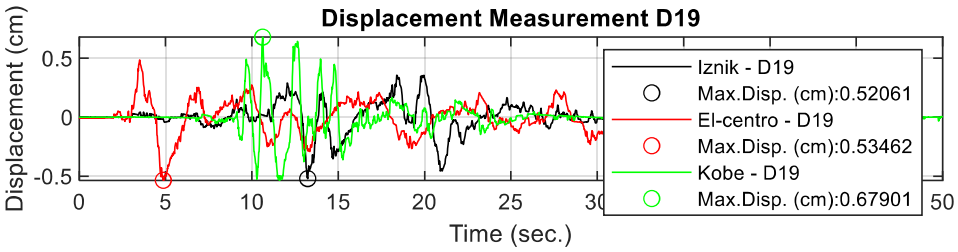



Figure 4-18. CASE 3: The displacement measurements of D19 under all earthquake motions.

## 4.4. Case 4

In this configuration, one layer of geogrid is placed below the pipe, while two layers are positioned above it. The acceleration responses on pipe (A7) and close to surface (A14) compared with maximum acceleration of input motions (A1) and displacement responses are presented for the case of three layers of geogrid. Maximum acceleration, displacement responses and settlement were presented.

### 4.4.1. Acceleration Response

Regarding the Kocaeli earthquake motion, the maximum acceleration close to surface (A14) was 0.152 g, showing a 2% amplification compared to the input motion. As for the El Centro earthquake motion, the surface maximum acceleration (A14) reached 0.323g, indicating a 10% amplification over the actual maximum acceleration of 0.294g. Under the Kobe earthquake motion, the surface maximum acceleration (A14) was 0.874g, reflecting an 11% amplification relative to the actual maximum acceleration.

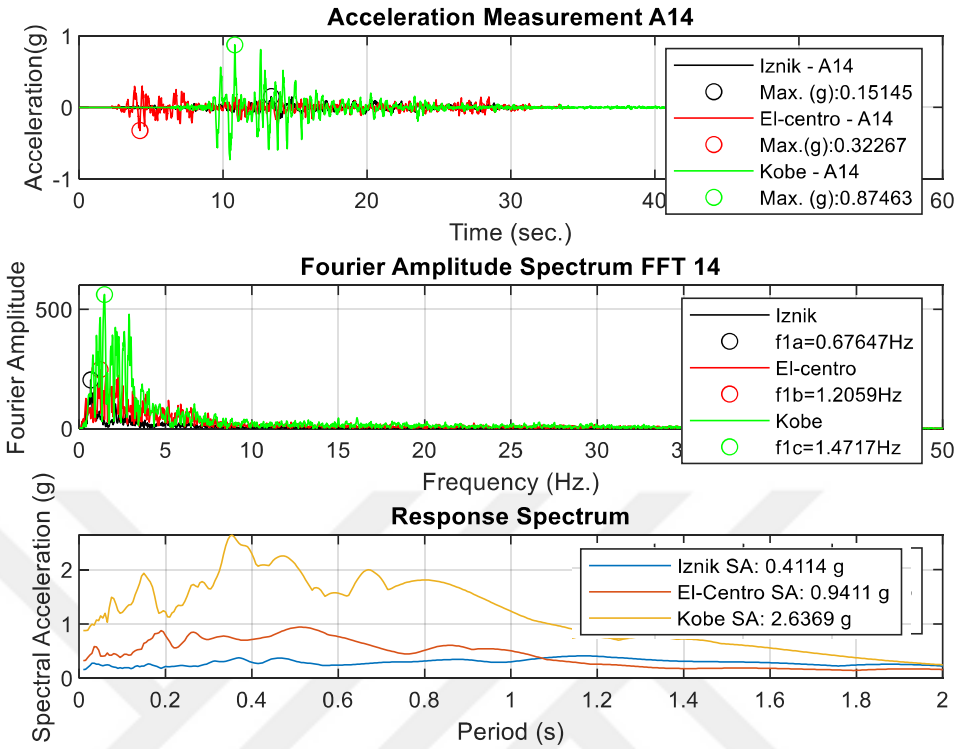



Figure 4-19. CASE 4: Time-history, Fourier amplitude spectrum, response spectrum graphs for A14 under all earthquake motions.

Under the Kocaeli earthquake motion, the maximum acceleration at A7 was 0.147 g, showing a slight deamplification of about 1% compared to the input motion (A1). Regarding the El Centro earthquake motion, the maximum acceleration on the pipe (A7) was 0.311 g, representing a 6% amplification compared to the maximum acceleration of input motion 0.294 g. Under Kobe earthquake motion, the maximum acceleration at input motion of pipe was 0.840 g, reflecting a 7% amplification compared to the input acceleration of 0.788 g.

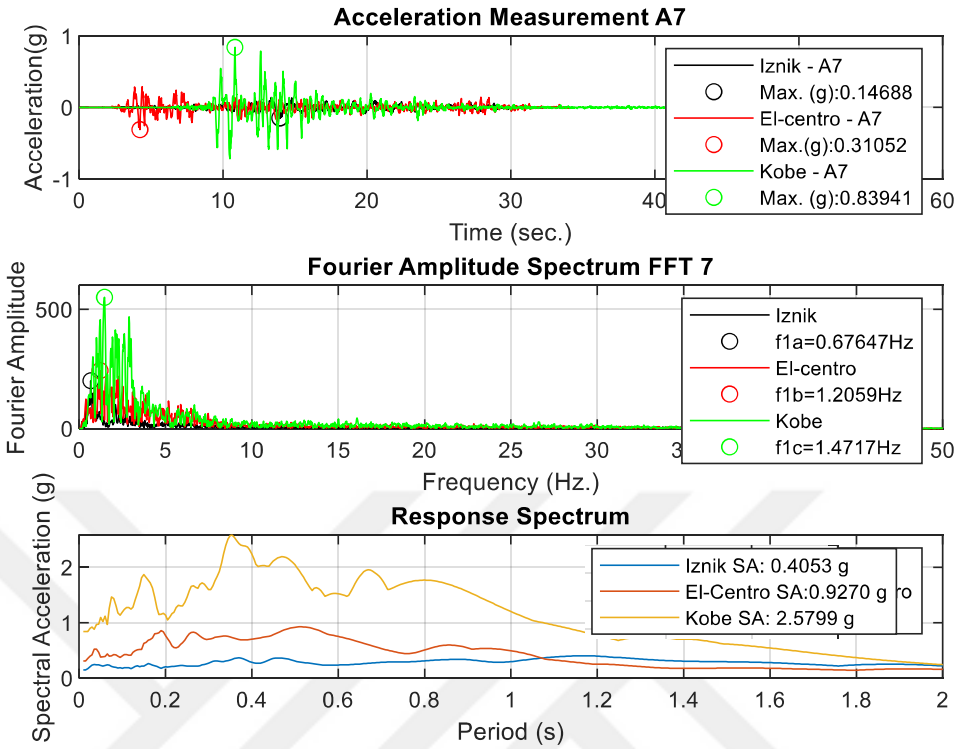



Figure 4-20. CASE 4: Time-history, Fourier amplitude spectrum, response spectrum graphs for A7 under all earthquake motions.

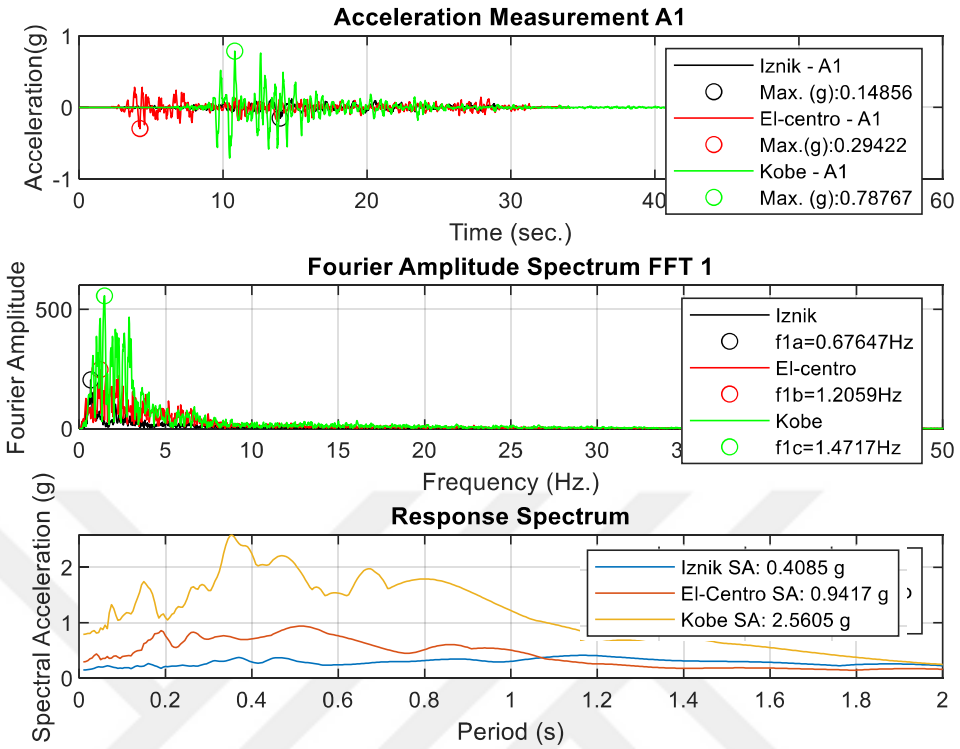



Figure 4-21. CASE 4: Time-history, Fourier amplitude spectrum, response spectrum graphs (A1) for all earthquake motions.

### 4.4.2. Displacement Response

In Figure 4-22 and Figure 4-23, soil box and horizontal pipe displacements of the pipe and shaking table were observed for all earthquake scenarios. The largest displacement values were observed for both shaking table and on pipe during the El Centro earthquake motion, measuring 9.87 cm and 9.14 cm respectively.

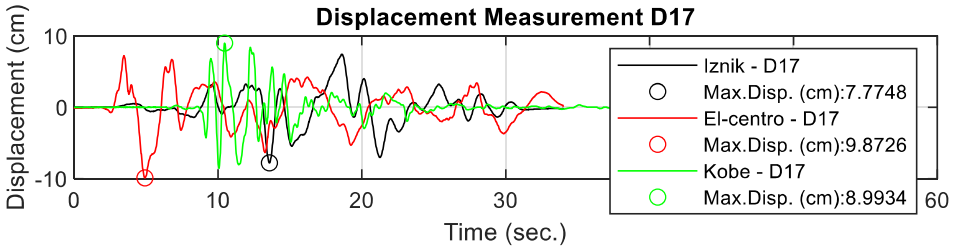



Figure 4-22. CASE 4: The displacement measurements of D17 under all Earthquake Motions.

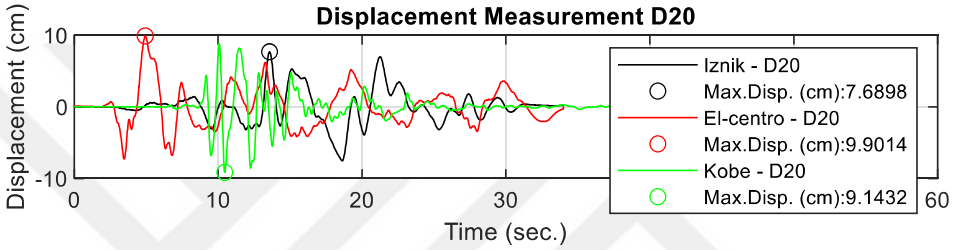



Figure 4-23. CASE 4: The displacement measurements of D20 under all Earthquake Motions.

As shown in Figures 4-22 and 4-23, the displacement of the pipe increased by 1% compared to that on the shaking table displacement under the Kocaeli earthquake motion. Under the El-Centro earthquake, there was almost no change in displacement from the shaking table to the pipe. Under the Kobe earthquake, 2% increase in displacement was observed in the pipe compared to the shaking table.

### 4.4.3. Settlement

In the Figure 4-24, D19 shows the surface settlement of the Case 4. The largest settlement was observed under the Kobe earthquake motion, measuring 0.53 cm,

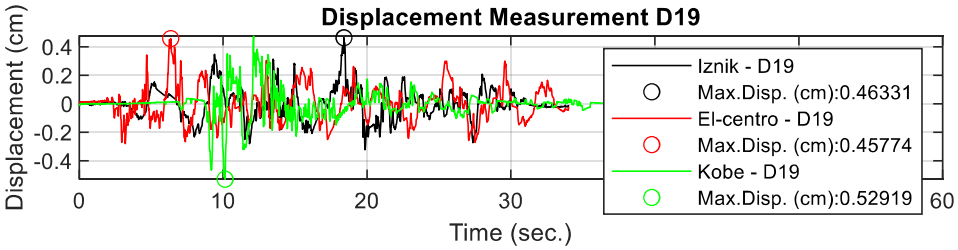



Figure 4-24. CASE 4: The displacement measurements of D19 under all Earthquake Motions.

## 4.5. Case 5

The acceleration responses on pipe (A7) and close to surface (A14) compared with PGA of input motions (A1) displacement responses and settlement are presented for the case of four layers of geogrid.

### 4.5.1. Acceleration Response

In the case of the Kocaeli earthquake motion, the maximum acceleration motion close to surface (A14) was 0.154 g, reflecting a small 3% amplification compared to the maximum acceleration of A1. Regarding the El Centro earthquake, the close to surface (A14) maximum acceleration was 0.324 g, showing an amplification of 12% over the actual maximum acceleration. Under the Kobe earthquake motion, the surface maximum acceleration (A14) reached 0.821 g, representing an 8% amplification compared to the maximum acceleration of input motion.

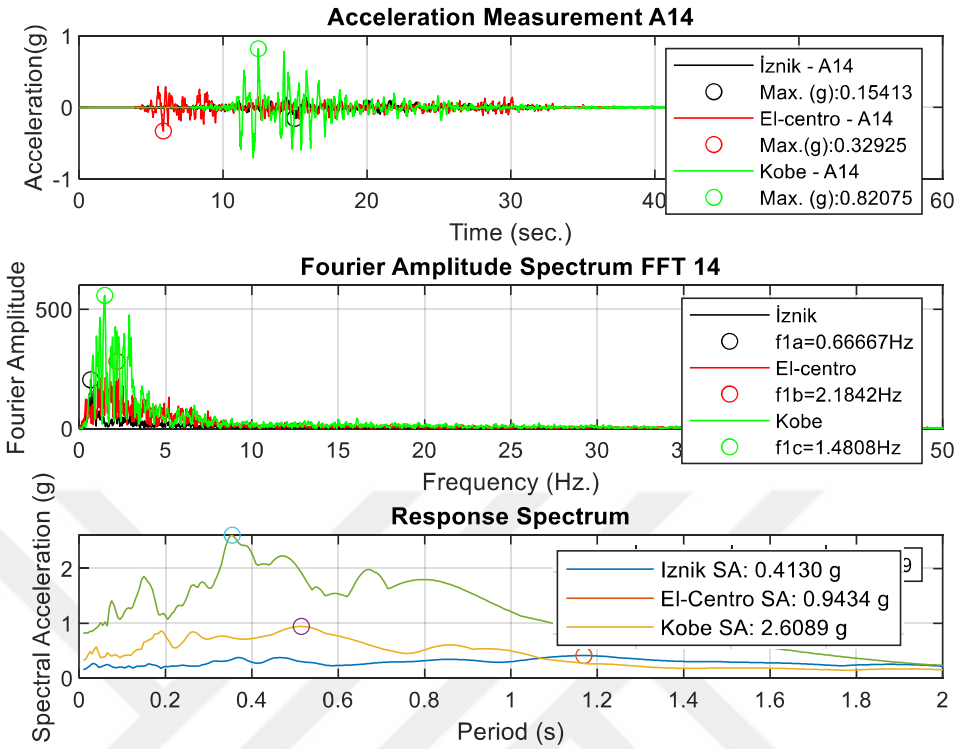



Figure 4-25. CASE 5: Time-history, Fourier amplitude spectrum, response spectrum graphs for A14 under all Earthquake motions.

Under Kocaeli earthquake motion, the maximum acceleration at A7 was 0.157 g, showing almost no change compared to the maximum acceleration motion of A1 of 0.150 g, indicating no significant amplification or deamplification. Under El Centro earthquake, the maximum acceleration on the pipe (A7) was 0.312 g, which represents a 6.1% amplification over the maximum acceleration of the input motion. Under Kobe earthquake motion, the pipe maximum acceleration was 0.793 g, reflecting a 4.5% amplification compared to the maximum acceleration of A1.

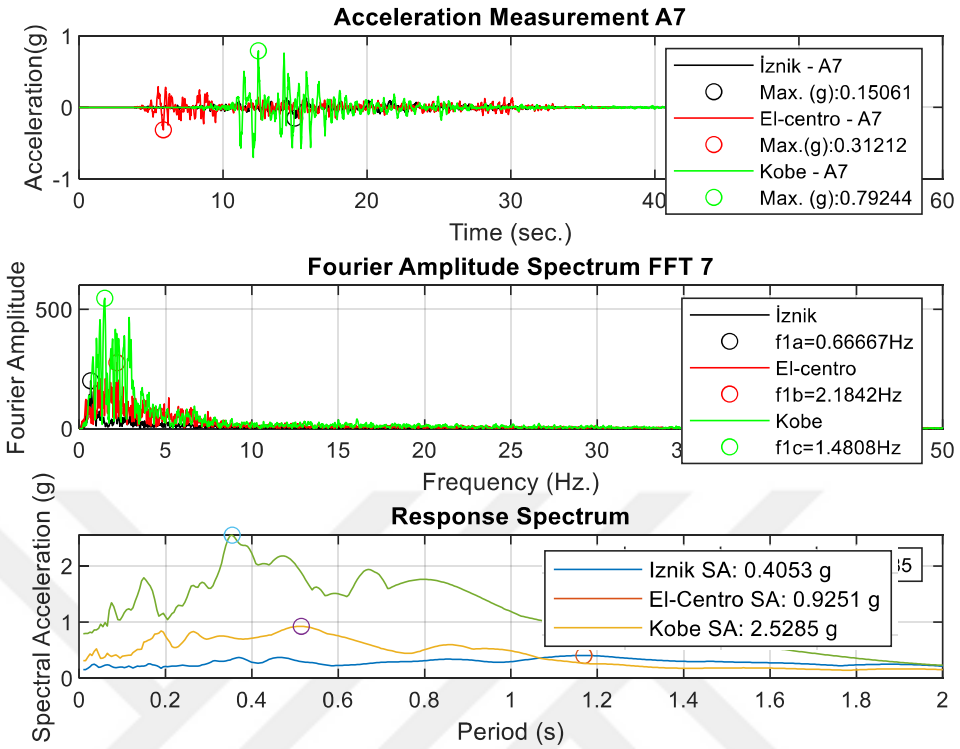



Figure 4-26. CASE 5: Time-history, Fourier amplitude spectrum, response spectrum graphs for A7 under all Earthquake motions.

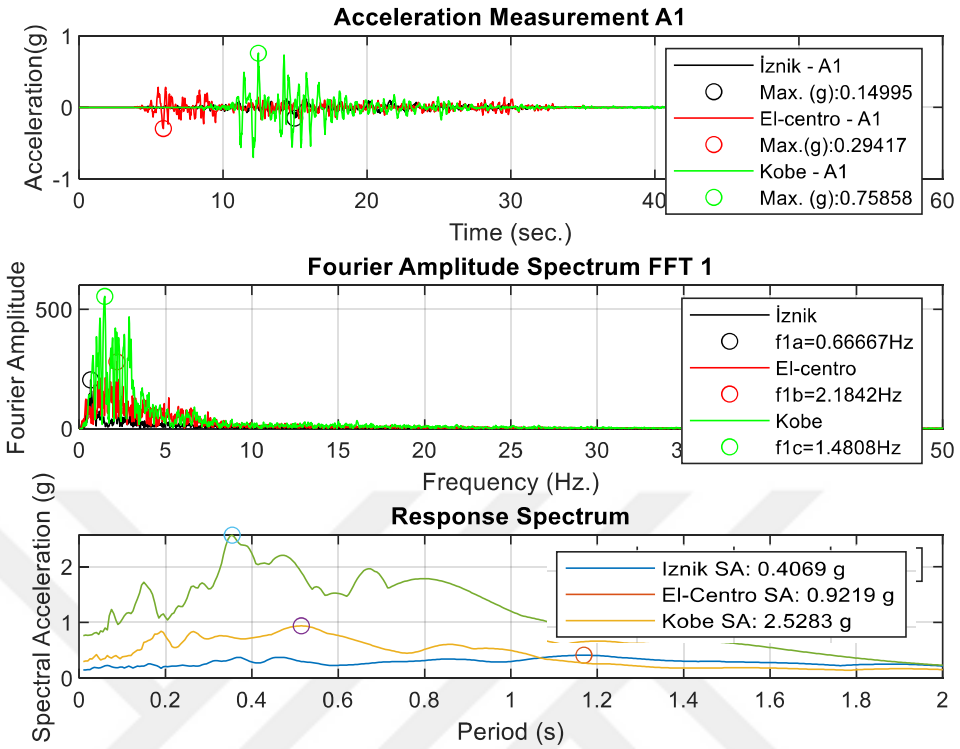



Figure 4-27. CASE 5: Time-history, Fourier amplitude spectrum, response spectrum graphs for A1 under all Earthquake motions.

### 4.5.2. Displacement Response

In Figure 4-28 and Figure 4-29, pipe displacements compared to the shaking table displacements were presented for all earthquake scenarios. The largest displacement value was obtained as 9.98 cm for shaking table under the El Centro earthquake. For lateral pipe displacement 9.94 cm was obtained for the use of four layers of geogrid.

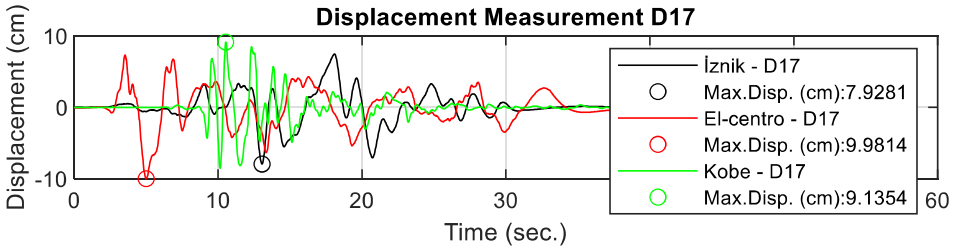



Figure 4-28. CASE 5: The displacement measurements of D17 under all Earthquake Motions.

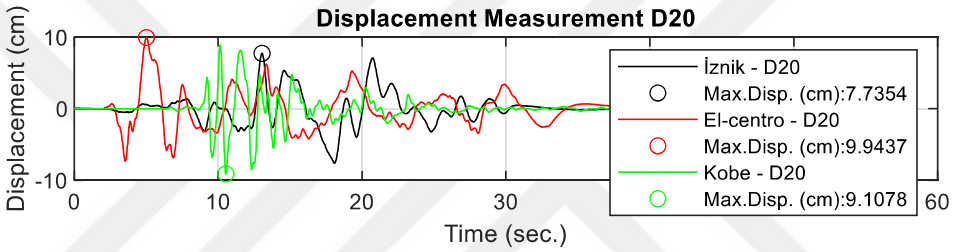



Figure 4-29. CASE 5: The displacement measurements of D20 under all Earthquake Motions.

As illustrated in Figures 4-28 and 4-29, the shaking table displacement decreased by 2% relative to that of the pipe during the Kocaeli earthquake motion. In contrast, under the El-Centro and Kobe earthquake motions, there was no change in the displacement of the pipe compared to that of the shaking table.

### 4.5.3. Settlement

In Figure 4-12, D19 shows the surface settlement of the Case 5. The largest settlement was observed during the El Centro earthquake, measuring 1.19 cm.

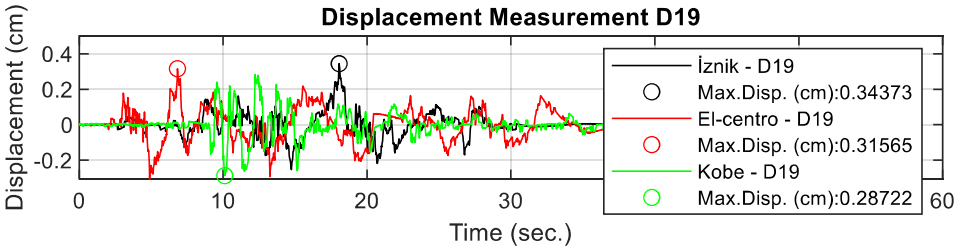



Figure 4-30. CASE 5: The vertical displacement measurements of D19 under all Earthquake Motions.

# 5. DISCUSSION AND CONCLUSION

In this chapter, the seismic performance of buried pipes with different geosynthetic reinforcement configurations is examined. A series of experiments were conducted using high-density polyethylene (HDPE) pipes, both with and without geogrid reinforcement, under various earthquake scenarios. The effects of geogrid layers on the seismic performance of the buried pipes were observed and compared.

In the following sections, the impact of geogrids on the seismic performance of buried pipes are analysed in detail. Section 5.1 focuses on the influence of geogrid arrangement type, examining how different configurations of geosynthetic reinforcement affect the pipe's response during seismic loading. Section 5.2 investigates the effect of the number of geogrid layers on improving the pipe's performance. Lastly, Section 5.3 shows the role of the earthquake's characteristics in determining the effectiveness of the geogrid reinforcement.

In order to ensure a more comprehensive understanding of the test results, instrumentation at different locations in the experimental setup was chosen for analysis. One of these is A7, positioned directly on top of the pipe, while the other is A14, located 20 cm above the pipe, close to the surface and embedded in the soil. Also, in order to conduct a more effective comparison of the displacement values for different geogrid arrangement types, displacement measurements are taken from point D20, which is located at the mouth of the pipe. D20 represents the lateral movement of the pipe in the x-direction. Similarly, D17 measures the lateral movement of the shaking table. On the other hand, D19 shows the settlement, representing the vertical displacement of the soil surface.

A total of 15 experiments were conducted using three different earthquakes. The comparisons presented in this study have been made based on the best and most observable outputs from the previously described scenarios, ensuring that the most relevant results are selected for analysis.

All evaluations were conducted using the improvement percentage formula. The improvement percentages were calculated based on the following equation: a negative percentage signifies a detrimental effect, while a positive percentage indicates an improvement.

$$\text{Improvement percentage} = \frac{(\text{Case 1} - \text{Case n})}{\text{Case 1}} \text{x} 100 \quad (5.1)$$

## 5.1. Effect Of Geogrid Arrangement Type

In this section, the differences in seismic performance improvement based on geogrid arrangement types are analysed. Specifically, the improvement variations between the wrap arrangement and the layer arrangement are compared by considering acceleration, displacement, and spectral acceleration. Specifically, the improvement variations between Case 2 (pipe fully wrapped with geogrid) and Case 3 (one layer of geogrid below and above the pipe) are compared.

To ensure more clearer observation of the results, the Kocaeli and El Centro earthquake records were selected for analysis as they represent the best scenarios, providing more definitive and reliable results.

### 5.1.1. Acceleration Response

5.1.1.1. Comparison of Case 2 and Case 3 on-Pipe under Kocaeli Earthquake Motion. The Figure 5-1 and Figure 5-2 illustrate the acceleration recorded at the top of the pipe sensor (A7) under the Kocaeli earthquake (Iznik station) motion.

As shown in the section 4, the maximum acceleration for the control case (A1) is 0.156g. According to Figure 5-1 and Figure 5-2, the acceleration values recorded for the Kocaeli earthquake motion by sensors located on top of the pipe show that there is an

improvement of 3.49% in Case 2 and 6.52% in Case 3, when compared to the control case (Case 1)

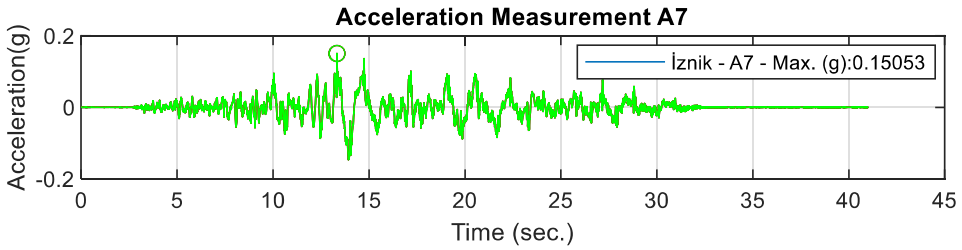



Figure 5-1. Time history for Case 2 (on pipe) under Kocaeli Earthquake (Iznik station).

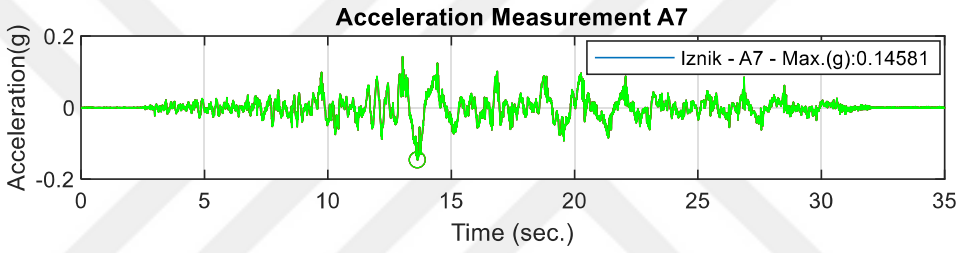



Figure 5-2. Time history for Case 3 (on pipe) under Kocaeli Earthquake motion (Iznik station).

5.1.1.2. Comparison of Case 2 and Case 3 on-Pipe under El-Centro Earthquake Motion.

When analysing the graphs for the El Centro earthquake (Imperial Valley station) in Figure 5-3 and 5-4, where the control case maximum acceleration is 0.321g, Case 2 shows a 4.5% improvement compared to Case 1, while Case 3 shows a 5.88% improvement.

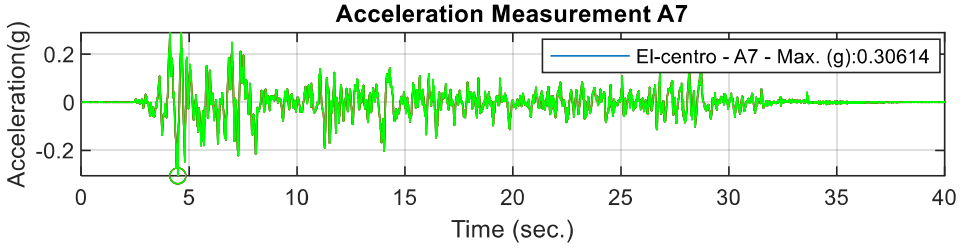



Figure 5-3. Time history for Case 2 (on pipe) under El-Centro Earthquake motion (Imperial Valley station).

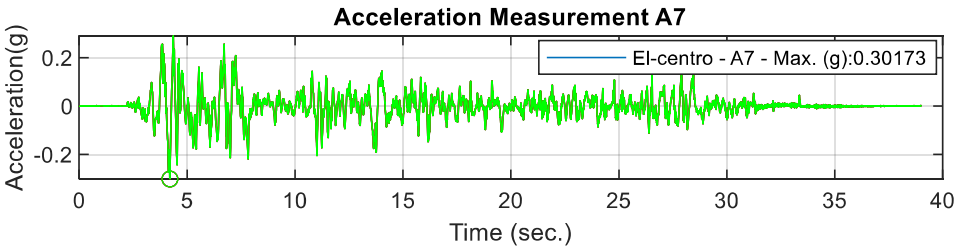



Figure 5-4. Time history for Case 3 (on pipe) under El-Centro Earthquake motion (Imperial Valley station).

So, these results indicate that, for the accelerometers positioned on top of the pipe, using a layered geogrid arrangement is more effective than fully wrapping the pipe with geogrid.

5.1.1.3. Comparison of Case 2 and Case 3 for Close to Surface under Kocaeli Earthquake Motion. The Figures 5-5 and Figures 5-6 present the time history recorded by the sensor located 20 cm above the pipe (A14) under the El Centro and Kocaeli earthquake motions. Under Kocaeli earthquake motion, the control case recorded maximum acceleration value of 0.169g for the sensor located in the upper layer (A14). Compared to the control case (Case 1), the wrapping geogrid case shows an improvement of 6.95%, while the layered geogrid case shows an improvement of 13.53%.

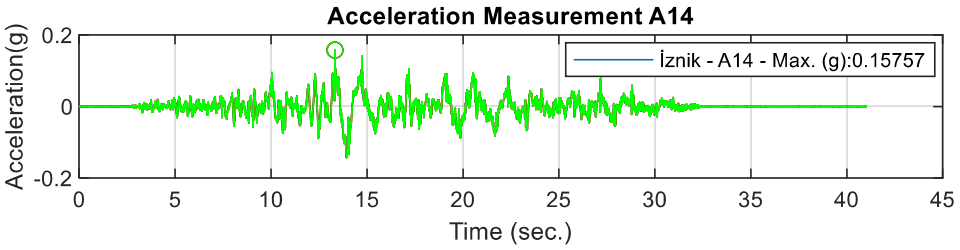



Figure 5-5. Time history for Case 2 (close to surface) under Kocaeli Earthquake motion (Iznik station).

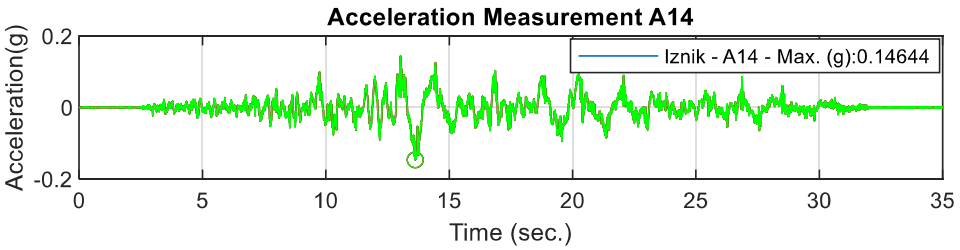



Figure 5-6. Time history for Case 3 (close to surface) under Kocaeli Earthquake motion (Iznik station).

5.1.1.4. Comparison of Case 2 and Case 3 for Close to Surface under El-Centro Earthquake Motion. As mentioned in Section 4, under the El Centro earthquake motion, the control case (without geogrid) recorded a value of 0.349g for the same sensor (A14). In comparison to the control case, the improvement in the wrapping geogrid case is 13.07%, while the improvement in the layered geogrid case is 13.19%. These values are quite similar, indicating that both geogrid configurations can be effective in enhancing seismic performance.

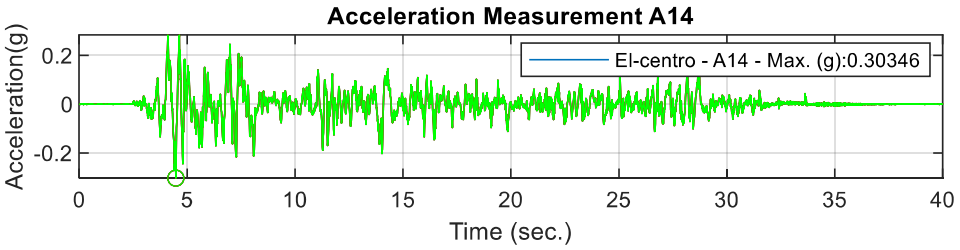



Figure 5-7. Time history for Case 2 (close to surface) under El-Centro Earthquake motion (Imperial Valley station).

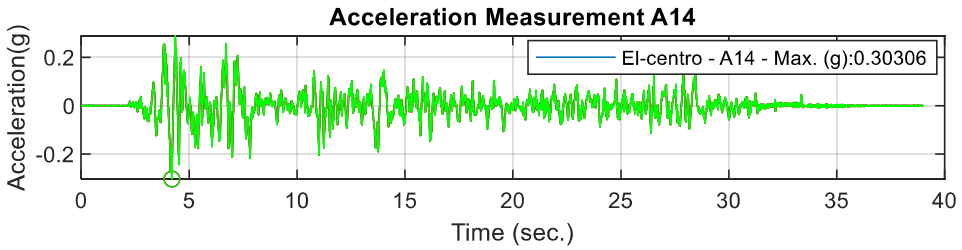



Figure 5-8. Time history for Case 3 (close to surface) under El-Centro Earthquake motion (Imperial Valley station).

### 5.1.2. Displacement Response

The comparison was made to observe the effects of different geogrid arrangement types, specifically wrapping and layered configurations, on the horizontal displacement behaviour.

In the following graphs, the lateral movement at D20 has been analysed, with the selected best scenarios focusing particularly on the Kobe and El Centro earthquake motions. These observations show the behaviour of the pipe's mouth under seismic events, in terms of lateral displacements. The analysis shows the response of the pipe structure to seismic forces by offering a detailed understanding of how the geogrid arrangement can influence the displacement.

5.1.2.1. Comparison of Pipe Displacement in Case 2 and Case 3 under El-Centro Earthquake Motion. According to the data presented in Figure 5-9 for El-Centro earthquake motion, the sensor on the pipe indicates a change of 0.61% for the pipe wrapping in comparison to the control case, while the layered geogrid arrangement has a change of 0.47%.

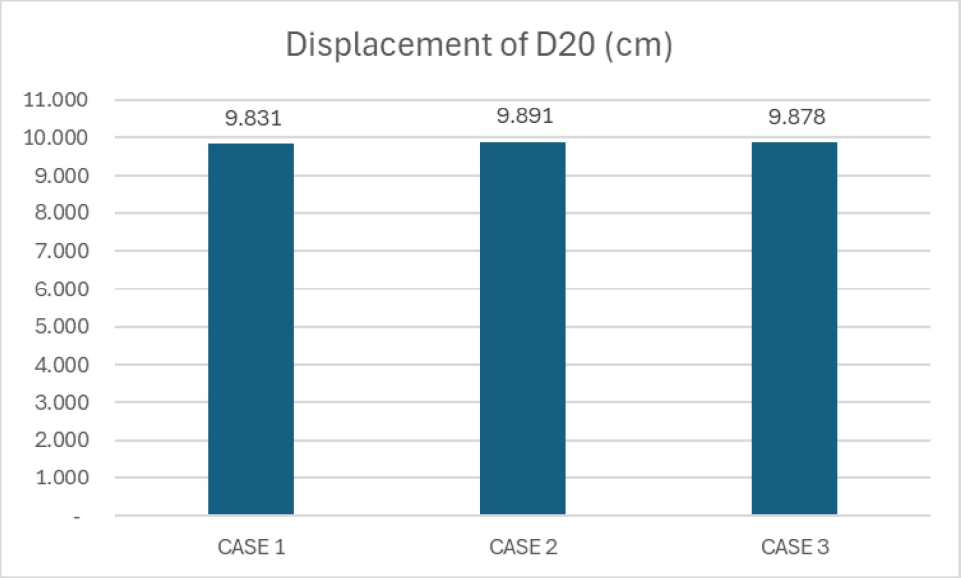



Figure 5-9. Maximum horizontal pipe displacements for Case 1, Case 2, and Case 3 under El-Centro Earthquake motion.

5.1.2.2. Comparison of Pipe Displacements in Case 2 and Case 3 under Kobe Earthquake Motion. Similarly, when considering the Kobe earthquake motion, displacement data shows that pipe wrapping exhibits an improvement of 0.32%, while the layered geogrid shows an improvement of 0.43%.

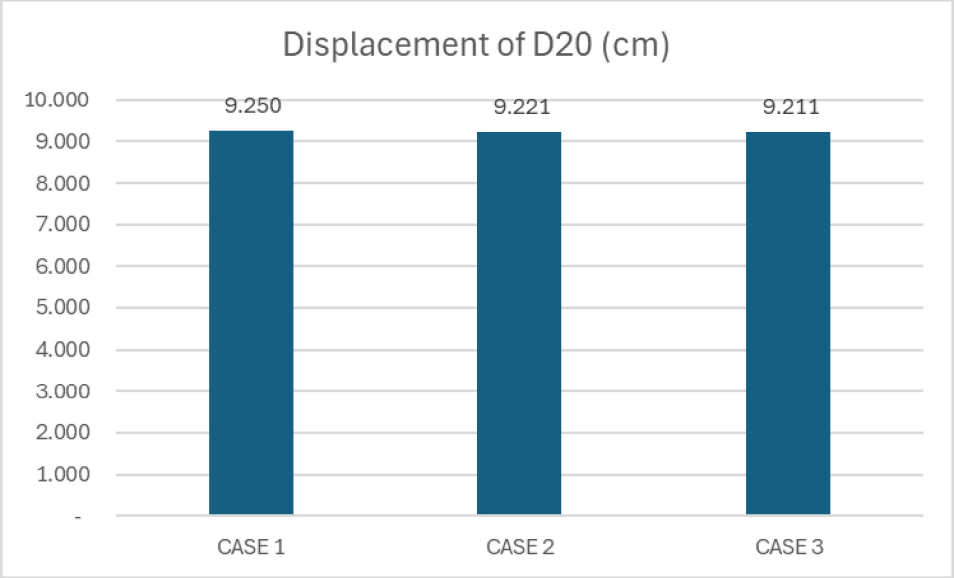



Figure 5-10. Maximum horizontal pipe displacement for Case 1, Case 2, and Case 3 under Kobe Earthquake motion.

These findings suggest that the inclusion of the geogrid has a limited impact on displacement.

### 5.1.3. Spectral Acceleration

Spectral acceleration indicates how the pipe responds to seismic loads at various vibration periods. To summarize the findings for the three earthquakes, the Kocaeli and Kobe earthquake motion were selected as the best results obtained.

5.1.3.1. Comparison of Spectral Acceleration Close to Surface for Case 2 and Case 3 under Kocaeli Earthquake Motion. Comparison of the spectral acceleration for different geogrid arrangement types, calculated from a close to surface accelerometer placed at various depths under the Kocaeli earthquake. Case 2 and Case 3 exhibit almost identical spectral acceleration (SA) values, both reaching approximately 0.405 g at a period of 1.69 seconds as given in Figure 5-11, Figure 5-12, and Figure 5-13.

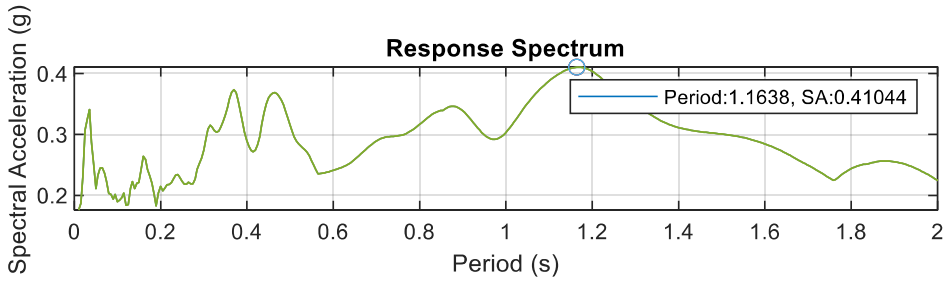



Figure 5-11. Response spectrum for A14 (close to surface), Case 1 under Kocaeli Earthquake motion.

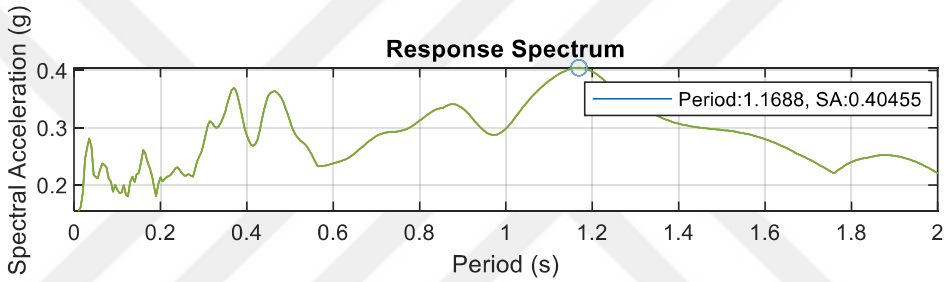



Figure 5-12. Response spectrum for A14 (close to surface), Case 2 under Kocaeli Earthquake motion.

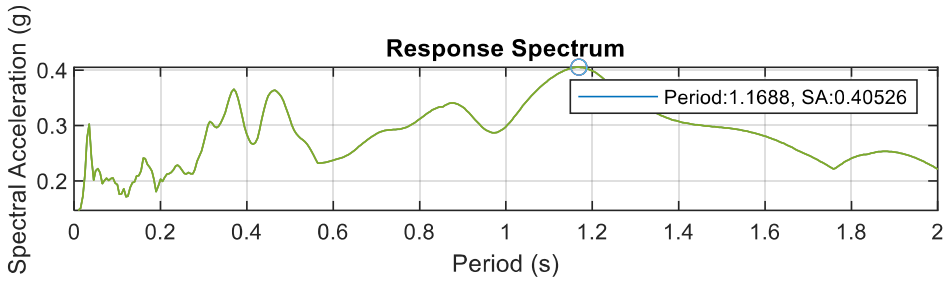



Figure 5-13. Response spectrum for A14 (close to surface), Case 3 under Kocaeli Earthquake motion.

5.1.3.2. Comparison of Spectral Acceleration on Pipe for Case 2 and Case 3 under Kobe Earthquake motion. The spectral acceleration values obtained from sensor on pipe (A7) under the Kobe Earthquake motion are as follows: Case 1 recorded a value of 2.589 g, Case 2 recorded 2.598 g, and Case 3 recorded 2.587 g as shown in Figure 5-14, Figure 5-15 and Figure 5-16.

To evaluate the improvement performance, the percentage change for both Case 2 and Case 3 relative to Case 1 was calculated. Case 2 exhibits a slight improvement of approximately 0.35% compared to Case 1, indicating a minor enhancement in seismic performance. Conversely, Case 3 demonstrates a small reduction in spectral acceleration, with a negligible decrease of about 0.08% compared to Case 1.

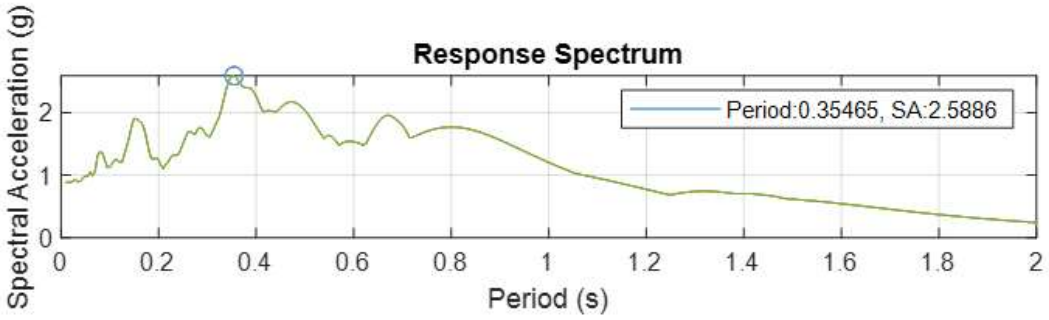



Figure 5-14. Response spectrum for A7 (on pipe), Case 1 under Kobe Earthquake motion.

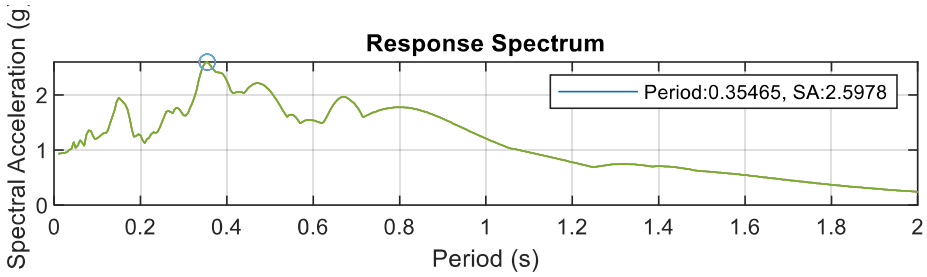



Figure 5-15. Response spectrum for A7 (on pipe), Case 2 under Kobe Earthquake.

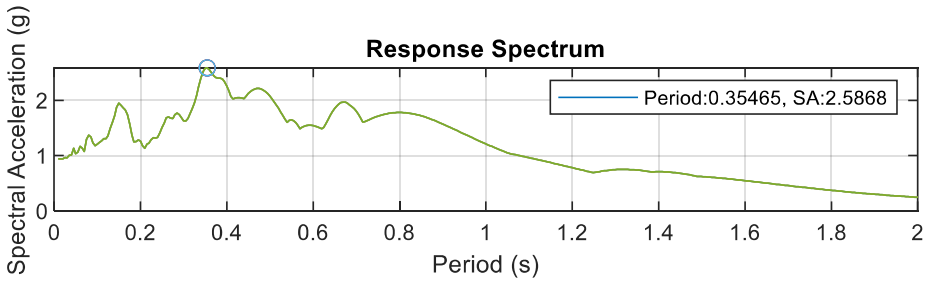



Figure 5-16. Response spectrum for A7 (on pipe), Case 3 under Kobe Earthquake.

In summary, Case 2 demonstrates a small positive change in spectral acceleration, while Case 3 shows no significant improvement relative to Case 1. There is no significant variation in the spectral acceleration values between Case 1, Case 2, and Case 3, indicating that there is no notable improvement among the cases.

### 5.1.4. Effect of Geogrid Configuration with Depth

This section examines the changes in geogrid configurations and their relationship with depth under seismic conditions within the soil sample, focusing on the El Centro earthquake scenario, which demonstrated the best performance. Using data from the El Centro earthquake motion, acceleration values at different depths were analysed to assess the impact of geogrid configurations (wrapping and layered) on accelerations.

Sensor A7 is positioned on the pipe, while A14 is located 20 cm above the pipe. Additionally, A1 measures the maximum acceleration from the shaking table. The results indicate that the maximum acceleration on the pipe closely aligns with that of the shaking table across all cases as shown in Figure 5-17. Moreover, the graphs show similar results for both the wrapped pipe with geogrid and the layered geogrid configurations.

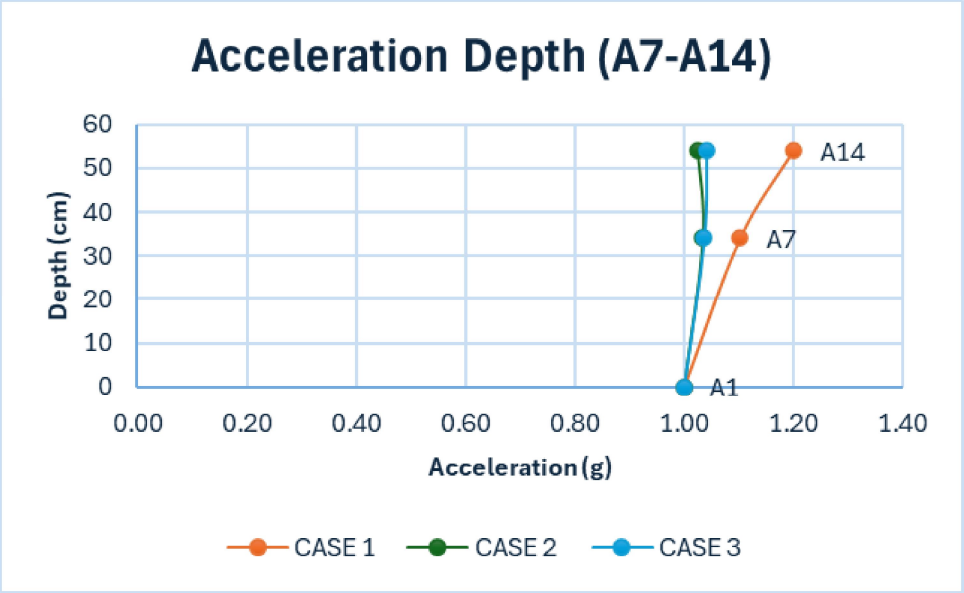



Figure 5-17. Variation of acceleration with depth under El-Centro Earthquake motion for Case 1, Case 2 and Case 3.

Figure 5-17 shows that the maximum acceleration values on top of the pipe are closer to the maximum acceleration of the input motion (A1). However, the most significant increase has occurred at the surface.

## 5.2. Effect Of Geogrid Layer Number

In order to understand the influence of geogrid reinforcement on the seismic performance of buried pipelines, an additional analytical investigation was conducted. This section focuses on evaluating the effects of varying the number of geogrid layers used as reinforcement for the pipe. This part covers to analyse whether an increase in the number of geogrid layers correlates with improvements in the seismic response of the buried pipes.

In this part, the effect of the number of geogrid layer investigated by comparing the maximum input acceleration, displacement measurements and spectral acceleration values obtained from analyses of Case 3 with two layers, Case 4 with three layers, and Case 5 with four layers.

### 5.2.1. Acceleration Response

5.2.1.1. Comparison of Case 3, Case 4 and Case 5 for Close to Surface under Kocaeli Earthquake Motion. Maximum acceleration values are generally higher at locations close to surface, the data from the A14 sensor was utilized for comparative analysis. The following examines the maximum accelerations for the Kocaeli earthquake motion considering configurations with 2, 3, and 4 layers of geogrid. Accordingly, when one layer is placed at the bottom and one layer at the top, a 6.95% improvement is observed compared to the unreinforced condition in Figure 5-18. For three layers, a 10.57% improvement is noted, and using four layers results in an 8.99% improvement as shown in Figure 5-19 and Figure 5-20.

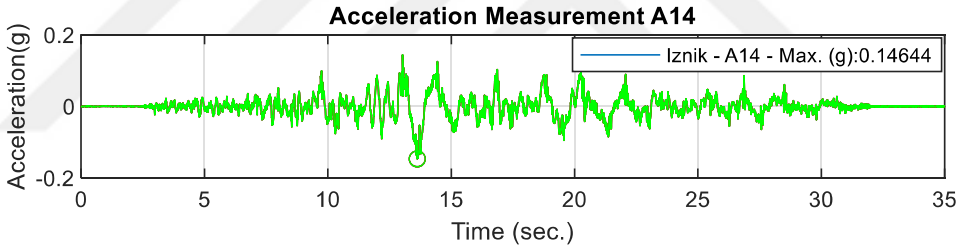



Figure 5-18. Case 3 - Time history for A14 (close to surface) under Kocaeli Earthquake motion (Iznik station).

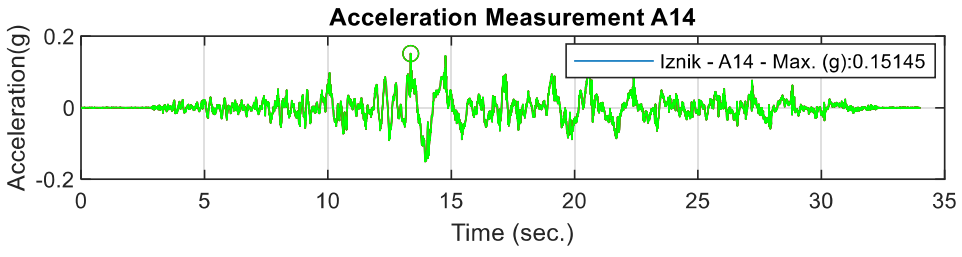



Figure 5-19. Case 4 - Time history for A14 (close to surface) under Kocaeli Earthquake motion (Iznik station).

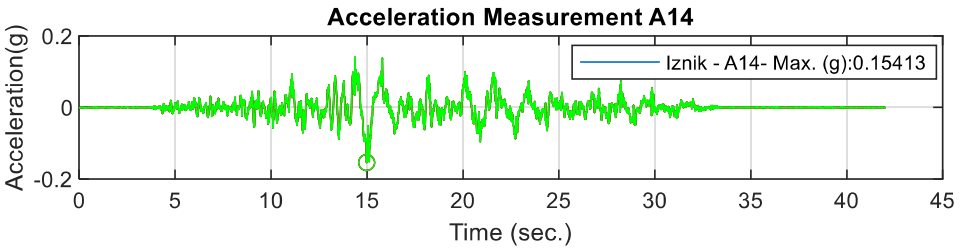



Figure 5-20 .Case 5 - Time history for A14 (close to surface) under Kocaeli Earthquake motion (Iznik station).

5.2.1.2. Comparison of Case 3, Case 4 and Case 5 for Close to Surface under El-Centro Earthquake Motion. Under the El-Centro earthquake motion, the maximum acceleration values are similar to those observed under Kocaeli earthquake motion.

When one layer is positioned at the base and another at the top, a 13.53% improvement is observed relative to the unreinforced scenario as shown in Figure 5-21. The implementation of three geogrid layers shows a 7.57% improvement, whereas the use of four layers results in a 5.68% improvement in Figure 5-22 and Figure 5-23.

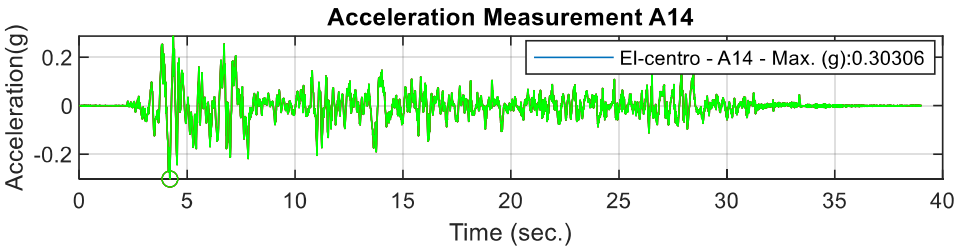



Figure 5-21. Time history for A14 (close to surface) under El-Centro Earthquake motion (Imperial Valley station) for Case 3.

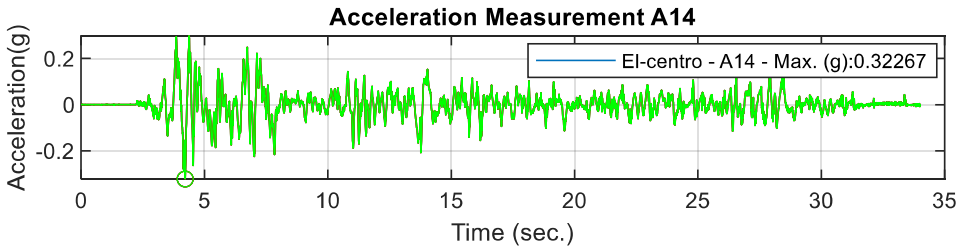



Figure 5-22. Time history for A14 (close to surface) under El-Centro Earthquake motion (Imperial Valley station) for Case 4.

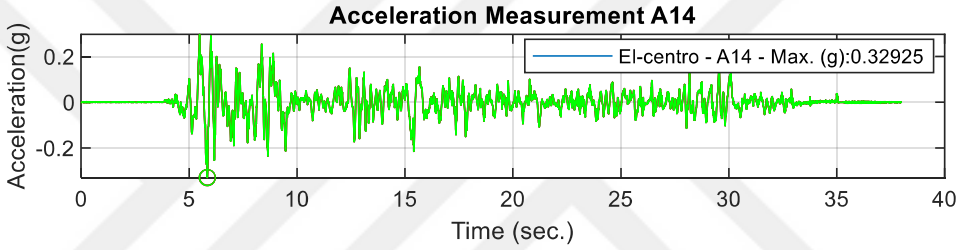



Figure 5-23. Time history for A14 (close to surface) under El-Centro Earthquake motion (Imperial Valley station) for Case 5.

5.2.1.3. Comparison of Case 3, Case 4 and Case 5 for Close to Surface under Kobe Earthquake Motion. In the case of the Kobe earthquake, the use of two layers of geogrid resulted in a 1.42% increase in acceleration. With three layers, an improvement was achieved, leading to a 4.09% increase in acceleration. The use of four geogrid layers resulted in the most significant improvement, achieving approximately a 10% increase in acceleration.

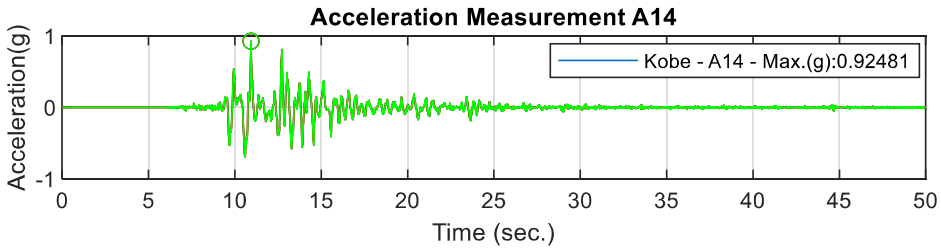



Figure 5-24. Time history for A14 (close to surface) under Kobe Earthquake motion (KJMA station) for Case 3.

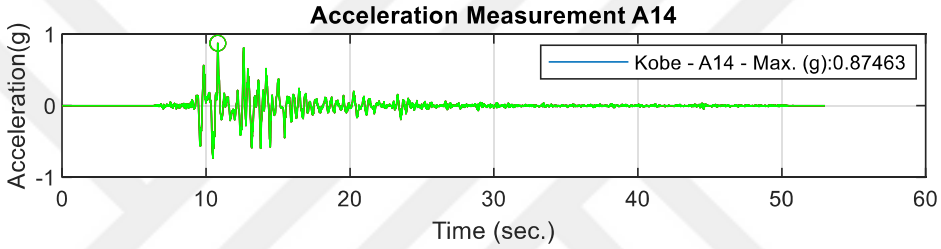



Figure 5-25 Time history for A14 (close to surface) under Kobe Earthquake motion (KJMA station) for Case 4.

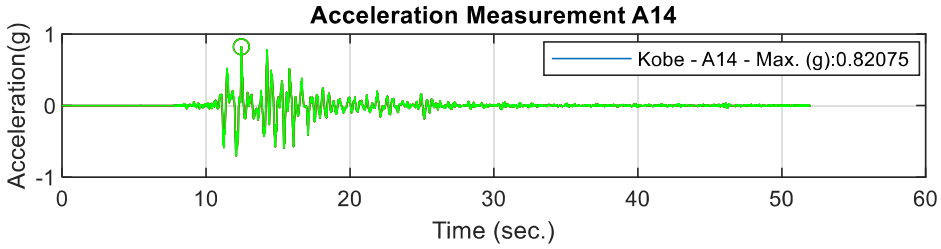



Figure 5-26. Time history for A14 (close to surface) under Kobe Earthquake motion (KJMA station) for Case 5.

### 5.2.2. Displacement Response

This section compared the effect of the number of geogrid layers on the seismic response of the buried pipe. To effectively compare the displacement values for different

number of geogrid layers, displacement measurements were taken from point D20 at the pipe end, representing lateral movement in the x-direction, while D19 indicates the vertical surface displacement (settlement) of the soil surface.

5.2.2.1. Comparison of Pipe Horizontal Displacement Between Case 1, Case 3, Case 4, and Case 5 under Kobe Earthquake Motion. The measured maximum displacement indicates a consistent reduction in displacement compared to control case in Figure 5-27. The 2-layer geogrid configuration (Case 3) shows a slight decrease of 0.32%, while the 3-layer geogrid configuration (Case 4) shows a reduction of 0.43%. The reduction becomes more significant with the 3-layer geogrid, showing a 1.16% decrease, and is most pronounced with the 4-layer geogrid configuration (Case 5), which shows a 1.54% reduction. Although these reductions are relatively small, adding more geogrid layers results in a gradual improvement in reducing maximum lateral displacement, with the 4-layer geogrid configuration showing the best improvement.

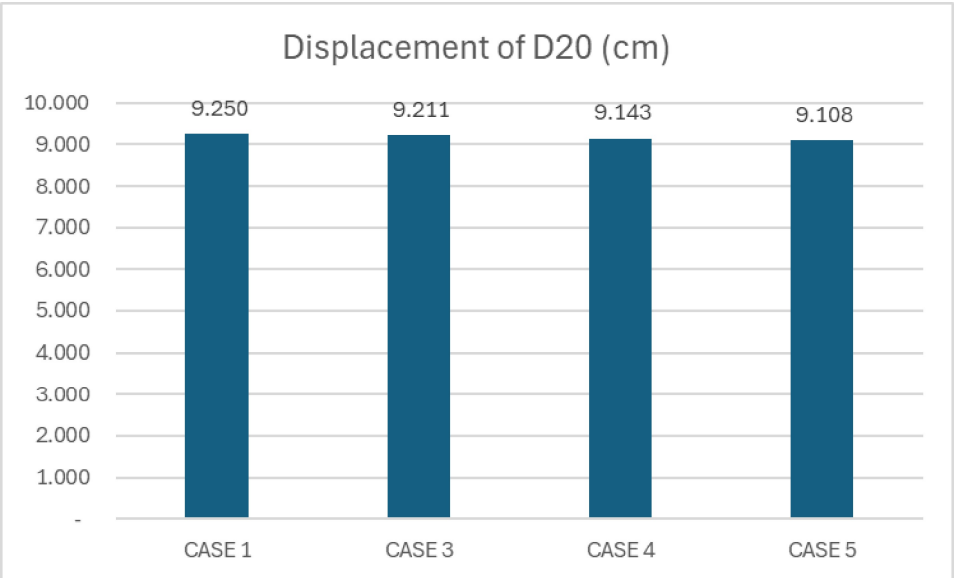



Figure 5-27. Maximum horizontal pipe displacement at D20 for Case 1, Case 3, Case 4, and Case 5 under Kobe Earthquake motion.

In detail, the analysis of the maximum displacement value of for D20 shows that the addition of geogrid layers contributes to a decrease in maximum horizontal displacement. The reductions are observed in 3 and 4 layers of geogrid, achieves a 1.16% reduction in maximum displacement, indicating a more improvement in mitigating horizontal displacement. However, it is important to note that the improvements, are relatively small.

5.2.2.2. Comparison of Vertical Displacement of the Surface Between Case 1, Case 3, Case 4 and Case 5 for under El-Centro Earthquake motion. The analysis of the maximum displacement values reveal that the addition of geogrid layers can have varying effects on vertical displacement. While some configurations may lead to increased displacement, others can result in significant reductions in Figure 5-28.

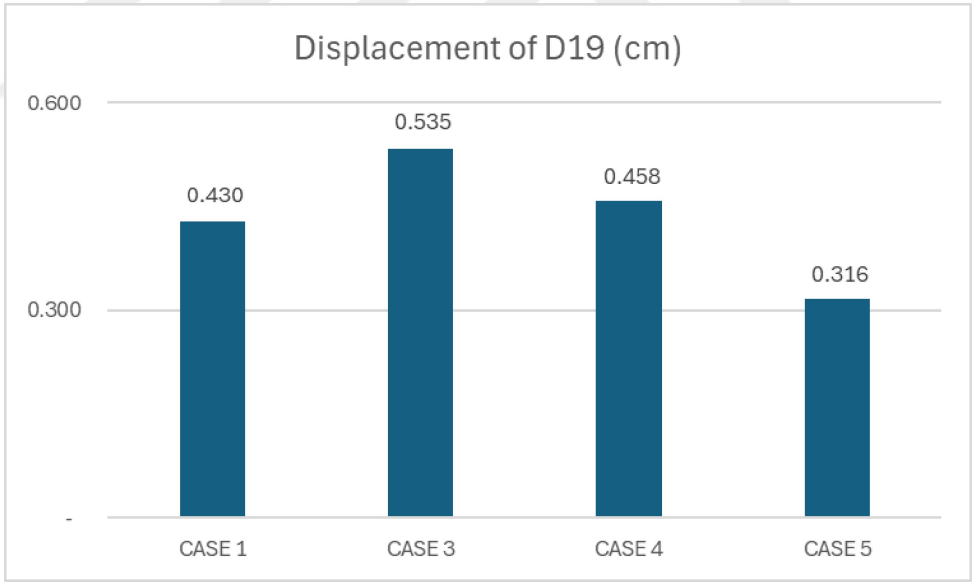



Figure 5-28. Comparison of maximum horizontal pipe displacement at D20 for Case 1, Case 3, Case 4, and Case 5 under El-Centro Earthquake motion.

In the control case, the observed maximum settlement was 0.430 cm, whereas in Case 3, with two layers of geogrid, it increased slightly to 0.535 cm. In Case 4, which utilized three layers of geogrid, the settlement was measured at 0.458 cm.

In Case 5, reduction of 23.19% in maximum settlement was observed compared to the control case. However, this reduction in settlement was not consistently reflected in the other cases, where displacement behaviour varied. The analysis of displacement data indicates that different geogrid configurations have a minor impact on displacement values as shown in Figure 5-28.

### 5.2.3. Spectral Acceleration

Spectral acceleration measures the pipe's response to seismic loads across different vibration periods. The findings under the three earthquake motions are summarized by analysing Kocaeli and Kobe earthquake motions because they represent the best results for all cases. the overall trend. The following analysis presents a comparison of spectral acceleration (SA) for experiments incorporating different numbers of geogrid layers placed at various depths within a soil box.

5.2.3.1. Comparison of Spectral Acceleration on Pipe Between Case 1, Case 3, Case 4 and Case 5 under Kocaeli Earthquake Motion. The results obtained for the Kocaeli Earthquake motion (Iznik Station) indicates that the spectral acceleration on the pipe exhibited negligible variation. Specifically, for configurations involving 2, 3, and 4 layers of geogrid, the SA value consistently remained around 0.405g as shown in Figure 5-29, Figure 5-30 and Figure 5-31.

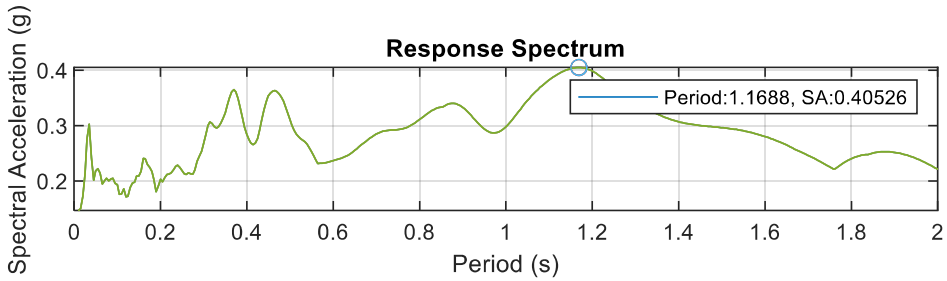



Figure 5-29. Response spectrum for A7 (on pipe), Case 3 under Kocaeli Earthquake motion.

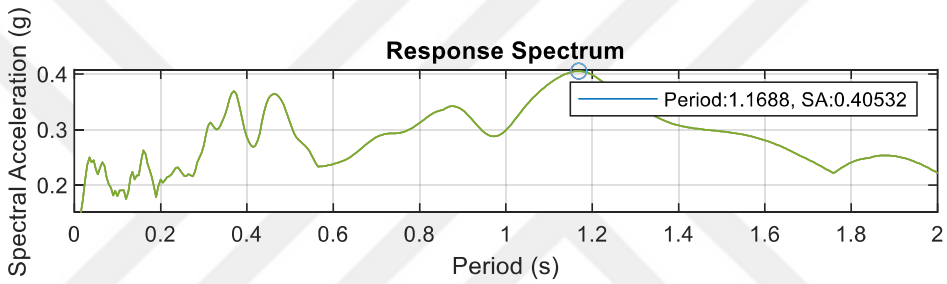



Figure 5-30. Response spectrum for A7 (on pipe), Case 4 under Kocaeli Earthquake motion.

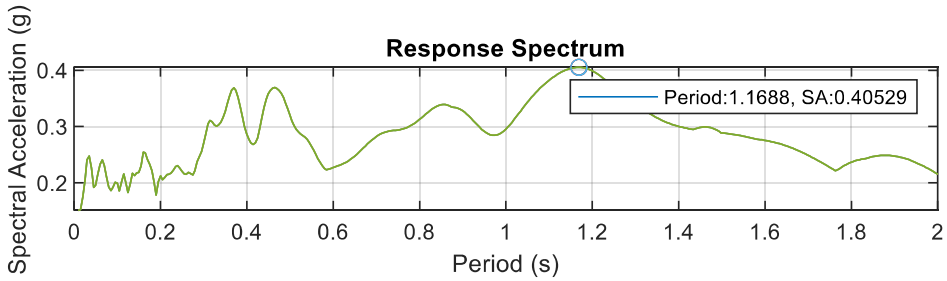



Figure 5-31. Response spectrum for A7 (on pipe), Case 5 under Kocaeli Earthquake motion.

Response spectrum graphs under Kocaeli earthquake motion show negligible variation in SA values, suggesting that the geogrid layers do not significantly change the pipe's response to seismic forces in this scenario.

5.2.3.2. Comparison of SA Between Case 1, Case 3, Case 4 and Case 5 on- pipe under Kobe Earthquake Motion. Under the Kobe earthquake motion, the spectral acceleration (SA) value without the use of geogrid is 2.589 g. The addition of geogrid layers led to a slight reduction in spectral acceleration values Specifically, with the addition of two geogrid layers, the SA value decreased to 2.587 g in Figure 5-32. This reduction continued with three layers, where the SA value further decreased to 2.580g in Figure 5-33, and with four layers, the SA value dropped to 2.549g in Figure 5-34. These results indicate that increasing the number of geogrid layers leads to a very small decrease in the spectral acceleration, with reductions of 0.08%, 0.35%, and 1.55%, respectively.

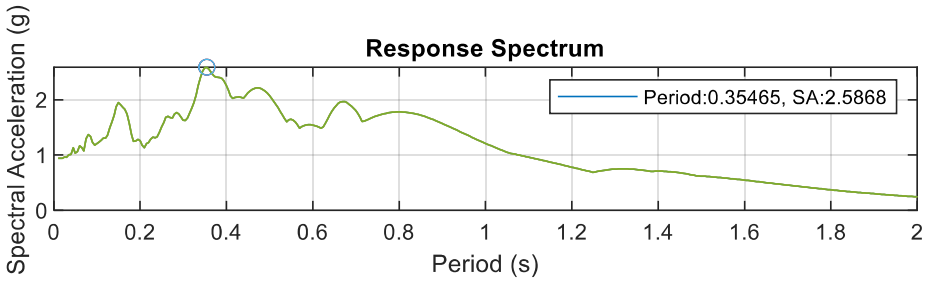



Figure 5-32. Response spectrum for A7 (on pipe), Case 3 under Kobe Earthquake motion.

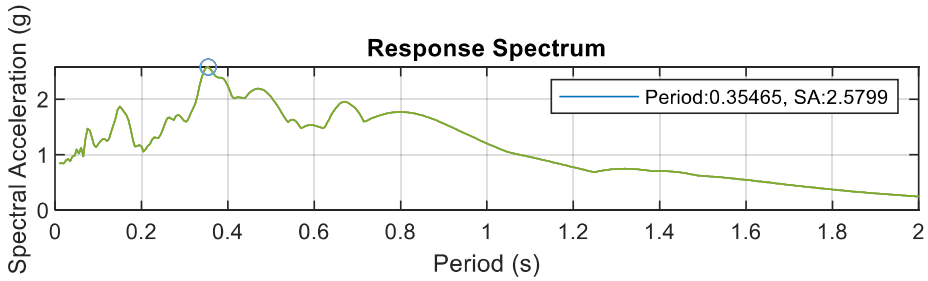



Figure 5-33. Response spectrum for A7 (on pipe), Case 4 under Kobe Earthquake motion.

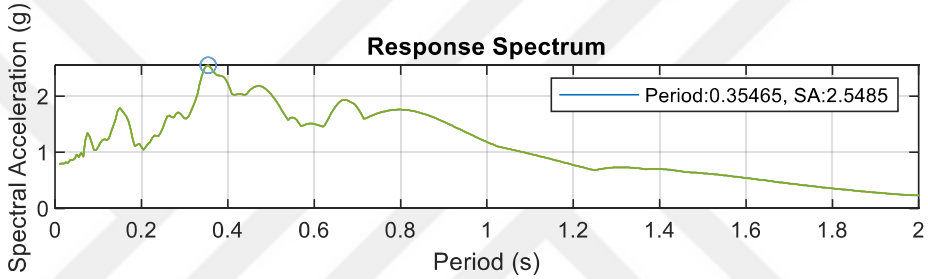



Figure 5-34. Response spectrum for A7 (on pipe), Case 5 under Kobe Earthquake motion.

This analysis highlights that while the addition of geogrid layers can slightly reduce the spectral acceleration on the pipe during seismic events, the overall impact is relatively minor. It demonstrates a small reduction in SA values with the addition of more geogrid layers, indicating a marginal improvement in the pipe's seismic performance.

### 5.2.4. Effect of Number of Geogrid Layer with Depth

This section examines the relationship between the number of geogrid layers and maximum acceleration values with depth under seismic conditions. The El Centro earthquake motion was chosen as the best results obtained. Using the El Centro earthquake motion, maximum acceleration values at various depths were analysed.

In Figure 5-35, A1 represents the maximum input acceleration under the El Centro earthquake motion. As shown, the close to surface acceleration values exceed the the maximum acceleration of input motion. The results show that the maximum acceleration on the pipe closely corresponds to maximum acceleration of input motion across all cases.

However, the most substantial increase occurs at the surface. The three-layer geogrid configuration shows significant improvement in A14 (close to surface), with a 13.53% reduction in acceleration, indicating enhanced seismic performance compared to other configurations.

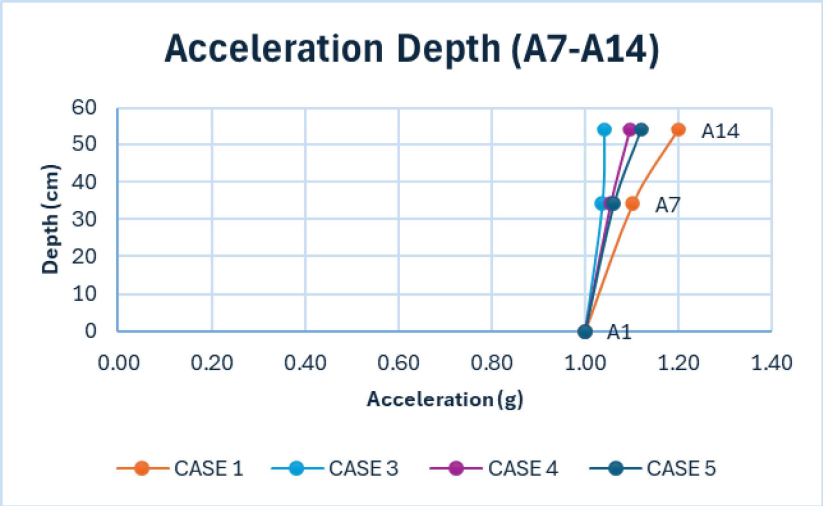



Figure 5-35. Variation of maximum acceleration with depth under El-Centro Earthquake motion for Case 1, Case 3, Case 4, and Case 5.

The test results indicate that geogrid layers reduce maximum acceleration values. The acceleration on the pipe is close to the maximum acceleration of input motion (A1) acceleration, and this trend remains consistent among the cases. In Case 1, where no geogrid is used, the recorded accelerations are generally higher. In scenarios where geogrids are used, the acceleration values decrease.

## 5.3. Effects of Earthquake Motions

In this section, the impacts of geogrid implementation on seismic performance of buried pipes under different earthquake motions are evaluated. The results of three earthquakes with different characterization were compared based on the acceleration values recorded close to soil surface (A14). The PGA (Peak Ground Acceleration) values for the earthquakes are as follows: Kocaeli earthquake (0.15g), El Centro earthquake (0.3g), and Kobe earthquake (0.82g). As expected, the earthquakes with higher PGA values resulted in proportionally higher maximum acceleration values at A14 (close to surface).

Figure 5-36 shows the comparison of cases with geogrid reinforcement and without geogrid reinforcement for A14 under all earthquake motions. When examining the percentage improvements in geogrid-reinforced cases, it becomes evident that the relationship between the earthquake's PGA value and the improvements in the surface acceleration is not directly proportional as shown in Figure 5-36.

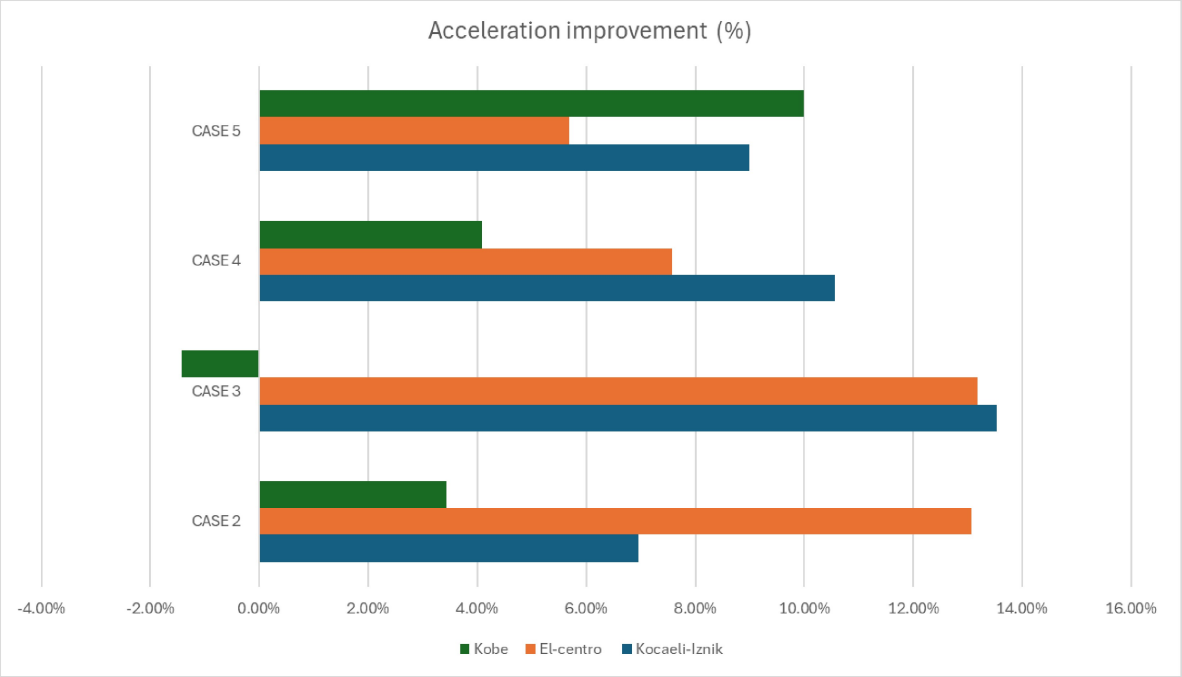



Figure 5-36 Acceleration improvement percentage for all cases under all earthquake motions (A14).

The acceleration improvements observed at the surface and at higher depths do not follow a linear or proportional relationship with the earthquake's PGA values. For instance, in Case 5, the highest percentage of improvement occurs during the Kobe earthquake motion (0.82 g), with an improvement of approximately 10%. In contrast, Case 3 demonstrates the highest percentage of improvement during the Kocaeli earthquake motion (0.15g), achieving around 13% for near-surface measurements. Conversely, for acceleration measurements under the El-Centro earthquake motion (0.15g) shows a higher percentage of improvement, approximately 13% for Case 2, while the Kobe earthquake motion exhibits a lower percentage of improvement of only 3%.

In conclusion, there is no clear relationship between PGA and the effectiveness of geogrid reinforcement arrangement and quantity. As shown in Figure 5-36 earthquakes with lower PGA values can lead to greater improvements, while those with higher PGA values may result in smaller enhancements.

# 6. CONCLUSIONS

Geogrid reinforcement enhances the seismic performance of buried systems primarily by increasing the overall stability and integrity of the soil-structure interaction. The geogrid acts as a reinforcing element within the soil matrix, distributing seismic forces more evenly and reducing the potential for differential movement or deformation of the soil and buried structures. This reinforcement helps to limit the development of strain and displacement in the soil, effectively reducing the seismic loads transferred to the buried pipes. Additionally, the inclusion of geogrids improves the load-bearing capacity of the soil and enhances its shear strength.

In this thesis, 15 shaking table tests have been conducted with and without use of geogrids. Analyses have been conducted using data obtained from 17 accelerometers and 6 LVDTs placed at various locations. The analyses have been carried out under three main sections: (1) Comparison of different geogrid arrangements, (2) comparison of the number of geogrid layers, and (3) the effect of earthquake characteristics on seismic performance of the buried pipes.

First, the impact of geogrid reinforcement on seismic performance have been examined based on the geogrid arrangement types, specifically comparing the improvement percentages between Case 1-2 and Case 1-3. Then, the relationship between arrangement type and depth have been analysed.

The conclusions from thesis can be summarized for geogrid arrangement types as follows:

i. The wrapping configuration resulted in an improvement of 3.49%, while the layered geogrid demonstrated a more significant improvement of 6.52% on the pipe maximum acceleration. This suggests that the layered arrangement provides better performance in reducing seismic accelerations on the pipe compared to wrapping.

ii. Close to the surface, the wrapping geogrid resulted in an improvement of 6.95%, whereas the layered configuration achieved a more substantial improvement of 13.53% on the surface maximum acceleration. This indicates that layered geogrids are more effective in mitigating surface-level seismic impacts.

iii. The spectral acceleration values have been almost the same for the configurations, with the value of 0.405 g. This suggests that the geogrid arrangement type had no significant effect on the spectral acceleration values.

iv. Lateral displacement of the pipe changes were minimal, with variations of 0.32% for the wrapping arrangement and 0.43% for the layered arrangement. These small changes indicate that the type of geogrid arrangement had a negligible impact on lateral displacement.

The key findings related to the comparison of geogrid layer numbers can be summarized as follows:

i. A two-layer geogrid arrangement resulted in a 13.53% improvement in maximum acceleration values, which appears sufficient for this scenario. However, in a different earthquake scenario, a 10% improvement was observed with four layers of geogrid. This is still notable for four layers of geogrid.

ii. The spectral acceleration values for the two-layer and four-layer geogrid configurations were 0.1% and 1.55%, respectively. Although four layer of geogrid provided slightly better results, the small differences in SA suggest that the number of geogrid layers had a limited impact on spectral accelerations.

iii. The percentage change in maximum horizontal displacement ranged from 0.32% to 1.54% for all cases. Similarly, the impact of the geogrid layer number on displacement was minimal, indicating no significant effect.

Lastly, in this thesis mentioned the effectiveness of geogrid reinforcement using different geogrid arrangements, especially the layered configuration, in reducing

acceleration response both on pipe and close to surface. However, its impact on spectral acceleration and displacement is relatively minor. A two-layer geogrid setup generally provides adequate improvement. Overall, the layered geogrid arrangement stands out as the most effective in seismic performance, particularly by reducing acceleration response, even though its influence on spectral acceleration and displacement remains limited.

In this thesis, the test results can be valid for the specific experimental setup and input motion applied.

This thesis presents preliminary test results. In the future, more complex test setups with different geosynthetics types, pipe material types, and pipe dimension types should be prepared under a wider range of earthquake motions.

# REFERENCES

[1] Nair, G., and S. R. Dash, "Review of seismic mitigation techniques for buried pipelines in fault zones", *Structural Engineering Convention,* pp. 2794-2810, 2015.

[2] Koerner, G. R., and R. M. Koerner "Geosynthetic use in trenchless pipe remediation and rehabilitation", *Geotextiles and Geomembranes, 14(3-4)*, pp. 223-237, 1996.

[3] Bossio S., M. Blondet , and S. Rihal, "Seismic Behavior and Shaking Direction Influence on Adobe Wall Structures Reinforced with Geogrid," *Earthquake Spectra,* pp. 59-84, 2013.

[4] Wu T., N. Jiang, C. Zhou, X. Luo, H. Li, and Y. Xia, "Dynamic response and safety assessment of buried gas pipe subjected to ground surface explosion", *International Journal of Pressure Vessels and Piping,* vol. 194, 2021.

[5] Dave, M. M., and C. H. Solanki, "Protection of buried pipelines using geosynthetics under different loading conditions—a review", *In Advances in Computer Methods and Geomechanics: IACMAG Symposium 2019 Volume 1 Springer Singapore,* pp. 249-262, 2020.

[6] O'Rourke, M. J., and X. Liu, Response of buried pipelines subject to earthquake effects, New York: Mceer, 1999.

[7] Bülent A., M. J. O'Rourke, E. Uçkan, J. Shen, and M. Çağlar, "Performance-Based Design Of Buried Steel Pipes At Fault Crossings", *Pressure and Vessels & Piping Conference*, Boston, 2015.

[8] Chian, S. C., K. Tokimatsu, and G. Madabhushi, "Soil liquefaction-induced uplift of

underground structures: physical and numerical modeling", 2014.

[9] Toprak S., B. Wham, E. Nacaroglu, M. Ceylan, O. Dal, A. E. Senturk, "The Effects Of February 6, 2023 Kahramanmaras Earthquakes On Pipelines," *18th World Conference of Earthquake Enginneering On Pipelines*, Milan, Italy, 2024.

[10] "Australian Earthquake Engineering Society," [Online]. Available: https://aees.org.au/gallery/1988-tennant-creek/. [Accessed 17 07 2022].

[11] Uckan E. , M. Aksel, O. Atas, S. Toprak, and E. S. Kaya, "The performance of transmission pipelines on february 6th,2023 Kahramanmaras earthquake: a series of case studies", *Bulletin of Earthquake Engineering,* 2024.

[12] Koerner R. M, Designing with Geosynthetics-6.th Edition Vol 1, Xlibris Corporation, 2012.

[13] Kumar S. S., Geosynthetics and Their Applications, London, UK: Thomas Telford Publishing, 2002.

[14] Mitchell, J. K., R. B. Seed, and H. B. Seed, "Kettleman Hills Waste Landfill Slope Failure. I: Liner-System Properties", *Journal of Geotechnical Engineering,* pp. 647–668, 1990.

[15] Koerner, G. R., and R.M. Koerner, "Geosynthetic use in trenchless pipe remediation and rehabilitation," *Geotextiles and Geomembranes,* Vols. 14(3-4), pp. 223-237, 1996.

[16] Selvadurai, A., "Enhancement of the Uplift Capacity of Buried Pipelines by the Use of Geogrids," *Geotechnical Testing Journal,* vol. 12, no. 3, pp. 211-216, 1989.

[17] Khalaj, O., N. J. Darabi, S. N. M. Tafreshi, and B. Mašek, "Protection of Buried Pipe under Repeated Loading by Geocell Reinforcement", in *IOP Conference Series Earth and Environmental Science*, 2017.

[18] Kim H., B. Choi, and J. Kim, "Reduction of Earth Pressure on Buried Pipes by EPS Geofoam Inclusions", *Geotechnical Testing Journal,* vol. 33, no. 4, pp. 1-10, 2010.

[19] Corey, R., J. Han, K. Deep, and P. Robert, "Laboratory Study on Geosynthetic Protection of Buried Steel-Reinforced HDPE Pipes from Static Loading." *Journal of Geotechnical and Geoenvironmental Engineering,* p. 140, 2014.

[20] Anil Ö., R. T. Erdem, and E. Kantar, "Improving the impact behavior of pipes using geofoam layer for protection," *International Journal of Pressure Vessels and Piping,* Vols. 132-133, pp. 52-64, 2012.

[21] Hatami, K., and A. F. Witthoeft, "A numerical study on the use of geofoam to increase the external stability of reinforced soil walls", *Open PDF Geosynthetics International,* vol. 15, no. 6, pp. 452-470, 2008.

[22] Bathurst, R. J., S. Zarnani, and A. Gaskin, "Shaking table testing of geofoam seismic buffers," *Soil Dynamics and Earthquake Engineering,* vol. 27, p. 324–332, 2007.

[23] Wang, J., and J. Huang, "Full-scale field study of using geofoam to reduce earth pressures on buried concrete culverts", *Geotextiles and Geomembranes,* vol. 49, no. 5, pp. 1355–1367, 2021.

[24] Lingwall, B., and S. Bartlett, "Full-Scale Testing of an EPS Geofoam Cover System to Protect Pipelines at Locations of Lateral Soil Displacement.," *Pipelines,* 2014.

[25] Beju, Y. Z., and J. N. Mandal, "Combined Use of Jute Geotextile-EPS Geofoam to Protect Flexible Buried Pipes: Experimental and Numerical Studies", *International*

*Journal of Geosynthetics and Ground Engineering,* vol. 3, pp. 1-20, 2017.

[26] Söylemez B., and N. H. Sarıhan, "Effect of geofoam location and density on the improvement of buried flexible pipe," in *11th International Conference on Geosynthetics (11ICG), (16 - 21 Eylül 2018)*, Seoul, Güney Kore, 2018.

[27] Kılıç, H., and E. Akınay, "Effects of Using EPS Geofoam as Compressible Inclusion on HDPE Pipe Behavior", *Journal of Pipeline Systems Engineering and Practice,* vol. 10(2), 2019.

[28] Palmeira, E. M., and H. K. P. A. Andrade, "Protection of buried pipes against accidental damage using geosynthetics", *Geosynthetics International,* vol. 17(4), pp. 228–241, 2010.

[29] Palmeira, E. M., and D. F. Bernal, "Uplift resistance of buried pipes anchored with geosynthetics" *Geosynthetics International, 22(2),* pp. 149–160, 2015.

[30] Adams, M. T., J. Nicks, T. Stabile, J. T. H. Wu, and W. Schlatter, Geosynthetic Reinforced Soil Integrated Bridge System, Synthesis Report, *Federal Highway Administration*, 2015.

[31] Puppala, A. J., A. Banarjee, and S. S. Congress, "Geosynthetics in Geo-Infrastructure Applications," *Geotechnique,* vol. 11, pp. 339-353, 2020.

[32] Marto, A., M. Oghabi, and A. Eisazadeh, "The Effect of Geogrid Reinforcement on Bearing Capacity Properties of Soil Under Static Load; A Review", *Electronic Journal of Geotechnical Engineering,* vol. 18, pp. 1881-1896, 2013.

[33] Ling, H. I., D. Leshchinsky, and F. Tatsuoka, Reinforced Soil Engineering: Advances in Research and Practice, CRC Press, 2009.

[34] El-Sherbiny, R., and K. Abdel-Rahman, "Seismic Performance of Geosynthetic-Reinforced Soil Structures", *Journal of Geotechnical and Geoenvironmental Engineering,* vol. 139(8), pp. 1386-1395, 2013.

[35] Tran, V. D. H., M. A. Meguid, and L .E. Chouinard, "Three-Dimensional Analysis of GeogridReinforced Soil Using a Finite-Discrete Element Framework," *International Journal of Geomechanics,* vol. 15, 2015.

[36] Pinho-Lopes, M., A. M. Paula, and M. D. L. Lopes, "Pullout Response of Geogrids After Installation", *Geosynthetics International,* vol. 22, pp. 339-354, 2015.

[37] Elshesheny, A., M. Mohamed, and T. Sheehan, "Performance of Buried Rigid Pipes Under the Application of Incrementally Increasing Cyclic Loading", *Soil Dynamics and Earthquake Engineering,* vol. 125, p. 105729, 2019.

[38] El Naggar, H., A. Turan, and A. Valsangkar, "Earth Pressure Reduction System Using Geogrid-Reinforced Platform Bridging for Buried Utilities", *Journal of Geotechnical and Geoenvironmental Engineering,* vol. 141, p. 04015024, 2015.

[39] Ahmed, M. R., V. D. H Tran, and M. A. Meguid, "On the Role of Geogrid Reinforcement in Reducing Earth Pressure on Buried Pipes: Experimental and Numerical Investigations", *Soils and Foundations,* vol. 55, pp. 588-599, 2015.

[40] Shewbridge, S. E., and N. Sitar, "Formation of Shear Zones in Reinforced Sand", *Journal of Geotechnical Engineering,* vol. 122, pp. 873-88., 1996.

[41] Seed, R. B., K.O. Cetin, R .E. Moss, A. M. Kammerer, J. Wu, J. M. Pestana, M. F. Riemer, R. B. Sancio, J. D. Bray, R. E. Kayen, and A. Faris, "Recent Advances in Soil Liquefaction Engineering: A Unified and Consistent Framework." *Proceedings of the 26th Annual ASCE Los Angeles Geotechnical Spring Seminar,* 2003.

[42] Tafreshi, S. M., N. J . Durabi, and A. R. Dawson, “Combining EPS Geofoam with Geocell to Reduce Buried Pipe Loads and Trench Surface Rutting” *Geotextiles and Geomembranes,* vol. 48, pp. 400-418, 2020.

[43] Brachman, R. W., I. D. Moore, and R. K. Rowe, “The performance of a laboratory facility for evaluating the structural response of small-diameter buried pipes” *Canadian Geotechnical Journal,* vol. 38(2), pp. 260-275, 2001.

[44] Kawabata, T., K. Uchida, Hirai, T., Mohri, Y., Ling, H. I., and N. Koyama, “Experiments on buried pipe using backfill of cover with geosynthetics”, *In New Pipeline Technologies, Security, and Safety,* pp. 1271-1278, 2003.

[45] Tupa, N., and E. M. Palmeira, “Geosynthetic reinforcement for the reduction of the effects of explosions of internally pressurised buried pipes.” *Geotextiles and Geomembranes,* vol. 25(2), pp. 109-127, 2007.

[46] Tafreshi, S. M., and O. Khalaj, “Laboratory tests of small-diameter HDPE pipes buried in reinforced sand under repeated-load” *Geotextiles and Geomembranes,* vol. 26, pp. 145-163, 2008.

[47] Pires, A. C., and E. M. Palmeira, , “The influence of geosynthetic reinforcement on the mechanical behaviour of soil-pipe systems ,” *Geotextiles and Geomembranes, 49(5),* pp. 1117-1128., 2021.

[48] Kawabata, T., K. Uchida, K., H.I. Ling, H. Nakase, Y. Sawada, T. Hirai, and K. Saito, “Lateral loading tests for buried pipe with geosynthetics”, *Geotechnical Engineering for Transportation Projects,* pp. 609-616, 2004.

[49] Potyondy J. G., “Skin friction between various soils and construction materials”, *Géotechnique 11,* vol. 4, pp. 339–353, 1961.

[50] Dove, J. E, and J. D. Frost, “Peak Friction Behavior of Smooth Geomembrane-Particle Interfaces”, *Journal of Geotechnical and Geoenvironmental Engineering, American Society of Civil Engineers,* vol. 125, pp. 544-555, 1999.

[51] Lemos L. J. L., and P. R. Vaughan , “Clay–interface shear resistance” *Géotechnique,* vol. 67, pp. 18-30, 2017.

[52] Ganesan, S., Kuo, M. and Bolton, M. “Influences on Pipeline Interface Friction Measured in Direct Shear Tests”, *Geotechnical Testing,* vol. 37, 2014.

[53] Suits, L., T. Sheahan, A. Corfdir, P. Lerat, I, Vardoulakis, “A Cylinder Shear Apparatus”, *Geotechnical Testing Journal,* vol. 27, 2004.

[54] DeJong J. T., and Z. J. Westgate, “Role of overconsolidation on sand–geomembrane interface response and material damage evolution”, *Geotextiles and Geomembranes,* vol. 23, no. 6, pp. 486-512, 2005.

[55] Boukpeti, N. and D. J. White, “Interface shear box tests for assessing axial pipe–soil resistance,” *Géotechnique,* vol. 67, no. 1, pp. 18-30, 2017.

[56] Quej-Aké L., N. Nava, M. A. Espinosa-Medina, H. B. Liu, J. L. Alamilla and E. Sosa, “Characterisation of soil/pipe interface at a pipeline failure after 36 years of service under impressed current cathodic protection”, *The International Journal of Corrosion Processes and Corrosion Control,* vol. 50, no. 4, pp. 311-319, 2014.

[57] Anderson, C., D. Wijewickreme, C. Ventura, & A. Mitchell, “Full-Scale Laboratorty Testing of Soil-Pipe Interaction in Branched Polyethylene Pipelines”, *Experimental Techniques,* vol. 29, no. 2, pp. 33-37, 2005.

[58] Bilgin, Ö., and H. E. Stewart, “Effect of temperature on surface hardness and soil interface shear resistance of geosynthetics”, *Proc., 8th Int. Conf. on Geosynthetics,*

vol. 1, p. 251–254, 2006.

[59] Bilgin, Ö., and H .E. Stewart, “Pullout Resistance Characteristics of Cast Iron Pipe”, *Journal of Transportation Engineering,* vol. 135, p. 730–735, 2009.

[60] Bilgin, Ö., and H. E. Stewart, “Design guidelines for polyethylene pipe interface shear resistance”, *Journal of Geotechnical and Geoenvironmental Engineering. ASCE,* Vols. 135, No. 6, pp. 809-818, 2009.

[61] Bilgin, Ö., and H. E. Stewart, “Studying Buried Pipeline Behavior Using Physical and Numerical Modeling” *GeoCongress 2012: State of the Art and Practice in Geotechnical Engineering,* 2012.

[62] Eid, H. T., N. M. Al-Nohmi, D. Wijewickreme, and R.S. Amarasinghe, “Drained Peak and Residual Interface Shear Strengths of Fine-Grained Soils for Pipeline Geotechnics”, *Journal of Geotechnical and Geoenvironmental Engineering,* pp. 145, 2019.

[63] Lawrence L., A.Diambra, M. S. Dietz, G. Mylonakis, and H. Milewski, “Interface shear strength of polypropylene pipeline coatings and granular materials at low stress level” in *E3S Web of Conferences 92*, Glasgow, 2019.

[64] Isaev, O. N., and R. F. Sharafutdinov, “Soil Shear Strength at the Structure Interface” *Soil Mechanics and Foundation Engineering,* 2020.

[65] Yan, K., J. Zhang, Z. Wang, W. Liao, and Z. Wu, “Seismic responses of deep buried pipeline under non-uniform excitations from large scale shaking table test”, *Soil Dynamics and Earthquake Engineering,* pp. 180-192, 2018.

[66] Feng, X., Z. Yunlong, X. Yuan, and P. Zhang, “An Experimental Study on Frictional

Properties of Concrete Pipe–Soil Interface", *ASCE,* 2022.

[67] Alzabeebee S., "Seismic response and design of buried concrete pipes subjected to soil loads", *Tunnelling and Underground Space Technology,* no. 103084, p. 93, 2019.

[68] Wang, L. R. L., and H. Zhang, "Buried pipeline system in a liquefaction environment" in *Proc. 10 WCEE*, Madrid, Spain, 1992.

[69] Lanzano, G., E. Salzano, F. Santucci de Magistris, and G. Fabbrocino, "Seismic vulnerability of gas and liquid buried pipelines", *Journal of Loss Prevention in the Process Industries,* pp. 72-78, 2014.

[70] Sarvanis, G. C., S. A. Karamanos, P. Vazouras, E. Mecozzi, A. Lucci, and P. Dakoulas, "Permanent earthquake-induced actions in buried pipelines: Numerical modeling and experimental verification", *Earthquake Engineering & Structural Dynamics,* vol. 47(4), 2018.

[71] Sterling R. S., P. Hadala, and F. Akl, "The effect of pipe bursting on nearby utilities, pavement, and structures", *Technical Report, Trenchless Technology Center, Louisiana Tech University,* 1997.

[72] Sahoo S., B. Manna and K. G. Sharma, "Seismic Behaviour of Buried Pipelines: 3D Finite Element Approach", *Hindawi Publishing Corporation, Journal of Earthquakes,* 2014.

[73] Marston, A., and A. O. Anderson, "The theory of loads on pipes in ditches and tests of cement and clay drain tile and sewer pipe", *Iowa Engineering Experiment Station,* pp. 31, 1913.

[74] Marston, A., "The theory of external loads on closed conduits in the light of the latest

experiments," *In Highway research board proceedings,* vol. 9, 1930.

[75] Spangler, M. G, "The Structural Design of Flexible Pipe Culverts," *The Iowa State College Bulletin, Iowa Engineering Experimental Station, Iowa State College.,* vol. Vol. XL, p. M30, 1941.

[76] Wang, L. R. L., and Y .H. Yeh, "A refined seismic analysis and design of buried pipeline for fault movement", *Earthquake engineering & structural dynamics,* vol. 13(1), pp. 75-96, 1985.

[77] Çalıkoğlu M., "Experimental Study of Foundation Isolation Using Geosynthetics", Master's thesis, Boğaziçi University, Istanbul, Turkey, 2014.